12-2015

All-Acrylic Multigraft Copolymers: Synthesis and Structure-Property Relationship for Producing Next Generation Thermoplastic Elastomers

Andrew Brown Goodwin
University of Tennessee - Knoxville, agoodwi2@vols.utk.edu

To the Graduate Council:

I am submitting herewith a dissertation written by Andrew Brown Goodwin entitled "All-Acrylic Multigraft Copolymers: Synthesis and Structure-Property Relationship for Producing Next Generation Thermoplastic Elastomers." I have examined the final electronic copy of this dissertation for form and content and recommend that it be accepted in partial fulfillment of the requirements for the degree of Doctor of Philosophy, with a major in Chemistry.

Jimmy W. Mays, Major Professor

We have read this dissertation and recommend its acceptance:

Sheng Dai, Alexei Sokolov, Roberto Benson

Accepted for the Council:

Carolyn R. Hodges

Vice Provost and Dean of the Graduate School

(Original signatures are on file with official student records.)

All-Acrylic Multigraft Copolymers:

Synthesis and Structure-Property Relationship for

Producing Next Generation Thermoplastic Elastomers

A Dissertation Presented for the

Doctor of Philosophy

Degree

The University of Tennessee, Knoxville

Andrew Brown Goodwin

December 2015

This work is dedicated in memory of Walter ‘Curley’ Brown.

“Imagination is usually regarded as a synonym for the unreal. Yet is true imagination healthful and real, no more likely to mislead than the coarser senses. Indeed, the power of imagination makes us infinite.”

-John Muir

ACKNOWLEDGMENTS

The work presented in this dissertation would not have been possible without the guidance and help, both scientific and non-scientific, from numerous people. First and foremost I would like to thank Professor Jimmy Mays for his technical guidance and patience during this long endeavor. I would also like to thank the rest of my thesis committee members, Prof. Roberto Benson, Prof. Sheng Dai, and Prof. Alexi Sokolov, for your help throughout this process. Additionally, none of this would have been possible without the day-to-day interactions with Dr. Durairaj Baskaran and Dr. Nam-Goo Kang who took the time to share both their knowledge and experiences with me and whom I will always consider my friends. Others I would like to thank include Dr. Kunlun Hong, Dr. Yangyang Wang, Dr. Dmitry Voylov, Dr. Vikram Sirvastiva, Dr. Justin Roop, Dr. Sachin Bobade, Dr. Beom-Goo Kang, Dr. Kostas Misichronis, Dr. Ravi Aggarwal, Dr. Wade Holley, Christopher Hurley, Weiyu Wang, Hongbo Feng, Wei Lu, Xinyi Lu, Robert Ripy, Huiqun Wang, Tom Malmgren, and all the other Mays' group members past and present.

I would not be here today without the love and encouragement from my fiancée Dr. Kimberly Nelson, thank you for your tireless support. To my parent's, Ronnie and Debbie Goodwin, for always believing in me. It was your countless sacrifices and continuous guidance that allowed me to embark on this great venture and I will always be grateful for that.

ABSTRACT

Polymer architecture and the advancement of molecular design using anionic and other controlled polymerization methods continues to be of significant research interest because of the tunable approach it provides, which can impact numerous applications ranging from thermoplastics to drug delivery systems. Among the numerous branched structures currently investigated, comb and graft copolymers continue to provide tailored materials which exhibit superior mechanical properties when compared to their di- and triblock linear counterparts. More specifically, the incorporation of two or more monomers into graft and multigraft constructions where the side chains are composed of a plastic (high T_g [glass transition temperature]) segment attached to a rubbery (low T_g) backbone has displayed much improved elastomeric properties for use in thermoplastic elastomer (TPEs) applications. These elastomeric materials continue to be dominated by compositions of styrene-isoprene or styrene-butadiene with little attention to all-acrylic systems in which both the soft and hard segments are made of acrylic monomers. By using anionic polymerization, methyl methacrylate macromonomers were synthesized and subsequently copolymerized with n-butyl acrylate using reversible addition-fragmentation chain transfer polymerization. In this manner we were able to construct the desired multigraft structures *via* a grafting-through methodology. The fundamental structure-property relationships were then studied to see how compositional changes such as branch point number, branch point

functionality, side chain molecular weight, and volume percent of the glassy PMMA [poly(methyl methacrylate)] segments affects the overall mechanical performance of the branched material. This allowed us to show the ability to dramatically control the overall strength and elasticity of the all-acrylic multigraft copolymers, as well as to demonstrate a versatile synthetic technique that has the ability to be adapted for the synthesis of more complex architectures using a vast array of hard and soft segments.

TABLE OF CONTENTS

LIST OF TABLES

LIST OF FIGURES

LIST OF SCHEMES

CHAPTER 1.

INTRODUCTION AND SYNTHESIS OF COMB AND GRAFT POLYMERS BY ANIONIC POLYMERIZATION

Abstract

This introduction reviews the current synthetic methodology for producing comb and other graft architectures, with an emphasis on branched copolymers that are analogs to linear triblock copolymers used in thermoplastic elastomeric applications. In addition to the synthetic procedure, a brief discussion into the structure-property relationship for multigraft copolymers will be presented to emphasize how architecture can be used as a tailorable parameter to optimize the physical properties of a material. It will become apparent that styrene-isoprene systems, including both linear and branched materials, have been extensively investigated, and have laid the blueprint for more in-depth work for all-acrylic materials that are also major contributors to the commercial market as elastomers and impact resistant applications.

1.1 Background

The polymerization of vinyl monomers, notably styrene, alkyl methacrylates, alkyl acrylates, vinyl chloride, dienes, acrylic and methacrylic acids, are of significant importance with about half of the commercially produced polymeric materials based on them.[1] These vinyl monomers exhibit a wide variety of unique physical properties which allows them to be used in applications such as elastomers, surface coatings, insulation, flooring, packaging, piping, impact modifiers, to just name a few.[1-3] Additionally, the properties that are exhibited by vinyl polymers are governed by compositional make up that includes molecular weight (which include number-average (M_n) and weight-average (M_w) molecular weight), chain architecture, and chain functionality.[1, 4, 5] The physical properties displayed by the polymer can be significantly effected by parameters such as molecular weight distribution (M_n/M_w, MWD) and by both the number and length of the chain branching. The ability to control the molecular parameters of molecular weight, MWD, and branching depends on the polymerization method employed to synthesize them. Vinyl monomers are capable of being polymerized by numerous methods including free radical, ionic (both anionic and cationic), and coordination polymerization processes. Among these processes classical free radical polymerization (FRP) is the most widely used in industry, but is being expanded to the techniques of controlled radical polymerization (CRP) and ionic methods, which allows for superior control and the synthesis of more well-defined polymers.

In general, there are three basic steps in the synthesis of polymeric materials:[5-8]

Initiation: The initiation step decides the polymerization method and can consist of the dissociation of a neutral molecule into two primary radicals (R*) or a charged nucleophile or electrophile (produced by carbanion or carbocation, respectively), all of which are generically termed the initiator (I).[6, 9] Monomers that bear polymerizable vinyl double bonds are attacked by the initiator species, starting the polymerization, to produce the propagating chain-end (P*).

Propagation: The process where the propagating monomer adds to the double bonds of monomers repetitively and the polymeric chain grows in the number of repeat units, termed the degree of polymerization (DP), and molecular weight.

Termination: The quenching of the propagating polymer chain and can occur under desired conditions to promptly end the polymerization reaction or arise from undesirable chain-end coupling, disproportionation, or backbiting side reactions. The use of CRP and ionic polymerization techniques reduces the effects of propagating polymer termination by undesirable side reactions to produce a 'living' or 'quasi-living' system resulting in more narrowly disperse samples and will be discussed in the later sections.

1.2 Anionic Polymerization

Living anionic polymerization, which was elegantly performed by Michael Szwarc in 1956, provides a versatile method for the synthesis of macromolecules having a low degree of compositional heterogeneity.[10-14] The term 'living' refers to the ability to grow polymer anions that retain their reactivity for sufficient time allowing for the continued

propagation without termination or chain transfer reactions.[10] It is this living property to makes anionic polymerization well suited for achieving linear block copolymers and various types of branched structures including stars, combs, and dendrimers.[3, 15-18] The most elementary of anionic polymerizations is that of styrene initiated by an organometallic compound, commonly *sec*-butyllithium (*s*-BuLi), in hydrocarbon solvent under inert conditions (Scheme1.1).

The general mechanism for anionic polymerization is again broken down into the three basic steps of initiation, propagation, and termination. The initiation mechanism and the rate of initiation for anionic polymerization each depend on the structure of both the initiator and monomer. Ideally, the rate of initiation happens much more rapidly than the rate of propagation, allowing for very narrow MWDs, and happens by either the direct ion addition, as in the case with the lithium compounds, or by the formation of more ionic bonds, which is experienced with higher alkali metals.[6, 9] During the propagating stage of the polymerization styrene monomers are continuously added the propagating chain-end, free of termination, until the monomer is completely consumed. The rate of propagation is governed by a number of factors including strength of the counter ion, the monomer being polymerized, and solvent polarity. These factors result in different degrees of carbanion and counter ion association and results in different propagation rates. In nonpolar hydrocarbon solvent the larger alkali metal cations do not coordinate as strongly, producing a greater number of free chain-ends and a faster

Initiation:

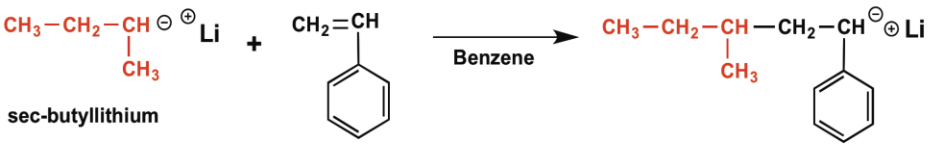

Propagation:

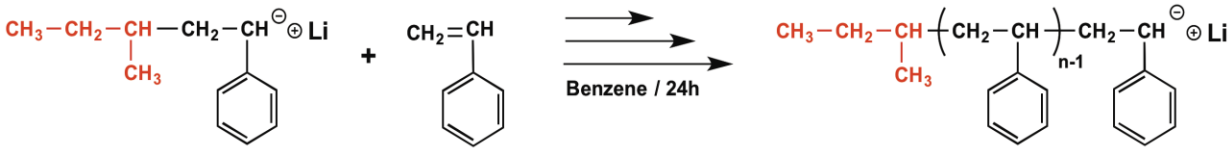

Termination:

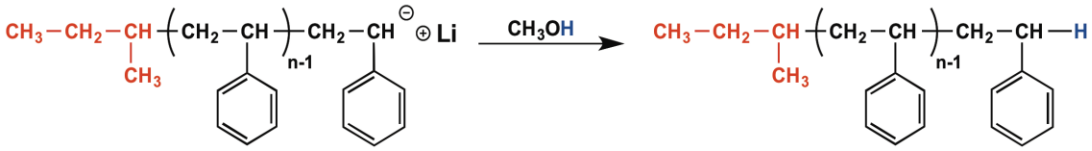

Scheme 1.1. Anionic polymerization of styrene using *sec*-butyllithium as an initiator.

propagation rate. Additionally, in the case of alkyl-lithium initiators in non-polar hydrocarbon solvent the length of the carbon chain and connectivity aids in the solvation of the initiating species, reducing ion-pair association, resulting in a faster initiation and enabling better control of the polymerization (Scheme 1.2 and Table 1.1).[19-21] When a more polar medium is used, such as tetrahydrofuran, lithium metal cations are more strongly solvated which reduces the effect of ion-pair association, again increasing the propagation rate. The order of solvating power and propagating rate constant for polystyrene can be seen in Table 1.2.[9]

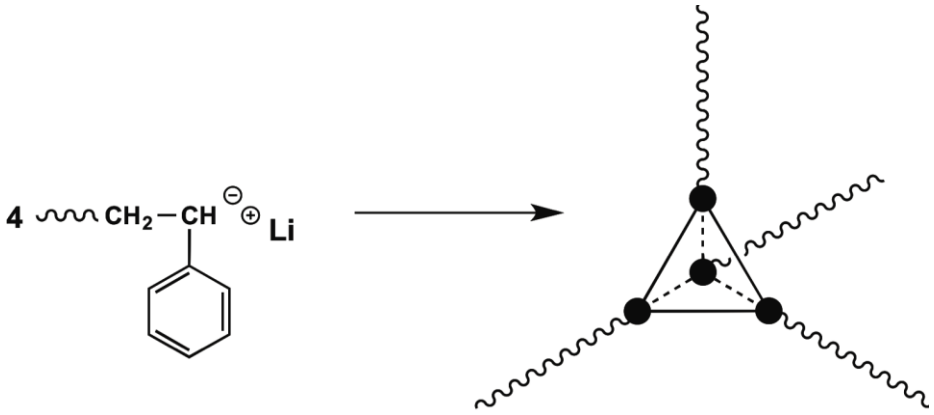

Scheme 1.2. Aggregation of Li^+ counterion from the initiation with s-butyllithium in non-polar solvent.

Table 1.1. Lithium aggregation number in polar and non-polar solvent. [11]

Alkyl	N_{agg}		
	Non-polar	Polar	Solid state
Methyl	-	4	4
Ethyl	~6	4	4
n-Butyl	~6	~2.5	6
s-Butyl	4	~1	-
t-Butyl	4	~1	4

Table 1.2. Polymerization rate with different counterions in various solvents. [7]

Counterion	Solvent	k_p (L/mol s) at 25°C
Na^+	Tetrahydrofuran	80
Na^+	1,2-Dimethoxyethane	3600
Li^+	Tetrahydrofuran	160
Li^+	Benzene	$10^{-3} \leq X \geq 10^{-1}$
Li^+	Cyclohexane	(5-100) x 10^{-5}

Similarly, the monomer structure is another consideration for the initiation and propagation steps when using anionic polymerization, especially when synthesizing block copolymers by sequential monomer addition. Vinyl monomer stability is based on the anions formed by nucleophilic addition and the pKa value for the conjugate acid of those anions. Thus, the least stable monomers are those that have large pKa values for the corresponding conjugate acids and by increasing the electrophilicity one can increase the polymerization rate.[11] In the case of sequential addition to construct block copolymers monomer reactivity is again extremely important to consider because a monomer can only initiate a second monomer that is an equivalent or weaker electrophile (Figure 1.1).

As mentioned earlier, there are a few important consequences of having termination- and transfer-free polymerizations. First is the ability to synthesize polymers with predictable molecular weight. The number-average molecular weight, M_n, of the final polymer is the grams of reacted monomer/moles of initiator and because of the constant active chain-end the first-order time-conversion plot would be linear Figure 1.2.[13, 14, 22] Secondly, this technique allows for the preparation of macroinitiators, macromonomers, functional, graft, and star polymers that will be discussed in detail later in this chapter.

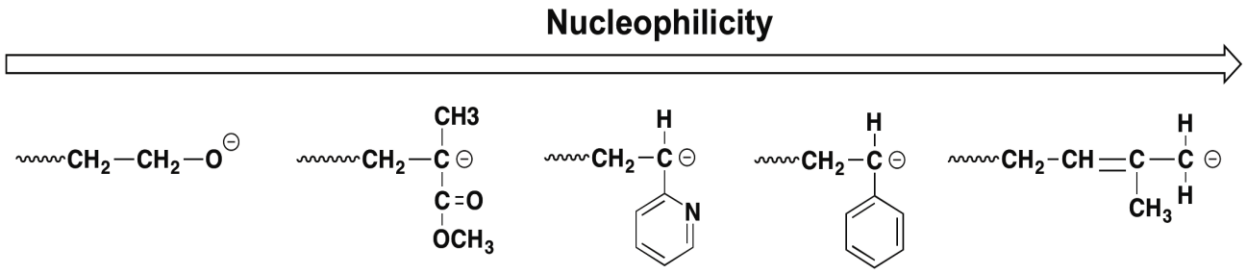

Figure 1.1. Relative nucleophilicity for commonly used monomers.

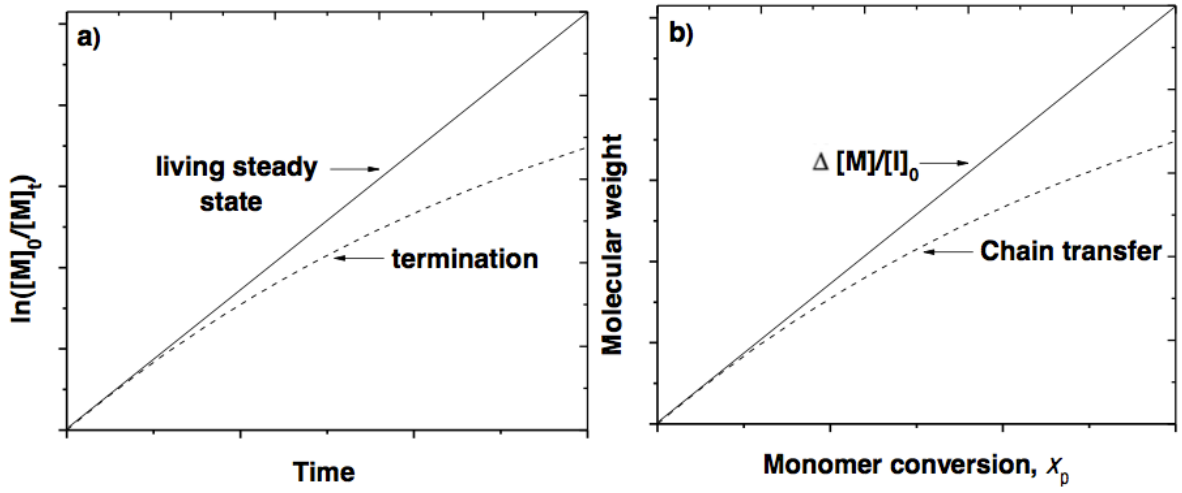

Figure 1.2. Ideal 'living' polymerization characteristics: (a) First-order time conversion plot and (b) molecular weight versus conversion plot for both a living (solid line) and non-living (dashed line) system.

1.3 Controlled Radical Polymerization

The general requirement for controlled radical polymerization is to reduce the undesirable occurrences of chain termination and chain transfer. In order to achieve the 'quasi-living' characteristic in CRP the propagating radical chain-end concentration is reduced by fast equilibrium between a dormant and active state.[23, 24] This exchange equilibrium through the active-deactivate process are frequent enough to allow all of the living chains to grow more uniformly which governs the molecular weight and MWD.[23] Several strategies have been developed to allow propagating chain-end radicals to exist in this reversible equilibrium, most notable are the techniques are that of atom transfer radical polymerization (ATRP), nitroxide mediated polymerization (NMP), and reversible addition-fragmentation transfer polymerization (RAFT), which all are based on the underlying principal of the rapid and dynamic equilibrium exchange between the dormant and active state such that the $k_{deact} >> k_{act}$.[25] In this thesis we will only focus on RAFT, but it worth noting that all CRP methods must meet the criteria of:[26-28]

1. The initiation of chains should be fast and quantitative ($R_i \geq R_p$).
2. The number of terminated chains should be small in comparison to the total chains.
3. The dynamic exchange between the dormant and active states must be relatively fast to the propagation rate.

Each CRP system has its own advantages and disadvantages and again we will be focusing on RAFT, but the recent works of Matyjaszewski and Grubbs are suggested for a general introduction to ATRP and NMP.[29, 30]

1.3.1 Reversible Addition-Fragmentation Chain Transfer (RAFT) Polymerization

The CRP technique of RAFT was first reported by Chiefari et al. in 1998 with the key feature being the addition-fragmentation equilibrium of the thiocarbonylthio compound, shown in Scheme 1.3.[31, 32] The initiation and radical-radical termination occur by the same mechanism as in conventional radical polymerization with the primary defining step of this system involving the use of a chain transfer agent (CTA) that caps the free radicals generated upon initiation. In the beginning stages of the polymerization, depicted in scheme 1.3, the addition of a propagating radical (P_n*) to the CTA and produce the [RS(Z)C-S-P_n (1)] compound is subsequently followed by the fragmentation of the intermediate radical providing the polymeric thiocarbonylthio compound of [P_nS(Z)C=S (2)] and a new radical (R*). The reaction of this newly formed radical (R*) with free monomers forms a new propagating radical chain-end (P_m*). The rapid exchange equilibrium between the active propagating radicals of P_n* and P_m* and the dormant polymeric thiocarbonylthio compounds (2 and 3) provides narrowly dispersed polymers because of the probability that all chains have equal probability to be in the dormant or active state.[31, 32] The steady state is attained by balancing the rate

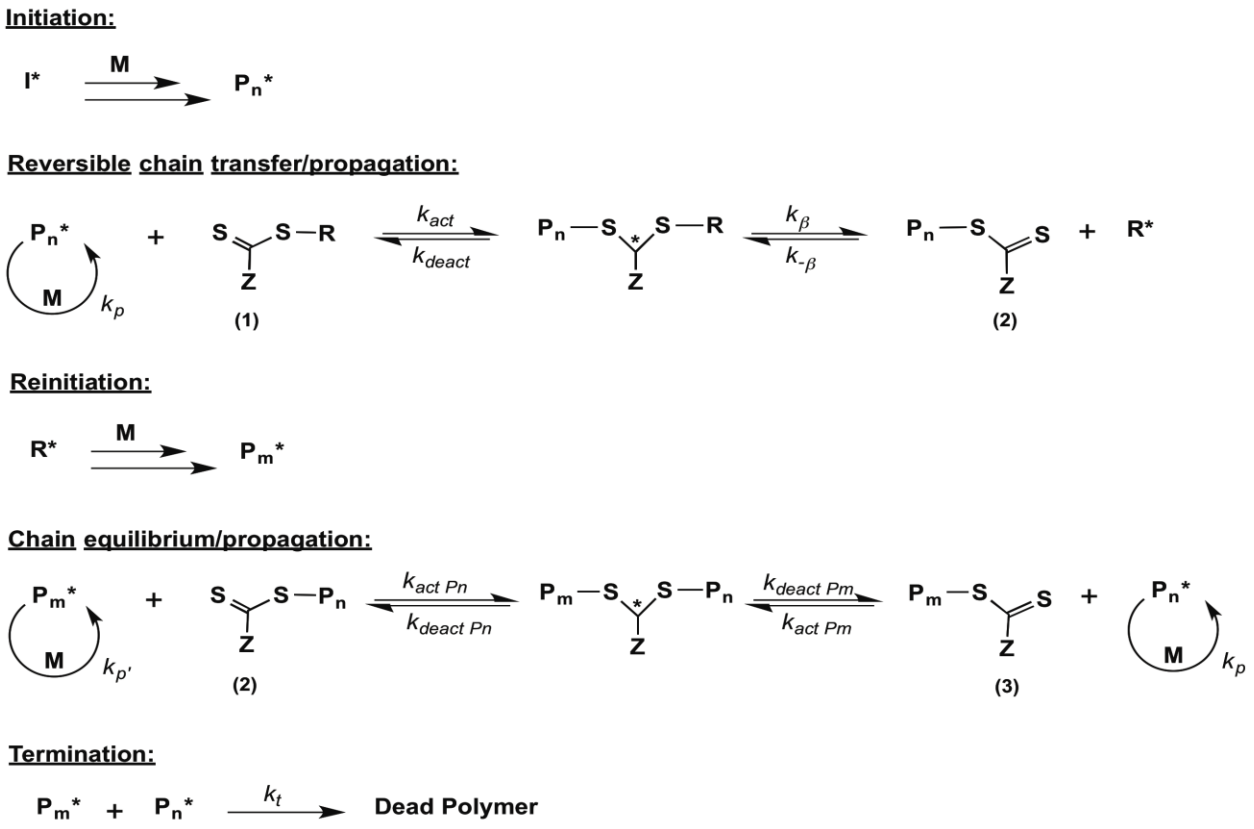

Scheme 1.3. The mechanism of RAFT polymerization by radical initiation and showing the addition and fragmentation stabilization during propagation.

constant of the active and deactivate state, opposed to the rate of initiation to the rate of termination as is the case for classical free radical polymerization, and molecular weights can be targeted similar to the anionic living system but by basing the number of polymer chains on the CTA concentration rather than on the initiator concentration.[23, 31] At the end of the reaction most polymer chains retain the thiocarbonylthio end-group and often produce a yellowish tint to the polymer powder.

A wide array of monomers have been polymerized using RAFT to give well-defined polymers with controlled molecular weights and compositions. Commonly investigated monomers such as styrene, acrylates, methacrylates, and vinyl acetates are known to be well suited for RAFT methodology, while monomers with unprotected primary and secondary amine functionality and dienes are generally incompatible with RAFT technology.[31] The monomers which bear vinyl conjugated systems are typically able to stabilize the propagating radical.

One of the major advantages of the RAFT technique is that it is carried out under the same conditions as classical free radical polymerization with exception to the addition of a CTA or RAFT agent.[33] The CTA is the defining feature of RAFT and a wide variety of thiocarbonylthio compounds, including dithioesters, dithiocarbanates, xanthates, and trithiocarbonates have been shown to effectively control the polymerization system.[34] The effectiveness of the CTA depends on the monomer being polymerized and is determined by the properties of the free radical leaving group (R) and the Z-group, which can be chosen and modified to stabilize the intermediate

radicals (Scheme 1.4).[31, 35-37] The following must be considered when choosing a RAFT agent:

1) The initial RAFT agent and the polymer-RAFT agent should have a reactive C=S double bond (high k_{act}).
2) The intermediate radicals should fragment rapidly and give no side reactions.
3) The intermediate should partition in favor of products.
4) The expelled radicals (R*) must efficiently re-initiate the polymerization.

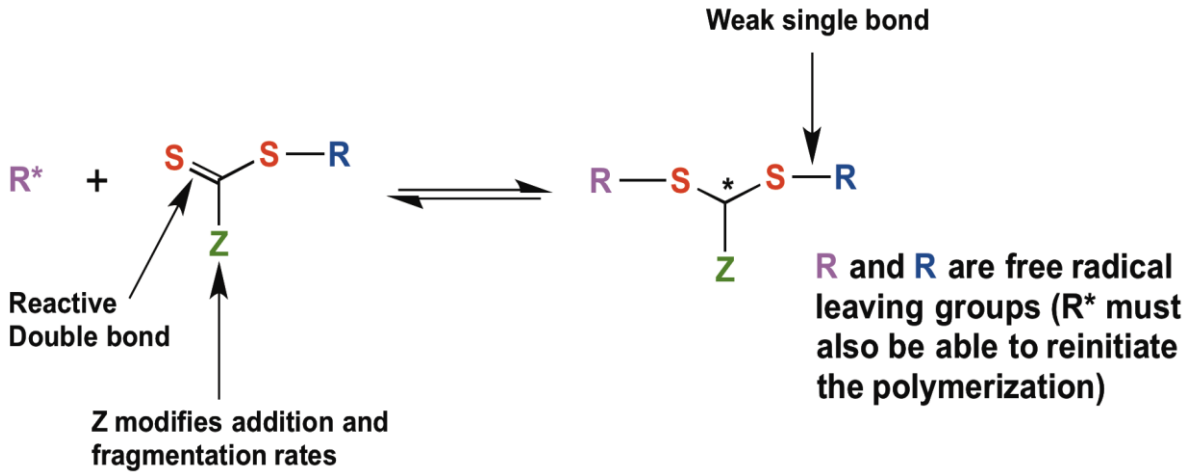

Scheme 1.4. The addition and fragmentation, creating the polymers dormant and active state, of a generic chain transfer agent used in RAFT polymerization.

Reaction conditions including initiator, temperature, pressure, and solvent have also been investigated to see there role in producing stable propagating chain-ends resulting in a controllable system. The general guideline for the initiator concentration for RAFT polymerization is that the molar ratio of the CTA to the amount of initiator decomposed should be 10:1.[31, 37] Additionally, because AIBN is a common radical source, the temperature of the reaction must be greater than the thermal decomposition temperature of the initiator, thus, RAFT polymerizations using thermal initiators are run between 50 °C and 100 °C. RAFT polymerizations have been demonstrated in both bulk and in solution where both systems provide good control. However, in the solution polymerization higher molecular weights are generally achieved with solvents such as toluene, benzene, DMF, and MEK being commonly employed because they provide good solubility for the monomer, CTA, resulting polymer, and do not interfere with the propagation chain causing transfer to solvent termination. Lastly, performing the polymerization under high vacuum and under inert gas pressure demonstrates the best quasi-living properties and reduces the termination events to produce more narrowly dispersed polymer samples.[38] These are only general guidelines for RAFT polymerization and may not apply to a specific system in question, but because of the usefulness and ease of the RAFT methodology a large literature library for individual systems have been constructed over the last decade.

Even though many systems have been produced and demonstrated to yield polymers with controlled molecular weights, narrow MWD and even branched systems;

the RAFT polymerization technique is not without its disadvantages. Three of the major draw backs include a) reactions of vinyl esters require high temperatures, b) the use of the highly efficient dithioesters as CTAs is expensive and leaves behind a color and odor, and c) there is always a low molecular weight radical available for termination. In spite of these shortcomings, the number of papers on applications of RAFT polymerizations continues to expand. At the same time, there has been no reduction in the number of investigators that explore RAFT polymerization and an increase in the number of papers that seek to both improve the process and further define the intimate details of the mechanism.[31]

1.4 General Aspects of Graft Copolymer Synthesis

Well-defined branched structures have continued to gain attention throughout the polymer community because of their unique properties that can be tuned through chemical design; therefore, these materials can address numerous applications ranging from thermoplastics elastomers and high-impact plastics to pressure-sensitive adhesives, additives, and foams.[17] Over the past twenty-five years, the synthesis of model branched structures has expanded to include a variety of living/controlled polymerization methods, as well as approaches incorporating a combination of techniques. These developments have been accelerated by advancements in anionic, cationic, and radical polymerization methods including: ring-opening polymerization, atom transfer radical polymerization, single electron transfer living radical

polymerization, reversible addition-fragmentation chain transfer polymerization, and nitroxide-mediated polymerization.[16, 18, 39] Although anionic polymerization methodology is limited to a rather small range of monomers, this method offers the maximum control over the polymerization without experiencing chain transfer or other termination events, incomplete monomer conversion, and decreased grafting efficiencies.[18, 40-43] Obtaining superior synthetic control is not only significant to synthetic polymer chemist, but the availability of well-defined, precisely tailored polymers is critical to polymer physicists and engineers for use in development of a fundamental understanding and correlation between polymer architecture, molecular composition, and physical properties to tailor and pursue materials for specific applications.[39]

Comb and graft copolymer architecture consist of a linear polymeric backbone having one or more polymer side chains attached by covalent bonds.[2, 17, 39] Comb structures are the simplest form of these branched materials because the molecular composition of the main chain and branches are comprised of the same. In contrast, graft copolymers are comprised of a backbone and side chains that differ in chemical composition.[15, 44, 45] The structures of both comb and graft copolymers are defined by three structural factors depicted in Figure 1.3: (1) the molecular weight of the main chain, (2) the molecular weight of the side chains, and (3) the distance between graft chains.[46]

Optimum control of the polymerization is the basis for the synthesis of precise, well-defined branched materials. Ideally, the comb and graft polymeric materials would

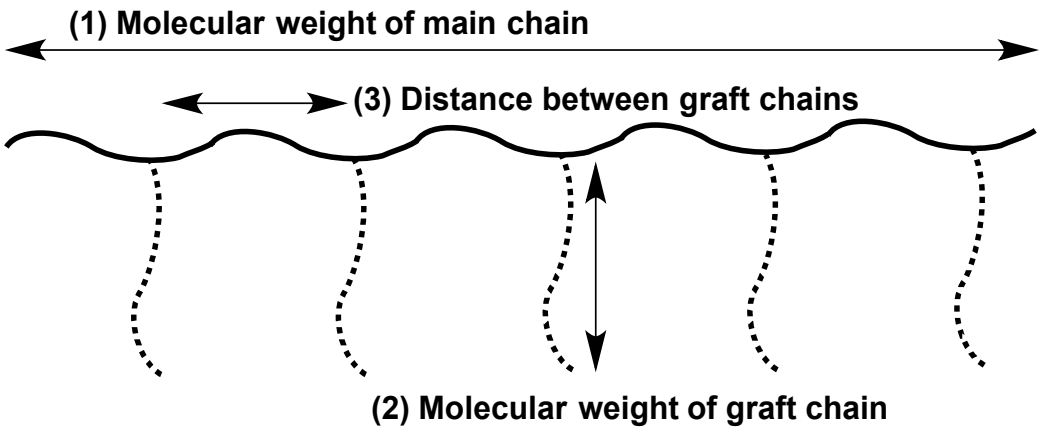

Figure 1.3. Structural parameters of branched polymers.

consist of monodisperse side chains covalently bound to a monodisperse main chain, with branch number, branch point spacing, and branch point functionality all being precisely controlled.[47] Anionic polymerization has most nearly achieved this ideal structural makeup, providing an array of branched structures, comprised of a verity of junction functionality and placement. However, most anionic graft copolymers synthesis reported to date, because of their mechanism, yield a controlled average number of graft branches per molecule and random spacing distribution of graft branches along the backbone.[11] There are three general methods for the synthesis of grafted polymers (Scheme 1.5):[11]

(1) *Grafting onto*: where the backbone polymer chain contains heterogeneously placed functional groups, X, that will react with another macromolecule with a chain-end antagonistic reactive functional group, Y.

(2) *Grafting from:* where the active sites are generated along the polymeric backbone, giving way to a pseudo multifunctional macroinitiator, to be used in the initiation of the second monomer.

(3) *Grafting through:* where a living polymer chains is end-capped with an unsaturated monomeric head-unit, forming a macromonomer that will undergo further homo- or copolymerization during the backbone construction.

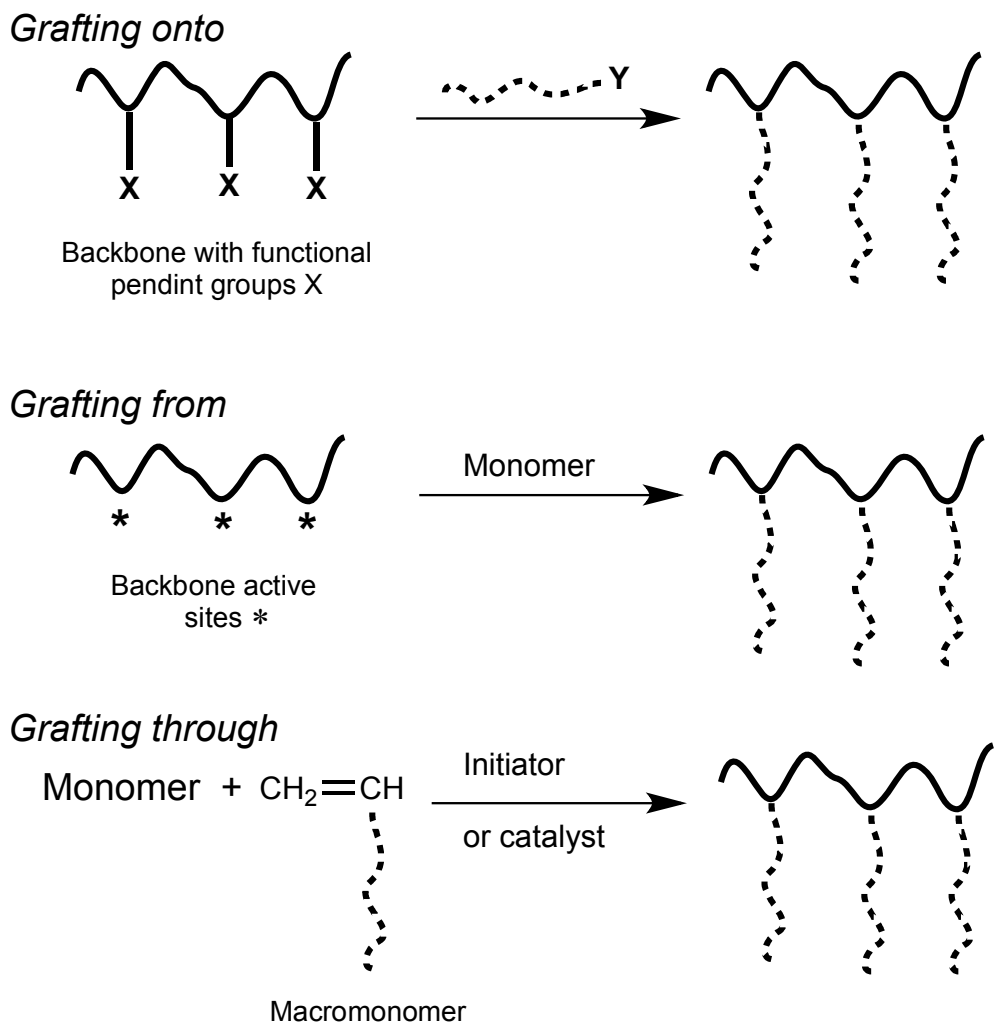

Scheme 1.5. The three general synthetic approaches to produce branched architectures.

1.4.1 Grafting Onto

The grafting onto method involves the nucleophilic attack of the living polymer side chains along the main chain at suitable electrophilic sites, with anhydrides, esters, pyridine, or benzylic halides functional groups being the most commonly utilized.[3, 18, 47] The branching sites along the polymer main chain can be generated by post-polymerization modification or by copolymerization with a monomer that bears the desired pendant functional group. Under appropriate reaction conditions, a coupling reaction between the backbone and side chains will result in the covalently bound comb of graft copolymer architecture. A key advantage to this method is that before the coupling reaction both the polymer side chains and polymer backbone can be characterized independently. Measuring the molecular weights of the grafted product and the homo- or copolymer precursor allows the number of branches, or the grafting efficiency, to be obtained.

The most common grafting onto approach utilizes chloromethylation of polystyrene depicted in Scheme 1.6.[48] Using this method and living poly(ethylene oxide) oxyanions by anionic polymerization results in the synthesis of PS-g-PEO.[53] Additionally, PS graft copolymers containing poly(2-vinylpyridine), poly(4-vinylpyridine), poly(methyl methacrylate), and poly(tert-butyl methacrylate) side chains were produced by the partial chloro- and bromomethylation of the anionically prepared PS main chain followed by the coupling reaction with the living chain-end anions of the side chains.[49-53] However, the reaction of many other polymeric carbanions and the chloromethyl

pendant group resulted in the undesirable metal-halogen exchange, altering the functionality of the branched polymer.[54-56] Conversion of the chloromethyl group into a chlorosilyl moiety, established by Rahlwes and coworkers, resulted in the quantitative reaction with poly(isoprenyllithium) to produce PS-g-PI.[57]

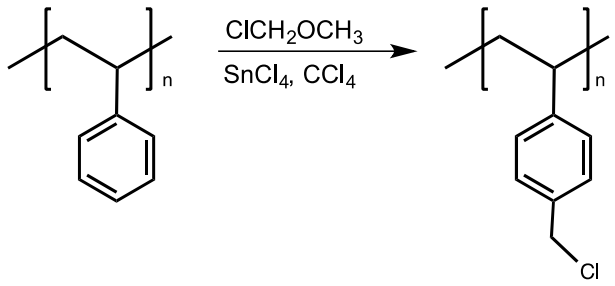

Scheme 1.6. The chloromethylation of poly(styrene) to introduce reactive pendent groups along the backbone.

The described linking reactions occur through nucleophilic attack of the living poly-anion upon the backbone, with the successful reaction often requiring the reduction of the reactivity of the chain-end anion to avoid side reactions. Living polycarbanions may be end-capped with 1,1-diphenylethylene (DPE) for this purpose.[58] By using the DPE and chloromethylated approach, more complex architectures have been synthesized by slight modifications to the grafting onto strategy. Graft copolymers with "V-shaped" and "Y-shaped" side chains were produced by the combination of controlled radical and living anionic polymerization techniques (Scheme 1.7).[59] The V- and Y-

shaped structures were obtained by the TEMPO-mediated copolymerization of styrene and vinybenzychloride to produce the backbone and the side chains were produced by a PS macromonomer, end-capped with a DPE derivative, reacting with a second living PS or PI side chain. Lastly, the final V- or Y-shaped living branched segments were reacted with the benzylchloride functionality randomly distributed along the backbone.

The final notable grafting onto approach is the preparation of poly(butadiene) and poly(isoprene) graft materials using a chlorosilylane after post-polymerization hydrosylation of the polydiene backbone.[60-62] The anionic polymerization of butadiene in benzene, results in a linear backbone with >90% 1,4-addition. The hydrosylation reaction using $(CH_3)SiHCl$ creates chlorosilate groups at the pendant double bonds of the 1,2-polybutadiene units. The subsequent reaction with living PS or PBd anions produces the randomly branched comb or graft copolymer structure Scheme 1.8. Additionally, increase functionality of the branching sites can be introduced through the use of multifunctional Si-Cl coupling agents during the hydrosilylation step.[3, 63, 64]

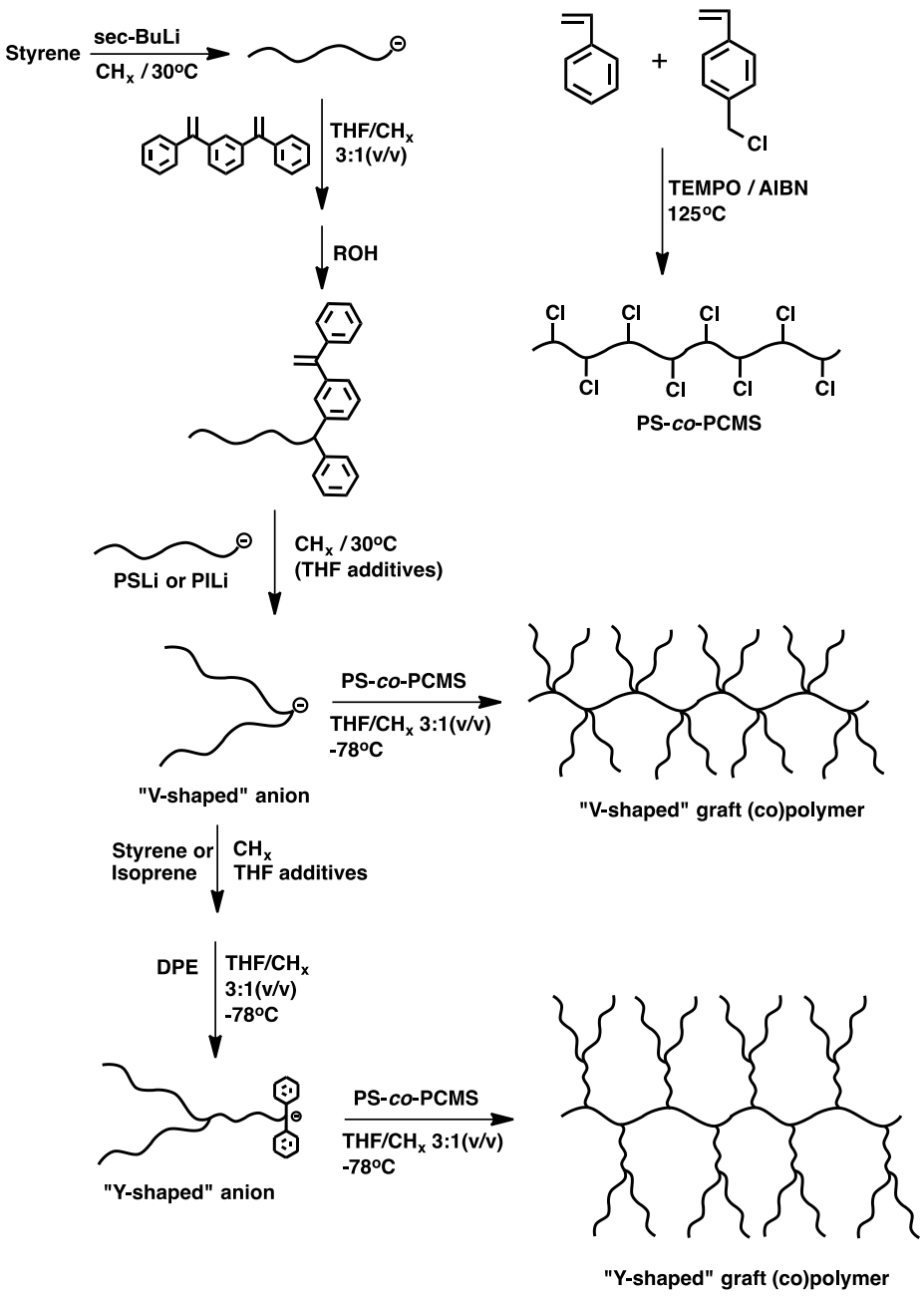

Scheme 1.7. The chloromethylation approach to produce v- and y-shaped side chains.

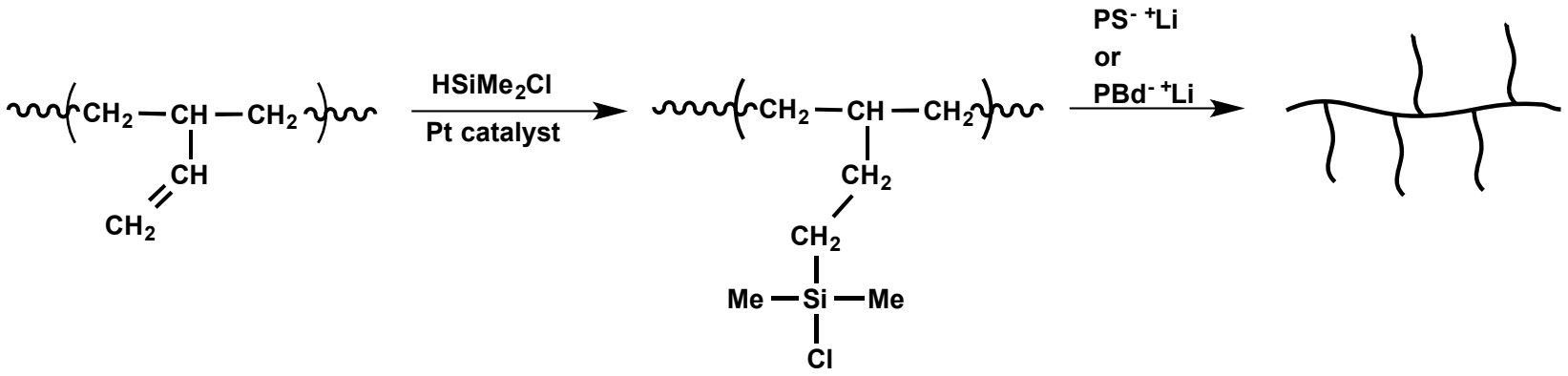

Scheme 1.8. The hydrosilylation of the pendent double bond present in the 1,2 poly(butadiene) units of the poly(butadiene) backbone.

1.4.2 Grafting From

The grafting from approach employs the creation of active sites along the polymer backbone, which serve to initiate the polymerization of the monomer that will become the side chains. The primary disadvantages of this approach is that the side chains cannot easily be isolated for independent characterization, making it more difficult to ascertain the chain length and grafting density. Secondly, the anionic synthetic procedure produces a rich ionic, macroinitiator composition that leads to poor solubility, which results in poor control of the polymerization.[3, 15, 47, 65] However, this methodology is considered particularly attractive for use in controlled radical polymerization techniques since there is a low concentration of instantaneous propagating species present, limiting coupling and other termination events, and the continuous growth of side chains effectively relieves steric effects.[39]

Grafting from by anionic polymerization is most often accomplished through acid-base chemistry, with the major advancement of this technique being the introduction of the *superbase*.[47, 66-68] This metallation by organometallic compounds, in the presence of a strong chelating agent, i.e. TMEDA, has been shown to produce main chain active sites of allylic, benzylic, and aromatic C-H bonds (Scheme 1.9). Several groups demonstrated this by producing various poly(diene-g-styrene) materials.[69-74]

A second important approach using the grafting from method is the removal of the acidic hydrogens on amide, alcohol, or phenol groups using tert-BuOK. The functional site is then capable of the anionic ring-opening polymerization of ethylene

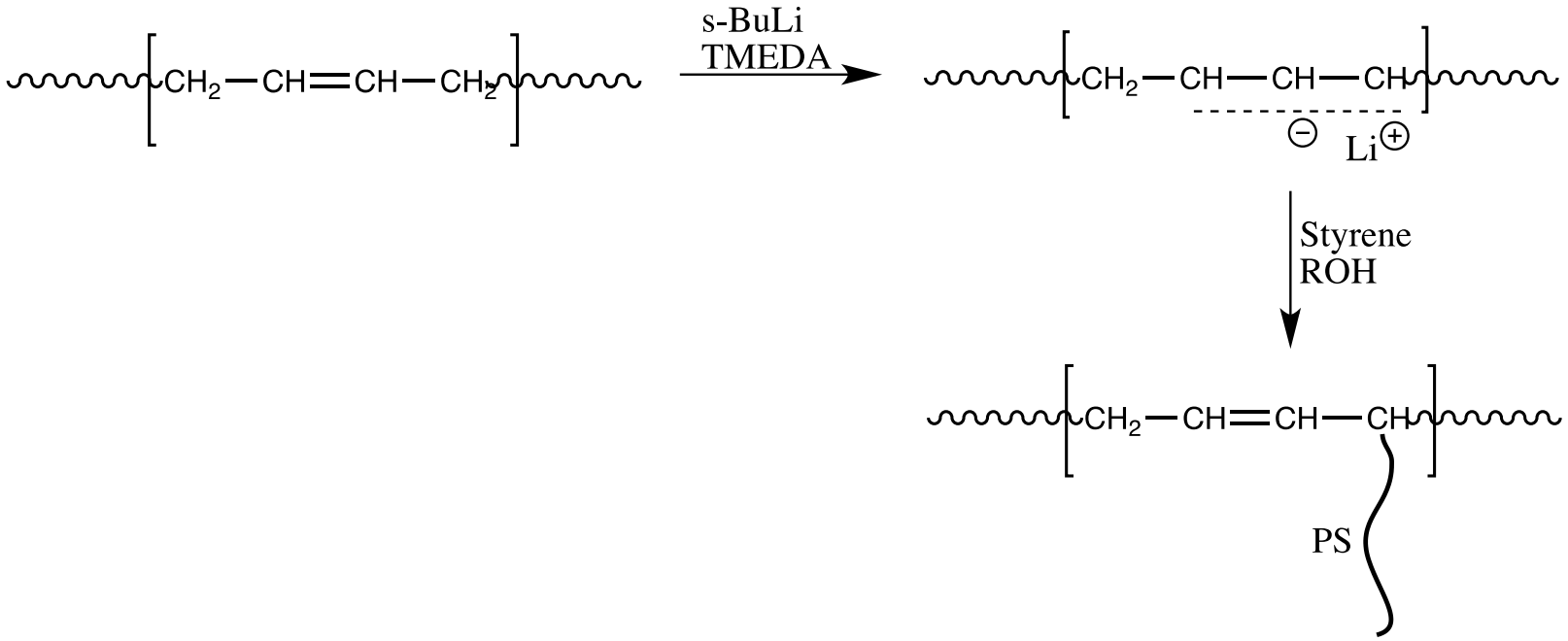

Scheme 1.9. Metallation of the 1,4 poly(butadiene) repeat units of poly(butadiene) capable of initiating styrene monomer.

oxide.[75] One example of this was demonstrated by Pispas and coworkers, where styrene and p-tert-butoxystyrene were copolymerized and after the deprotection of the tert-butyl group ethylene oxide was polymerized using phophazene base to produce the PS-g-PEO (Scheme 1.10).[76] Additionally, the same team synthesized thermo-responsive brush copolymers with poly(propylene oxide-r-ethylene oxide) side chains via the same strategy.[77]

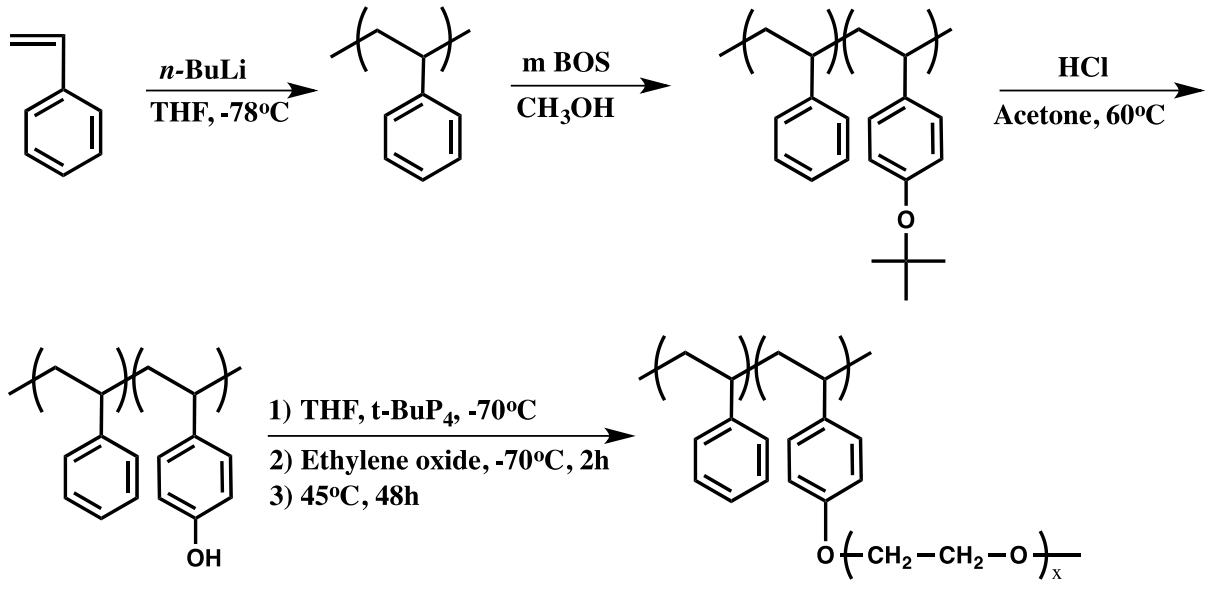

Scheme 1.10. A grafting from approach by ring opening poly(ethylene oxide) using a macroinitiator from functionalized styrene units.

1.4.3 Grafting Through (The Conventional Macromonomer Approach)

The grafting through method relies on the formation and polymerization of a macromonomer, which are oligo- or polymeric chains characterized by a polymerizable head group at the chain-end. Following this methodology, the side chains are first covalently bound to a polymerizable moiety at the chain-end to form the macromonomer. When the macromonomer undergoes the homopolymerization with itself molecular bush architecture is produced, but it is more commonly to copolymerize in the presence of a second monomer to produce the comb or graft architecture. The grafting through approach requires consideration of important synthetic factors, but offers access to reasonably well-defined grafted structures, with well-defined side chains and backbones, more easily than other grafting methods based upon anionic polymerization.[78, 79] The most important consideration is the reactivity disparity of the macromonomer (M_1) and the comonomer (M_2), typically expressed in reactivity ratios r_1 and r_2 described by the Mayo-Lewis copolymerization equation (eqn. 1.1):[80]

$$d[M_2]/d[M_1] = (1+r_2\,[M_2]/[M_1])/(1+r_1\,[M_1]/[M_2]) \qquad (1.1)$$

Generally, ionic mechanisms exhibit a greater discrepancy between r_1 and r_2, resulting in limited control of branch placement and number of branch point junctions. Additional factors of incompatibility between the macromonomer and the growing polymer chains,

fluctuations in concentration between the macromonomer and comonomer(s), and phase separation due to the formation of the copolymer can lead to greater compositional and molecular weight heterogeneity of the final branched product.[3, 15, 47] It is important to note the primary advantage to this strategy is the final graft architecture does not contain unreacted branch point junctions, that is to say there are no unreacted functional sites present along the main chain, allowing for confident determination in grafting efficiently and the average number of branch points.

The most common methodology for producing graft architectures by the grafting through approach is an *in situ* technique utilizing chlorosilyl moieties that do not require the isolation or the macromonomer as a purification step. The synthesis of the macromonomer involves the slow addition of living polymer to 4-(chlorodimethylsilyl)styrene (CDMSS) depicted in Scheme 1.11.[81, 82] This is made possible by the selectivity of the substitution reaction between the organolithium and silyl chloride rather than with the styrenic double bond. Additionally, end-capping the living polymer with a few butadiene units prior to the introduction of CDMSS provides greater control as a result of the selectivity for Si-Cl over the styrenic double bond being PBdLi > PILi > PSLi.[83] This method also allows for the synthesis of multifunctional macromonomers consisting of double and triple tailed structures to produce multifunctional branch point junctions, shown by Hadjichristidis and coworkers.[84, 85] More recently, the *in situ* macromonomer approach has been extended by Hadjichristidis and coworkers to synthesize a host of complex branched architectures,

including comb, star-comb, comb-on-comb, and double graft structures (Scheme 1.12).[86-88]

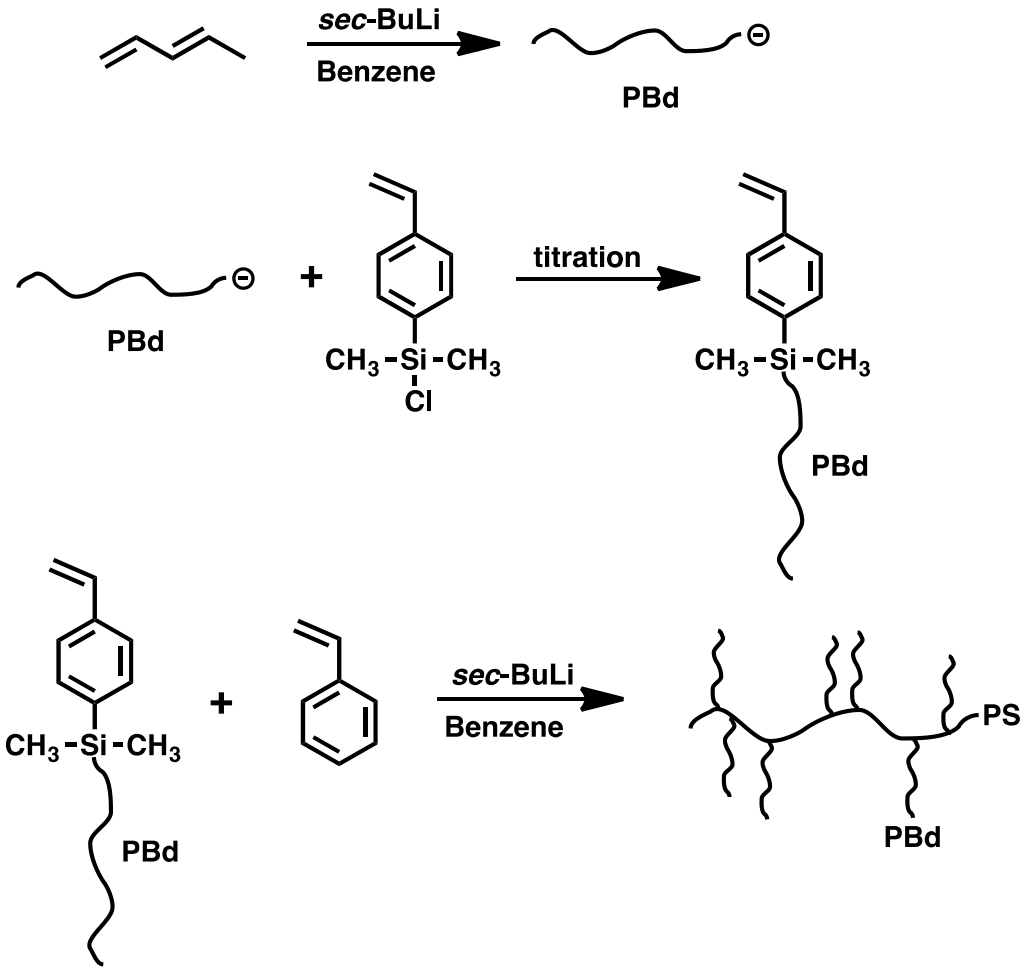

Scheme 1.11. The synthesis and subsequent polymerization of a poly(butadiene) macromonomer in with styrene to produce poly(styrene)-g-poly(butadiene) with randomly spaced branch point junctions.

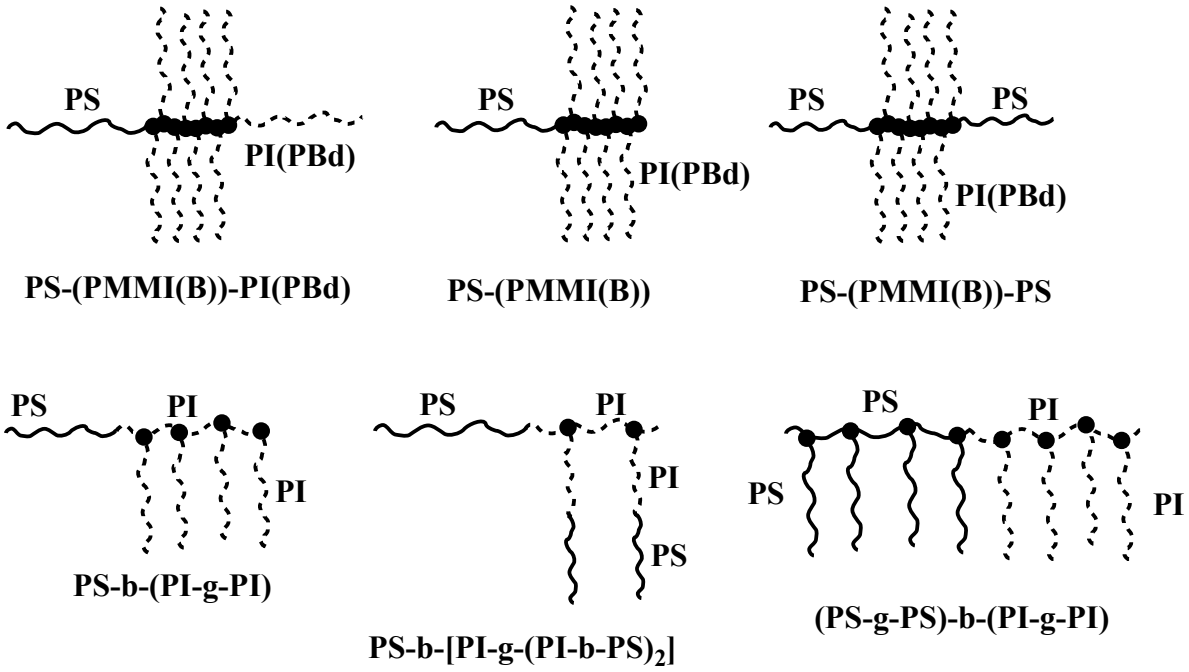

Scheme 1.12. In-situ approach to produce branched architectures by using a verity of macromonomers with the ability to lead to comb-comb and double graft architectures.

1.4.4 More Advanced Methods to Achieve Exact Graft Copolymers with Superior Control of Macromolecular Architecture

The methods discussed previously can, under appropriate and strict conditions, allow for control of side chain and backbone length. However, they provide only statistical control over the number of branch points per molecule and the spacing of the branch points. Over the last two decades progress in living anionic polymer synthetic techniques has prompted better control over these parameters and in the successful creation of many novel branched architectures including bottlebrush, π-shaped, H-shaped, super-H-shaped, pom-pom, and structures incorporating dendritic motifs.[41, 89-97] The synthesis of graft copolymer systems containing regular branch point spacing has been achieved primarily through the use of chlorosilane coupling chemistry, first demonstrated in 1990 with the synthesis of PI-g-PS.[98] This chemistry has evolved from essentially the production of an A2B miktoarm star to the synthesis of multigraft copolymers having regular branch point spacing and tunable branch point functionality.

This macromonomer strategy is based on step-growth polymerization to produce regularly spaced tri-, tetra-, and hexafunctional branch point junctions, termed regular comb, centipede, and barbwire architectures, respectively, and have been studied in detail for PI-g-PS systems (Figure 1.4).[99, 100] The construction of the tri-, tetra-, and hexafunctional multibranched architectures relies on the same general methodology of combining living anionic and condensation polymerizations, and only differing in the

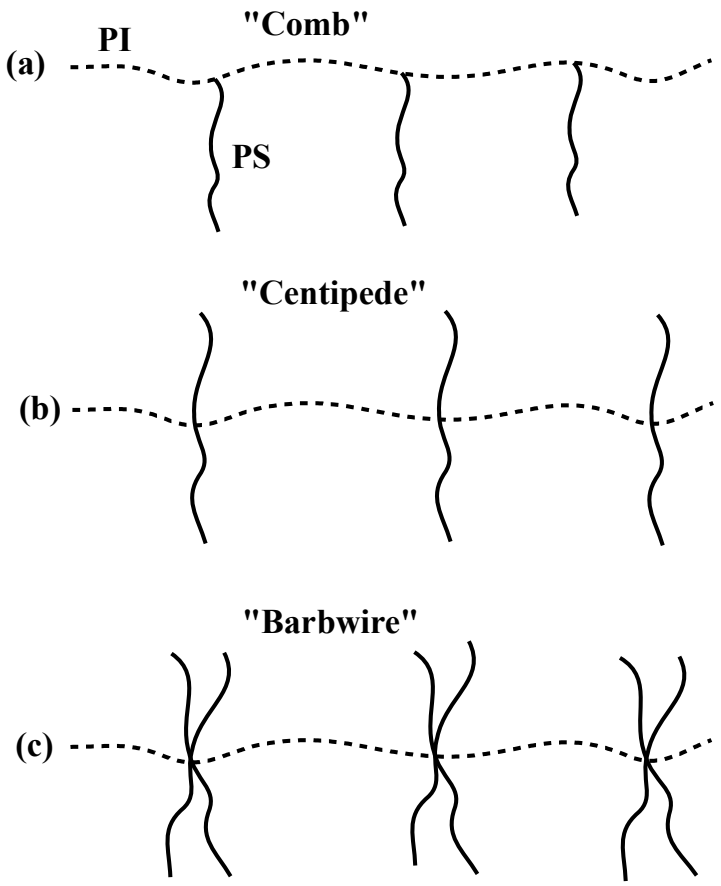

Figure 1.4. Poly(isoprene)-g-poly(styrene) multigraft copolymers termed (a) comb, (b) centipede, (c) and barbwire possessing tri-, tetra, and hexafunctional branch point junctions, receptively

choice of chlorosilane linking agent. In the case of the synthesis of the centipede structure, living PSLi is slowly added to $SiCl_4$ (vacuum titration) to obtain a coupled PS product with two terminal PS chain-ends and a $SiCl_2$ bonds in the middle of the chain. The PS-$SiCl_2$-PS chains are then reacted with difunctional PI, in slight excess, yielding the well-defined multigraft copolymers with a PI backbone and PS branches (Scheme 1.13).[99] It is important to note that the last step of this synthetic method is a polycondensation reaction yielding a PDI of 2 and allows for the number of branch point junctions to be controlled through stoichiometry. In contrast with the synthesis of the centipede and barbwire architectures, the synthesis of the comb structure requires no titration and is simply achieved by reacting living PS with an excess of methyltrichlorosilne, which can be removed by high-vacuum, and then introducing the difunctional living PI segments. This strategy produced branched polymers exhibiting regular branch point spacing, tunable branch point functionality, and is capable of extremely high molecular weights with the incorporation of more than 10 branch point junctions.[99, 100]

Additionally, the synthesis of ‘exact’ graft copolymers has been demonstrated by utilizing the macromonomer approach based on DPE moieties. Since DPE shows no self-addition behavior, the dependence on reactivity ratios of the macromonomer and comonomer can be avoided. This technique, seen in Scheme 1.14, was initially shown by Hadjichristidis and coworkers to produce comb, two and three branch symmetric,

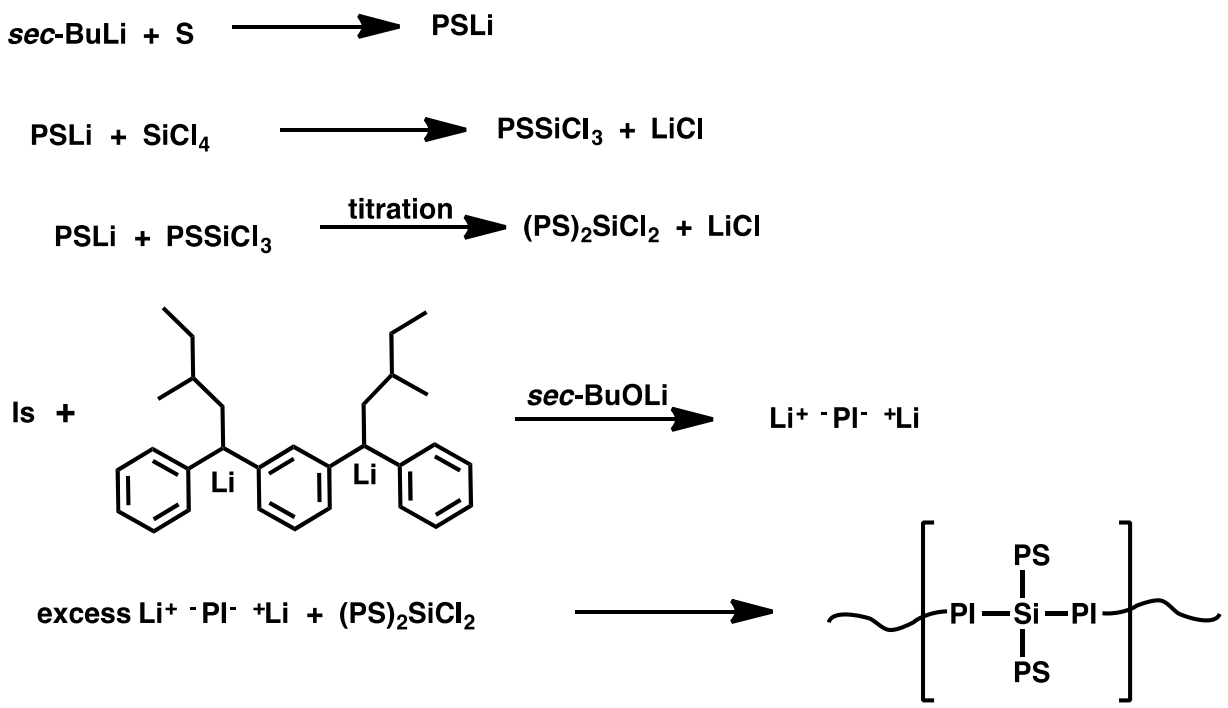

Scheme 1.13. Synthesis of the centipede poly(isoprene)-g-poly(styrene) multigraft copolymer with regularly spaced branch point junctions using vacuum titration.

and asymmetric structures through the use of the living polymer chains without initiation and propagation of the sterically hindered vinyl group. However, stoichiometry is crucial in this strategy in order to obtain complete initiation of the DCMSPDE double bond, without leading to linear side products.[81, 102, 103]

A second exact grafting strategy (Scheme 1.15) was developed by Hirao and coworkers involving the repeating of three reaction steps using a double-DPE macromolecule:[104]

(1) A transformation reaction of the α-terminal *tert*-butyldimethylsilyloxypropyl (SiOP) group into bromopropyl function via deprotection of the SiOP group followed by bromination.

(2) A linking reaction of α-SiOP-ω-DPE-functionalized living PS with α-terminal bromopropyl-functionalized PS to prepare an α-SiOP-in-chain-DPE-funtionalized PS backbone chain with the introduction of a DPE moiety between the two PS chains.

(3) An addition reaction of PSLi with the DPE moiety to introduce a PS graft chain.

This general synthesis method has been extended to the polymer of combinations of P2VP-g-PS, PtBMA-g-PS, PS-g-PI, PS-g-PMMA, and poly(ferrocenyl methylmethacrylate)-g-PS; the maximum number branches attached was 6 but in principle more branches can be achieved if adequate care is taken.[105-107]

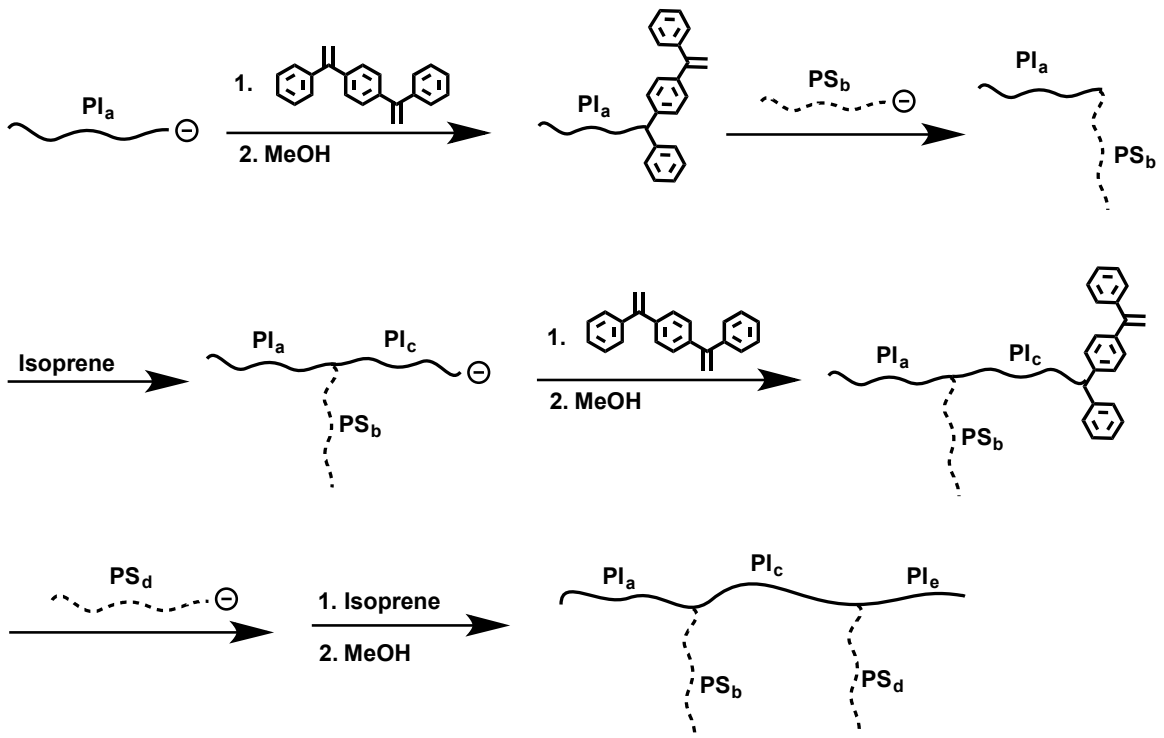

Scheme 1.14. Synthesis of poly(isoprene)-g-poly(styrene) with regularly spaced branch point junctions using multi-functional diphenylethylene moieties.

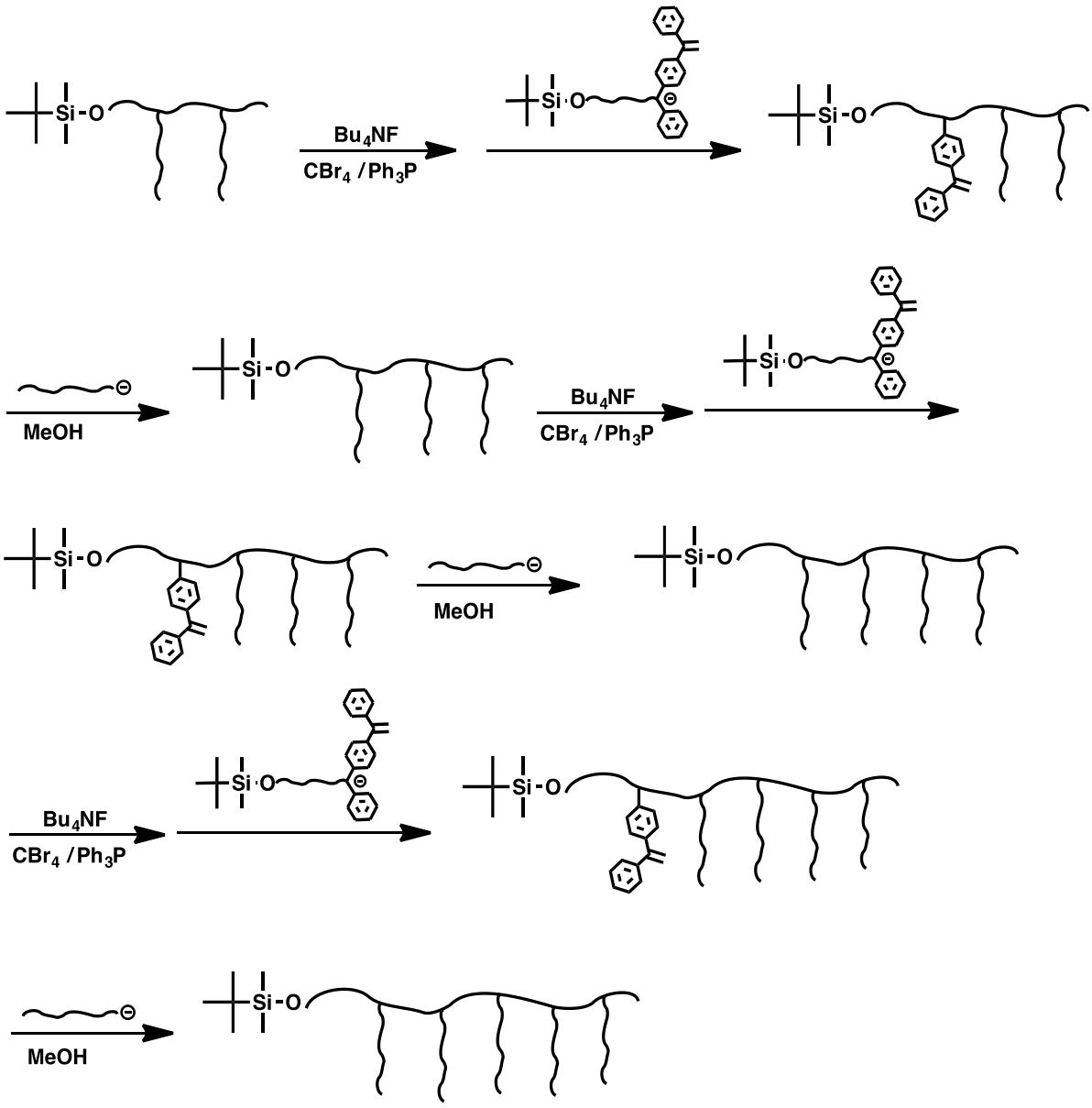

Scheme 1.15. Double-DPE approach to produce exact graft comb structures using various monomers.

1.5 Morphology of Graft Copolymer

It is well known that block copolymers undergo phase separation and self-organization on different length scale, ranging from nanometers to hundreds of nanometers as a result of molecular weight, block composition, the solvent chosen for film casting, annealing time and temperature, ect.[17] Additionally, it is the intrinsic parameters such as block copolymer architecture and the interaction parameter (χ) that determines the nature of the morphologies of these block copolymers.[108] Furthermore, by manipulating interactions between the two phases with individual control of the Flory-Huggins interaction parameter of the two blocks and the overall degree of polymerization (χN), or often displayed as the volume fraction (f) of each component, the micro-phase separation can be controlled to produce morphologies of spheres, cylinders, gyroid, and lamellae.[108-110] The morphology diagram for neutral, diblock copolymers has been mapped out by self-consistent field theory (SCFT) and is good agreement with experimental studies of these systems.[111-116] Figure 1.5 shows the phase diagram for A-B diblock copolymers exhibiting the various morphologies in a specific window of f and χN.

Until 20 years ago, very little was known about how long chain branching of polymers impacts the morphology of the material. It wasn't until Milner's work and development of the SCFT model for the effects of architecture and conformational asymmetry on "opposing polymer brushes," which approximated the morphology shift for miktoarm star copolymers.[117] In this work Milner predicted that by changing

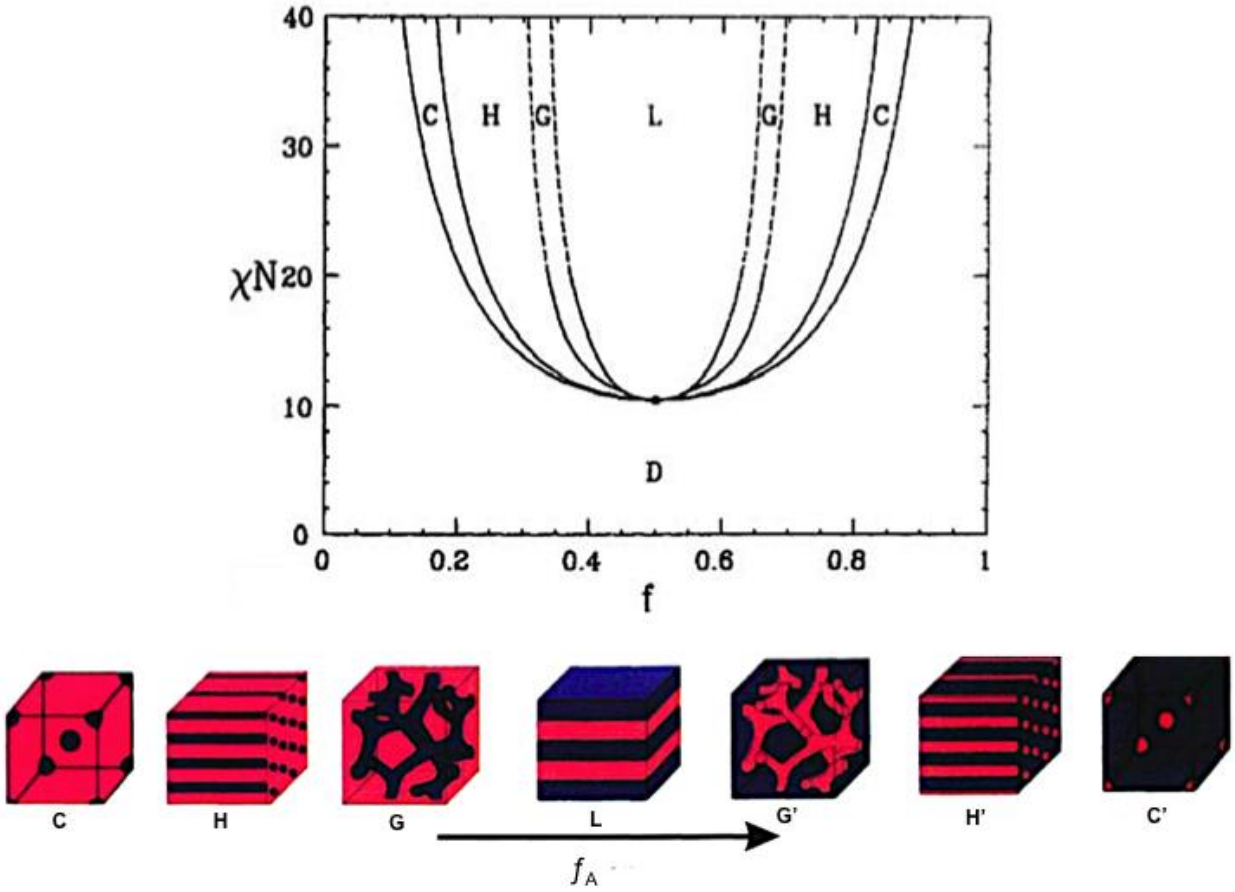

Figure 1.5. Phase diagram for general A-B linear diblock copolymers and their corresponding morphology with increasing f_A.

architecture from an AB diblock to A_2B, A_3B, and A_4B miktoarm stars, keeping the composition constant, would systematically alter the morphology of these materials in order to achieve the preferred flat interfacial region between segments. These predictions were subsequently verified through experimental results[117-120] To apply this theory to more complex multigraft copolymers, the constituting block copolymer hypothesis (Figure 1.6) must be employed. This concept is based on the premise that the overall phase behavior of a grafted copolymer is governed by the local behavior associated at each of the junction points.[95, 121-123] Additionally, the existing theories of miktoarm star and asymmetric linear diblocks can thus be applies to predict the overall behavior of the graft architectures because of their structural similarities at the local branched junctions.[117, 124-126]

Although controlling morphology of graft copolymers has been demonstrated, the main difference between the morphological ordering between linear diblock AB copolymers and the multigraft systems is that the branched graft materials do not exhibit the same degree of long range ordering. Furthermore, it has been shown experimentally that increasing the branch points per molecule further suppress the long range ordering.[127, 128] Figure 1.7 depicts the transmission electron microscopy (TEM) images of the microphase-separated domains of a hexafunctional PI-g-PS multigraft copolymer containing the same volume percent of PS with different branch point junctions and the increases in ordering as the number of branch points decreases.[99] Subsequently, small-angle X-ray scattering (SAXS) confirmed the morphology and allowed for the periodicity

of the microphase separation and agreed with the TEM image.[129] In addition to branch point number, the uniformity of branch placement has also been demonstrated to control the morphology of the material at large. This behavior is again related to the overall morphology being determined by the local microphase separation at the junction point subunits.[128] The findings also concluded that the branch point placement was more significant that the overall polydispersity of the sample.[121, 128]

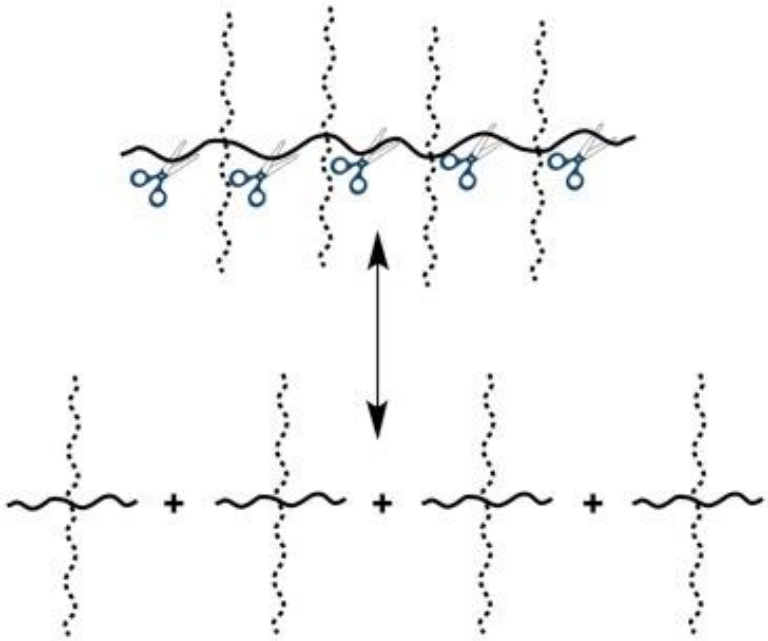

Figure 1.6. Representing a centipede multigraft copolymer as a series of connected A_2B_2 miktoarm stars.

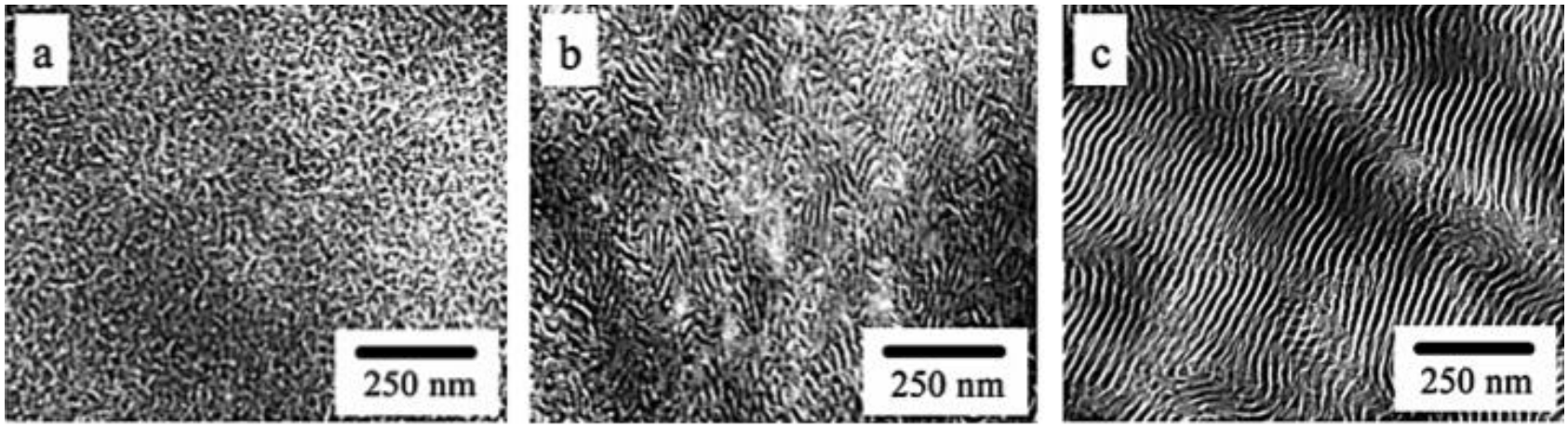

Figure 1.7. TEM images of barbwire poly(isoprene)-g-poly(styrene) multigraft copolymers that contains 21 vol.% PS with decreasing number of branch points from (a)5.3, (b)3.6, and (c) 2.7.[127]

1.6 Polymer Architecture and TPEs

One of the primary applications for these multigraft copolymer architectures is for use as thermoplastic elastomers, which are characterized by consisting of both plastic and elastomeric properties and do not rely on crosslinking to provide structural reinforcement and elastic recovery. Conventional TPEs are based on linear ABA triblock copolymers composed of glassy end blocks and an elastic middle block. Commercial examples of this class of materials are Kraton® from Kraton Polymers and products of BASF (Styroflex®), Chevron-Phillips, and others that use PS as the high glass transition (T_g) material and polydiene for the low T_g segment. Advanced nanostrength elastomers based on acrylic monomers are also present in the commercial market by Kuraray (Kurarity®) and Arkema that uses PMMA and P*n*BA as the hard and soft components, respectively. Although TPEs are more expensive than conventional crosslinked elastomers, they offer the advantages of faster, less energy intensive processing and the ability to be recycled and recast.

TPEs exhibit their desirable physical properties as a result of their morphological features. It is well understood that the soft, flexible phase controls the elastomeric properties while the hard, glassy phase controls the tensile stress of the material. The role of bulk morphology on the physical properties of the material is shown to strongly influence mechanical behavior and achieving high elasticity relies on the hard phases being dispersed in a continuous soft phase.[130-132] By tailoring the volume fraction of each component the mechanical properties and morphological ordering can be tuned

and exploited for the desired application. The influence of chain architecture of multigraft copolymers on the mechanical properties has been demonstrated to significantly improve the properties of strain and break and tensile strength. Figure 1.8 displays the stress-strain behavior of well-controlled PI-g-PS with regularly spaced branch point junctions and their rupture elongation exceeding their linear counterparts by nearly 500%.[127, 133, 134] Additionally, the authors showed that both strain at break and tensile strength was linearly dependent on the number of branch points (Figure 1.8) and that randomly branched structures yielded similar results.[127, 135, 136]

In addition to the commercially available TPEs based on styrene and isoprene or butadiene monomers, all acrylic linear triblock copolymers composed of alkyl methacrylates for the glassy block and alkyl acrylates for the rubbery block have also been commercialized. The advantage of the all-acrylic composition is the improved weatherability, UV and heat resistance, their optical transparency, and the large library of available functional acrylate monomers that can be incorporated into both the rubbery and glassy blocks. However, the two major limitations of these materials is the undesirable side reactions when producing the (meth)acrylate monomers by living anionic polymerization and the mechanical properties, such as stress and strain at break, of the materials are considerably lower when compared to SIS materials.[137, 138]

One of the major producers of these PMMA-P*n*BA-PMMA (MAM) materials is Kuraray, which has succeeded in designing a flawless living polymerization method,

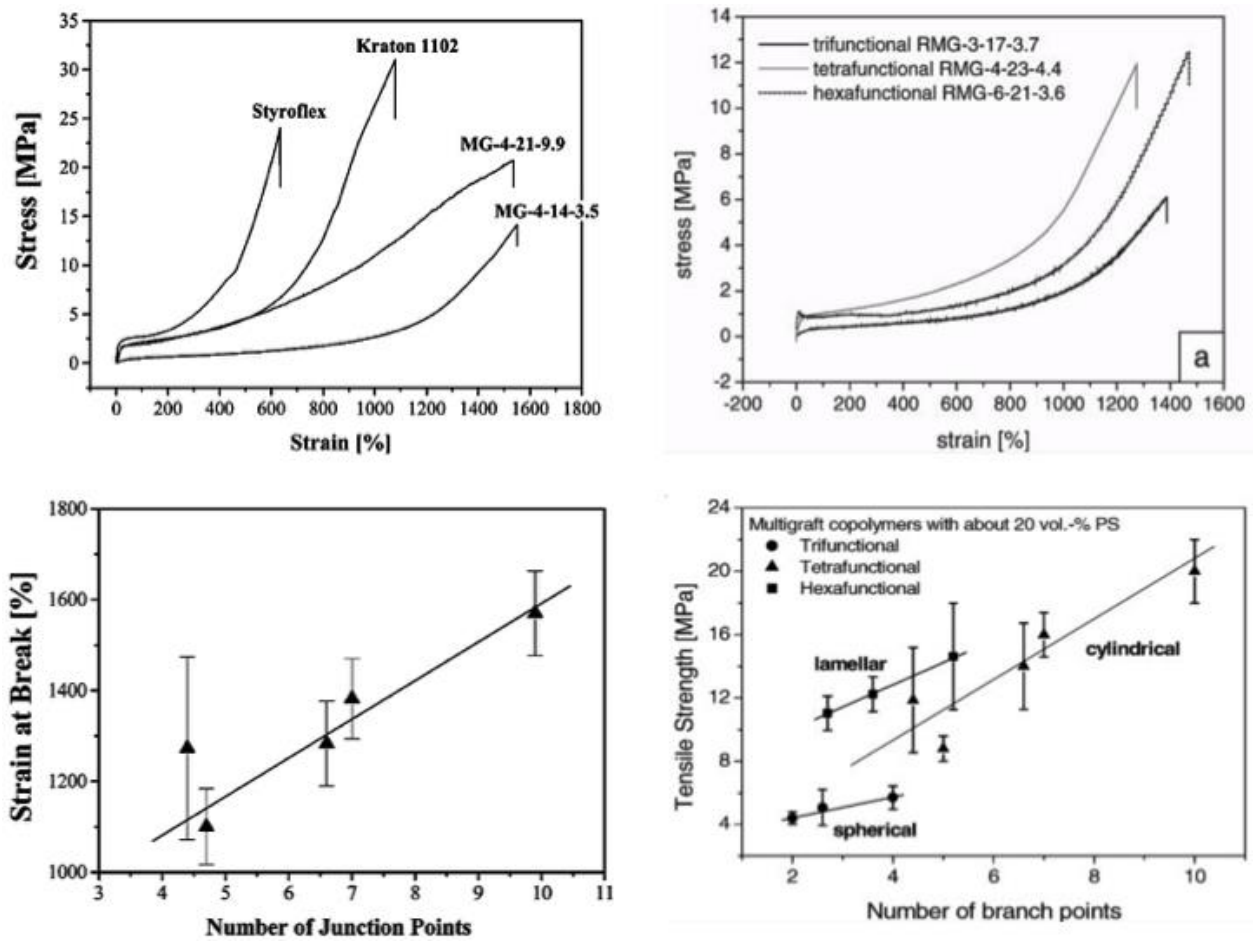

Figure 1.8. Stress versus strain curves of regularly spaced (top-left) and randomly spaced (top-right) multigraft PI-g-PS samples. The strain at break for regularly spaced centipede PI-g-PS multigraft copolymer samples with different number of branch points (bottom right) and the maximum tensile strength of various regularly spaced PI-g-PS multigraft samples with increasing number of branch points.[134]

termed the LA system, by using a Lewis base combined with di-phenoxyalkyl aluminum.[139, 140] The robust alkyl aluminum additive contributes to the stability of the enolate anion because of its steric structure (Figure 1.9), allowing insertion of the acrylic monomer under the most suitable conformations that exclusively results in no residual homo- or diblock segments and very narrow molecular weight distributions during the two-step monomer feeding polymerization (Figure 1.10).[141] The kinetic studies of the polymerization of MAM linear triblock copolymers by the LA system suggests that the aluminum acts as an accelerator for the propagating center and the polymerization rate is proportional to the aluminum concentration.[142] These results not only indicate the aluminum additive coordinates to stabilize the propagating chain-end, but at the same time, allows the polymerization to be performed at higher temperatures, optimized at -10 ^{o}C for the acrylate monomer and +50 ^{o}C for methacrylate monomer. Increasing the polymerization temperature reduces the slightly syndiotactic addition (rr/rm/mm = 61/36/3) within the P*n*BA segment and reduces the crystallization within the rubbery block which increases the softness and flexibility of the material at room temperature, preferred in elastomer applications (Figure 1.11).[142]

The MAM copolymers produced using the LA system commercially by Kuraray have great mechanical and morphological characteristics over analogous materials synthesized by controlled radical polymerizations, such as ATRP. The LA system technique produces a final bulk MAM material absent of any non-triblock chains, which are present in the other synthetic approaches, and act as plasticizers and reduce the

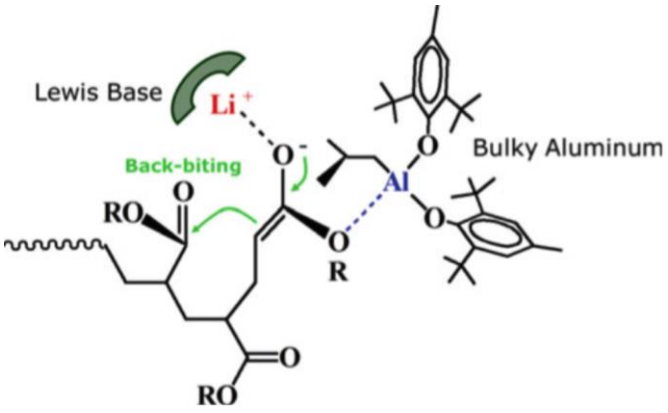

Figure 1.9. Stabilization structure of the anionically polymerized living acrylate monomer by the Aluminum additive used in the LA system.[142]

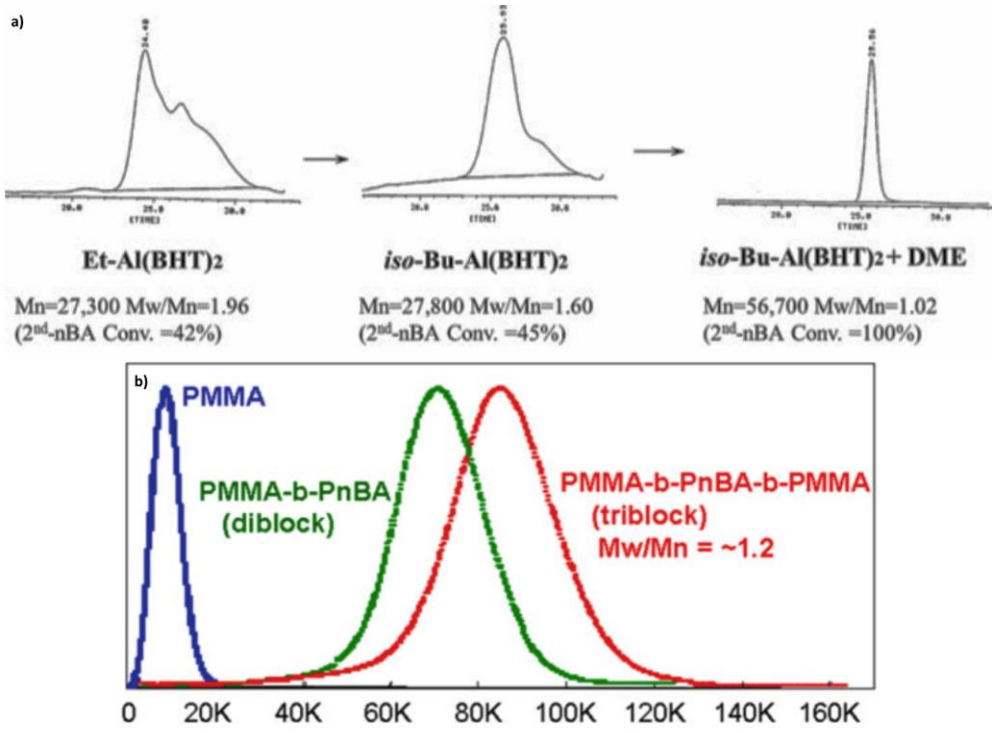

Figure 1.10. The effect of the steric alkyl groups of the Aluminum coordinating additive on the control of the polymerization (a) and the SEC elugram of the MAM linear triblock copolymer produced by Kuraray using the LA system (b).[142]

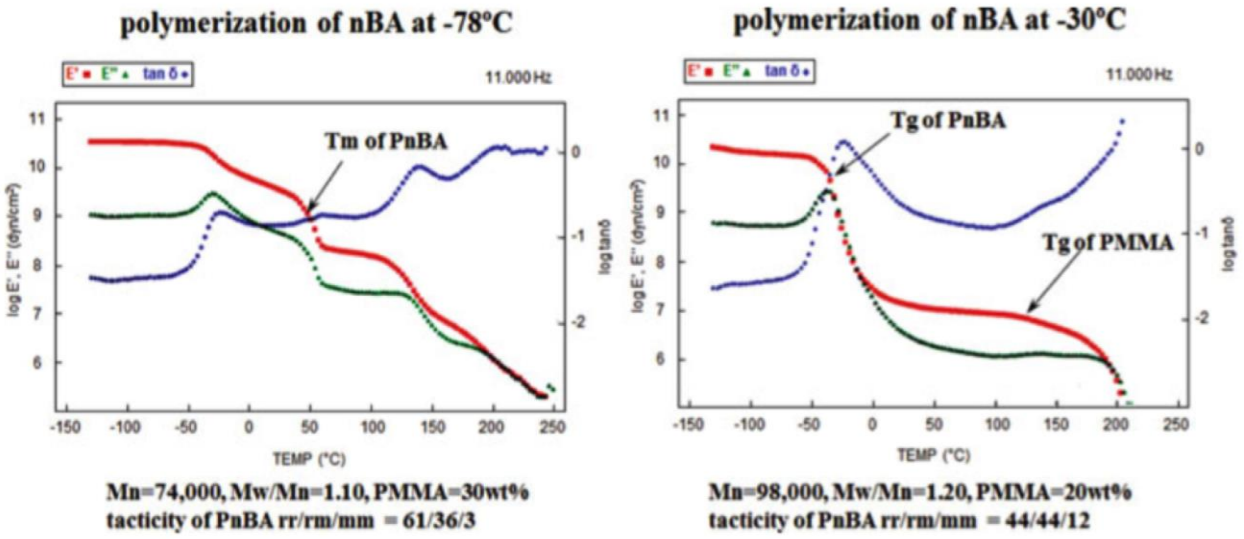

Figure 1.11. The partial syndiotactic addition of the nBA monomer and the resulting crystallization in the PnBA rubbery middle block (T_m at 50 °C) when the MAM triblock copolymers are synthesized a low temperature (-78 °C, left) which is not seen with polymerization of the nBA monomer at higher temperature (-30 °C, right).[142]

the overall mechanical and self-assembly characteristics of the material.[142, 143] The linear MAM triblock copolymer produced using the LA system by Kuraray goes by the trade name of Kurarity® and is produced at several grades, ranging from low to high PMMA content and molecular weights of ≥75 kg/mol (Figure 1.12), for a variety of applications.[142] The mechanical properties of the various grades of Kurarity® can be seen in Figure 1.13, where the tensile strength is highlighted in order to illustrate the effect of PMMA content on the observed strain and stress at break values.

Microphase separation between the rubbery P*n*BA and the glassy PMMA phases is also observed in commercially produced MAM linear triblock copolymers using both TEM and AFM. Kuraray has nicely illustrated by TEM both microphase separation and the presence of long range ordering to of their MAM triblock copolymers produced using the LA system, Figure 1.14.[142] The TEM images display partial sizes of the PMMA domains to be <50 nm and the transition from cylindrical to lamellar morphology as the PMMA wt.% is increased from around 20% to 50%. Additionally, the MAM linear triblock copolymers produced by ARKEMA were investigated using AFM and shown in Figure 1.15.[144] The triblock copolymer composed of 15 wt.% PMMA displays 10-20 nm spherical domains.

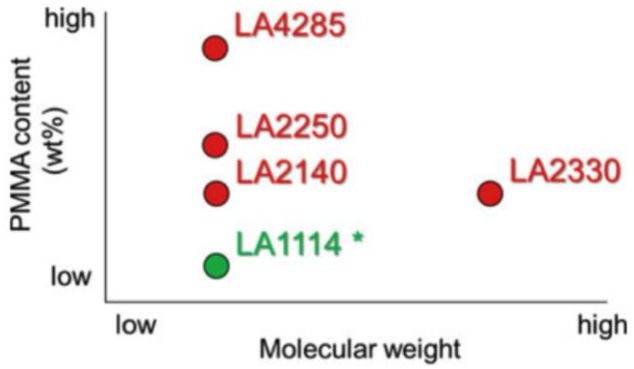

Figure 1.12. Grade map of MAM triblock copolymers produced by Kuraray.[142]

<Kuraray in-house data>

Property	Units	Test method	LA2140e	LA2330	LA2250	LA4285
Hardness [Type A]	(–)	ISO 7619-1	32	32	65	95
Hardness [Type D]		ISO 7619-1	<5	<5	18	46
Specific gravity	(–)	ISO 1183	1.08	1.08	1.08	1.11
Modulus at 100 %	(M Pa)	ISO 37	0.3	0.3	3.7	19
Tensile strength	(M Pa)	ISO 37	8.0	7.2	9.0	19
		ISO 527-2	–	–	–	19
Tensile elongation	(%)	ISO 37	570	490	380	140
		ISO 527-2	–	–	–	90
MFR [190 °C 2.16 kgf/cm²]	(g/10 min)	ISO 1133	31	3.7	25	1.5
MFR [230 °C 2.16 kgf/cm²]		ISO 1133	>350	42	330	31
Charpy impact (notched:1eA)	(KJ/m²)	ISO 179-1	NB	NB	NB	28
Flexural modulus	(M Pa)	ISO 178	–	–	–	650
Transmittance[3mmt]	(%)	ISO 13468-1	91<	91<	91<	91<
Haze[3mmt]	(%)	ISO 14782	2–6[a]	2–6[a]	2–6[a]	<2
Suitable applications	For PSA		+	+	+	
	For molding		-	-	+[b]	+
	For compound, additives		+[b]	+[b]	+[b]	+

Figure 1.13 Grade and mechanical properties of Kurarity®.[142]

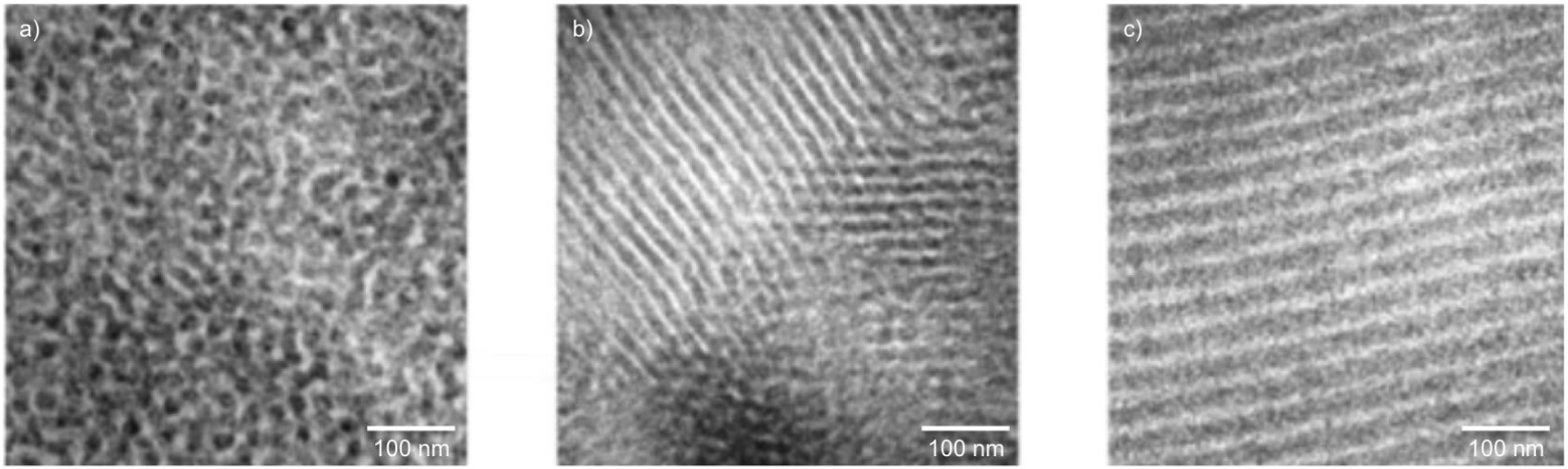

Figure 1.14. TEM images of Kurarity® composed of 23 wt.% (a), 30 wt.% (b), and >50 wt.% (c) PMMA (dark regions). The images depicted short cylindrical morphology (a), long cylindrical morphology (b), and lamellar morphology (c) with less than 50nm PMMA domain size.[142]

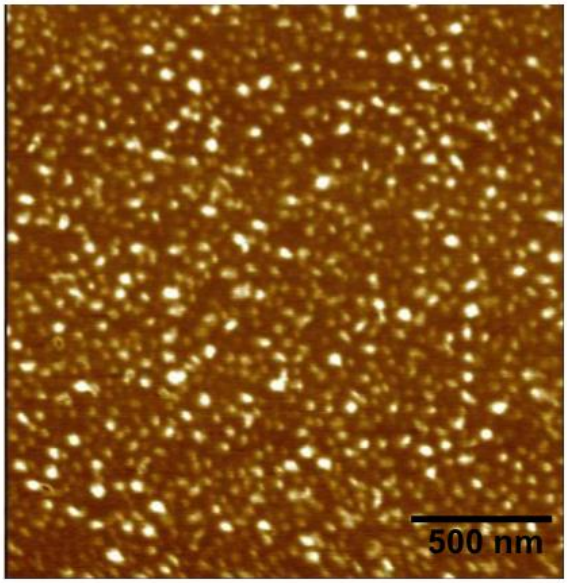

Figure 1.15. AFM phase image of an MAM linear triblock copolymer composed of 15 wt.% PMMA produced by Arkema. The PMMA domain size (bright regions) is 10-20nm.[144]

1.7 The Scope of this Thesis

The fundamental synthesis and properties of multigraft copolymers has been explored and the results have been discussed throughout this introductory chapter. To date, numerous synthetic procedures in order to produce unique branched materials and understand their structure/property relationship have been shown. Based on these previous works we have set out to extend the synthetic methodology for producing multigraft copolymers, keeping the possibility of industrial scale-up in mind, and to thoroughly investigate the lesser-studied acrylic-based TPEs, with the goal of understanding the fundamental aspects of their observed bulk mechanical properties and to optimize them through targeted synthesis.

Over the next few chapters three distinct portions of the all-acrylic multigraft copolymer for use in TPE applications will be discussed and provide a logical path through the synthesis, characterization, and structure/property relationship of these novel materials. We began by developing a synthetic strategy that would provide the controlled synthesis of PnBA-*g*-PMMA with controlling the tunable parameters of backbone and side chain molecular weights, volume fraction between the hard and soft acrylic segments, and the average number of branch point junctions per molecule. The numerous PnBA-*g*-PMMA samples were then well characterized in order to accurately define the structure and composition of the synthesized material. Subsequently the mechanical, thermal, and morphological properties were investigated to understand the role each parameter plays in the physical properties displayed by the bulk material.

Finally, we turned our attention to the synthesis and characterization of more advanced multigraft architectures that contained three phases and discuss the possibilities for not just all-acrylic TPEs but compositions containing both acrylic and non-acrylic monomers. This dissertation will close with our concluding remarks and suggestions for the future synthesis and bulk property optimization of multigraft copolymers.

References

1. Mishra, M.; Yagci, Y., *Handbook of Vinyl Polymers: Radical Polymerization, Process, and Technology.* 2nd ed.; CRC: Boca Raton, 2009.

2. Hadjichristidis, N.; Pispas, S.; Floudas, G., Block Copolymer Applications. In *Block Copolymers*, John Wiley & Sons, Inc.: 2003; pp 383-408.

3. Hadjichristidis, N.; Pitsikalis, M.; Pispas, S.; Iatrou, H. *Chemical Reviews* **2001,** 101, (12), 3747-3792.

4. Matyjaszewski, K.; Davis, T., *Handbook of Radical Polymerization.* Wiley-Interscience: New York, 2002.

5. Moad, G.; Solomon, D. H., *The Chemistry of Free Radical Polymerization* . Pergamon: Oxford, England, 1995.

6. Odian, G., *Priniciples of Polymerization*. Wiley-Interscience: New York, 1991.

7. Flory, P. J., *Principles of Polymer Chemistry*. Cornell University Press: Ithaca, 1953.

8. Flory, P. J. *Journal of the American Chemical Society* **1937,** 59, (2), 241-253.

9. Stevens, M. P., *Polymer Chemistry: An Introduction*. 3rd ed.; Oxford University Press: Oxford, England, 1999.

10. Baskaran, D.; Müller, A. H. E. *Progress in Polymer Science* **2009,** 32, (2), 173-219.

11. Hsieh, H. L.; Quirk, R. P., *Anionic Polymerization: Principles and Practical Applications* . Marcel Dekker: New York, 1996.

12. Morton, M., *Anionic Polymerization: Principles and Practice.* . Academic Press: New York, 1983.

13. Szwarc, M.; Levy, M.; Milkovich, R. *Journal of the American Chemical Society* **1956,** 78, (11), 2656-2657.

14. Szwarc, M. *Nature* **1956,** 178, (4543), 1168-1169.

15. Hadjichristidis, N.; Iatrou, H.; Pitsikalis, M.; Mays, J. *Progress in Polymer Science* **2006,** 31, (12), 1068-1132.

16. Hadjichristidis, N.; Pitsikalis, M.; Iatrou, H., Synthesis of Block Copolymers. In *Block Copolymers I*, Abetz, V., Ed. Springer Berlin Heidelberg: 2005; Vol. 189, pp 1-124.

17. Hadjichristidis, N.; Pispas, S.; Floudas, G., *Block Copolymers: Synthetic Strategies, Physical Properties, and Applications* . John Wiley & Sons, Hoboken : New Jersey, 2003.

18. Pitsikalis, M.; Pispas, S.; Mays, J.; Hadjichristidis, N., Nonlinear Block Copolymer Architectures. In *Blockcopolymers - Polyelectrolytes - Biodegradation*, Bellon-Maurel, V.; Calmon-Decriaud, A.; Chandrasekhar, V.; Hadjichristidis, N.; Mays, J. W.; Pispas, S.; Pitsikalis, M.; Silvestre, F., Eds. Springer Berlin Heidelberg: 1998; Vol. 135, pp 1-137.

19. Roovers, J. E. L.; Bywater, S. *Macromolecules* **1975,** 8, (3), 251-254.

20. Morton, M.; Fetters, L. J. *Rubber Chemistry and Technology* **1975,** 48, (3), 359-409.

21. Fetters, L. J.; Morton, M. *Macromolecules* **1974,** 7, (5), 552-559.

22. Waack, R.; Rembaum, A.; Coombes, J. D.; Szwarc, M. *Journal of the American Chemical Society* **1957,** 79, (8), 2026-2027.

23. Goto, A.; Fukuda, T. *Progress in Polymer Science* **2004,** 29, (4), 329-385.

24. Greszta, D.; Mardare, D.; Matyjaszewski, K. *Macromolecules* **1994,** 27, (3), 638-644.

25. Litvinenko, G.; Müller, A. H. E. *Macromolecules* **1997,** 30, (5), 1253-1266.

26. *Cationic Polymerizations: Mechanisms, Synthesis, and Applications*. Marcel Dekker: New York, 1996.

27. Mueller, A. H. E.; Zhuang, R.; Yan, D.; Litvinenko, G. *Macromolecules* **1995,** 28, (12), 4326-4333.

28. Matyjaszewski, K. *Journal of Physical Organic Chemistry* **1995,** 8, (4), 197-207.

29. Matyjaszewski, K. *Macromolecules* **2012,** 45, (10), 4015-4039.

30. Grubbs, R. B. *Polymer Reviews* **2011,** 51, (2), 104-137.

31. Moad, G.; Rizzardo, E.; Thang, S. H. *Aust. J. Chem.* **2009,** 62, (11), 1402-1472.

32. Chiefari, J.; Chong, Y. K.; Ercole, F.; Krstina, J.; Jeffery, J.; Le, T. P. T.; Mayadunne, R. T. A.; Meijs, G. F.; Moad, C. L.; Moad, G.; Rizzardo, E.; Thang, S. H. *Macromolecules* **1998,** 31, (16), 5559-5562.

33. Moad, C. L.; Moad, G.; Rizzardo, E.; Thang, S. H. *Macromolecules* **1996,** 29, (24), 7717-7726.

34. Moad, G.; Chiefari, J.; Krstina, J.; Mayadunne, R. T. A.; Postma, A.; Rizzardo, E.; Thang, S. H. *Polymer International* **2000,** 49, (9), 993-1001.

35. Rizzardo, E.; Moad, G.; Thang, S. H., RAFT Polymerization in Bulk Monomer or in (Organic) Solution. In *Handbook of RAFT Polymerization*, Wiley-VCH Verlag GmbH & Co. KGaA: 2008; pp 189-234.

36. Moad, G.; Solomon, D. H., *The Chemistry of Radical Polymerization*. 2nd ed.; Elsevier: Oxford, England, 2006.

37. Moad, G.; Rizzardo, E.; Thang, S. H. *Aust. J. Chem.* **2005,** 58, 379.

38. In *Handbook of RAFT Polymerization*, 1st ed.; Barner-Kowollik, C., Ed. Wiley-VCH Verlag GmbH & Co. KGaA: 2008.

39. Feng, C.; Li, Y.; Yang, D.; Hu, J.; Zhang, X.; Huang, X. *Chemical Society Reviews* **2011,** 40, (3), 1282-1295.

40. Liu, S.; Sen, A. *Macromolecules* **2001,** 34, (5), 1529-1532.

41. Tsoukatos, T.; Pispas, S.; Hadjichristidis, N. *Macromolecules* **2000,** 33, (26), 9504-9511.

42. Stehling, U. M.; Malmström, E. E.; Waymouth, R. M.; Hawker, C. J. *Macromolecules* **1998,** 31, (13), 4396-4398.

43. Beers, K. L.; Gaynor, S. G.; Matyjaszewski, K.; Sheiko, S. S.; Möller, M. *Macromolecules* **1998,** 31, (26), 9413-9415.

44. 1: Glossary of Basic Terms in Polymer Science (1996). In *Compendium of Polymer Terminology and Nomenclature: IUPAC Recommendations 2008*, Jones, R. G.; Kahovec, J.; Stepto, R.; Wilks, E. S.; Hess, M.; Kitayama, T.; Metanomski, W. V., Eds. The Royal Society of Chemistry: 2009; pp 3-21.

45. Jenkins, A. D.; Kratochvil, P.; Stepo, R.; Suter, U. W. *Pure and Applied Chemistry* **1996,** 68, (8), 1591-1595.

46. Hirao, A.; Goseki, R.; Ishizone, T. *Macromolecules* **2014,** 47, (6), 1883-1905.

47. Uhrig, D.; Mays, J. *Polymer Chemistry* **2011,** 2, (1), 69-76.

48. Reichenberg, D. *Journal of the American Chemical Society* **1953,** 75, (3), 589-597.

49. Pitsikalis, M.; Sioula, S.; Pispas, S.; Hadjichristidis, N.; Cook, D. C.; Li, J.; Mays, J. W. *Journal of Polymer Science Part A: Polymer Chemistry* **1999,** 37, (23), 4337-4350.

50. George, M. H.; Majid, M. A.; Barrie, J. A.; Rezaian, I. *Polymer* **1987,** 28, (7), 1217-1220.

51. Selb, J.; Gallot, Y. *Polymer* **1979,** 20, (10), 1273-1280.

52. Selb, J.; Gallot, Y. *Polymer* **1979,** 20, (10), 1259-1267.

53. Candau, F.; Afchar-Taromi, F.; Rempp, P. *Polymer* **1977,** 18, (12), 1253-1257.

54. Itsuno, S.; Uchikoshi, K.; Ito, K. *Journal of the American Chemical Society* **1990,** 112, (22), 8187-8188.

55. Candau, P. F.; Rempp, P. *Die Makromolekulare Chemie* **1969,** 122, (1), 15-29.

56. Altares, T.; Wyman, D. P.; Allen, V. R.; Meyersen, K. *Journal of Polymer Science Part A: General Papers* **1965,** 3, (12), 4131-4151.

57. Rahlwes, D.; Roovers, J. E. L.; Bywater, S. *Macromolecules* **1977,** 10, (3), 604-609.

58. Gauthier, M.; Moeller, M. *Macromolecules* **1991,** 24, (16), 4548-4553.

59. Yu, F.; He, J.; Wang, X.; Gao, G.; Yang, Y. *Journal of Polymer Science Part A: Polymer Chemistry* **2007,** 45, (17), 4013-4025.

60. Fernyhough, C. M.; Young, R. N.; Poche, D.; Degroot, A. W.; Bosscher, F. *Macromolecules* **2001,** 34, (20), 7034-7041.

61. Hadjichristidis, N.; Xenidou, M.; Iatrou, H.; Pitsikalis, M.; Poulos, Y.; Avgeropoulos, A.; Sioula, S.; Paraskeva, S.; Velis, G.; Lohse, D. J.; Schulz, D. N.; Fetters, L. J.; Wright, P. J.; Mendelson, R. A.; García-Franco, C. A.; Sun, T.; Ruff, C. J. *Macromolecules* **2000,** 33, (7), 2424-2436.

62. Cameron, G. G.; Qureshi, M. Y. *Die Makromolekulare Chemie, Rapid Communications* **1981,** 2, (4), 287-291.

63. Xenidou, M.; Hadjichristidis, N. *Macromolecules* **1998,** 31, (17), 5690-5694.

64. Roovers, J.; Toporowski, P.; Martin, J. *Macromolecules* **1989,** 22, (4), 1897-1903.

65. Ruckenstein, E.; Zhang, H. *Macromolecules* **1999,** 32, (19), 6082-6087.

66. Edgecombe, B. D.; Stein, J. A.; Fréchet, J. M. J.; Xu, Z.; Kramer, E. J. *Macromolecules* **1998,** 31, (4), 1292-1304.

67. Janata, M.; Lochmann, L.; Brus, J.; Holler, P.; Tuzar, Z.; Kratochvíl, P.; Schmitt, B.; Radke, W.; Müller, A. H. E. *Macromolecules* **1997,** 30, (24), 7370-7374.

68. Lochmann, L.; Fréchet, J. M. J. *Macromolecules* **1996,** 29, (5), 1767-1771.

69. Al-Jarrah, M. M. F.; Al-Kafaji, J. K. H.; Apikian, R. L. *British Polymer Journal* **1986,** 18, (4), 256-258.

70. Hadjichristidis, N.; Roovers, J. *Journal of Polymer Science: Polymer Physics Edition* **1978,** 16, (5), 851-858.

71. Falk, J. C.; Schlott, R. J.; Hoeg, D. F.; Pendleton, J. F. *Rubber Chemistry and Technology* **1973,** 46, (4), 1044-1054.

72. Falk, J. C.; Schlott, R. J.; Hoeg, D. F. *Journal of Macromolecular Science: Part A - Chemistry* **1973,** 7, (8), 1647-1662.

73. Falk, J. C.; Schlott, R. J. *Journal of Macromolecular Science: Part A - Chemistry* **1973,** 7, (8), 1663-1668.

74. Falk, J. C.; Hoeg, D. F.; Schlott, R. J.; Pendleton, J. F. *Journal of Macromolecular Science: Part A - Chemistry* **1973,** 7, (8), 1669-1676.

75. Jannasch, P.; Wesslén, B. *Journal of Polymer Science Part A: Polymer Chemistry* **1995,** 33, (9), 1465-1474.

76. Zhao, J.; Mountrichas, G.; Zhang, G.; Pispas, S. *Macromolecules* **2009,** 42, (22), 8661-8668.

77. Zhao, J.; Zhang, G.; Pispas, S. *Journal of Polymer Science Part A: Polymer Chemistry* **2010,** 48, (11), 2320-2328.

78. Ederle, Y.; Isel, F.; Grutke, S.; Lutz, P. J. *Macromolecular Symposia* **1998,** 132, (1), 197-206.

79. Rempp, P.; Franta, E., Synthesis and Applications of Macromonomers. In *Recent Advances in Anionic Polymerization*, Hogen-Esch, T.; Smid, J., Eds. Springer Netherlands: 1987; pp 353-361.

80. Mayo, F. R.; Walling, C. *Chemical Reviews* **1950,** 46, (2), 191-287.

81. Vazaios, A.; Hadjichristidis, N. *Journal of Polymer Science Part A: Polymer Chemistry* **2005,** 43, (5), 1038-1048.

82. Pantazis, D.; Chalari, I.; Hadjichristidis, N. *Macromolecules* **2003,** 36, (11), 3783-3785.

83. Norton, R. L.; McCarthy, T. J. *Macromolecules* **1989,** 22, (3), 1022-1025.

84. Nikopoulou, A.; Iatrou, H.; Lohse, D. J.; Hadjichristidis, N. *Journal of Polymer Science Part A: Polymer Chemistry* **2007,** 45, (16), 3513-3523.

85. Driva, P.; Iatrou, H.; Lohse, D. J.; Hadjichristidis, N. *Journal of Polymer Science Part A: Polymer Chemistry* **2005,** 43, (18), 4070-4078.

86. Zamurovic, M.; Christodoulou, S.; Vazaios, A.; Iatrou, E.; Pitsikalis, M.; Hadjichristidis, N. *Macromolecules* **2007,** 40, (16), 5835-5849.

87. Koutalas, G.; Lohse, D. J.; Hadjichristidis, N. *Journal of Polymer Science Part A: Polymer Chemistry* **2005,** 43, (18), 4040-4049.

88. Koutalas, G.; Iatrou, H.; Lohse, D. J.; Hadjichristidis, N. *Macromolecules* **2005,** 38, (12), 4996-5001.

89. Xie, C.; Ju, Z.; Zhang, C.; Yang, Y.; He, J. *Macromolecules* **2013,** 46, (4), 1437-1446.

90. Schüll, C.; Frey, H. *ACS Macro Letters* **2012,** 1, (4), 461-464.

91. Rahman, M. S.; Lee, H.; Chen, X.; Chang, T.; Larson, R.; Mays, J. *ACS Macro Letters* **2012,** 1, (5), 537-540.

92. Velis, G.; Hadjichristidis, N. *Macromolecules* **1999,** 32, (2), 534-536.

93. Avgeropoulos, A.; Hadjichristidis, N. *Journal of Polymer Science Part A: Polymer Chemistry* **1997,** 35, (4), 813-816.

94. Pispas, S.; Hadjichristidis, N.; Mays, J. W. *Macromolecules* **1996,** 29, (23), 7378-7385.

95. Gido, S. P.; Lee, C.; Pochan, D. J.; Pispas, S.; Mays, J. W.; Hadjichristidis, N. *Macromolecules* **1996,** 29, (22), 7022-7028.

96. Iatrou, H.; Avgeropoulos, A.; Hadjichristidis, N. *Macromolecules* **1994,** 27, (21), 6232-6233.

97. Roovers, J.; Toporowski, P. M. *Macromolecules* **1981,** 14, (5), 1174-1178.

98. Mays, J. *Polymer Bulletin* **1990,** 23, (3), 247-250.

99. Uhrig, D.; Mays, J. W. *Macromolecules* **2002,** 35, (19), 7182-7190.

100. Iatrou, H.; Mays, J. W.; Hadjichristidis, N. *Macromolecules* **1998,** 31, (19), 6697-6701.

101. Paraskeva, S.; Hadjichristidis, N. *Journal of Polymer Science Part A: Polymer Chemistry* **2000,** 38, (6), 931-935.

102. Nikopoulou, A.; Iatrou, H.; Lohse, D. J.; Hadjichristidis, N. *Journal of Polymer Science Part A: Polymer Chemistry* **2009,** 47, (10), 2597-2607.

103. Al-Muallem, H. A.; Knauss, D. M. *Journal of Polymer Science Part A: Polymer Chemistry* **2001,** 39, (20), 3547-3555.

104. Hirao, A.; Watanabe, T.; Kurokawa, R. *Macromolecules* **2009,** 42, (12), 3973-3981.

105. Hirao, A.; Uematsu, M.; Kurokawa, R.; Ishizone, T.; Sugiyama, K. *Macromolecules* **2011,** 44, (14), 5638-5649.

106. Hirao, A.; Murao, K.; Abouelmagd, A.; Uematsu, M.; Ito, S.; Goseki, R.; Ishizone, T. *Macromolecules* **2011,** 44, (9), 3302-3311.

107. Hirao, A.; Murano, K.; Kurokawa, R.; Watanabe, T.; Sugiyama, K. *Macromolecules* **2009,** 42, (20), 7820-7827.

108. Bates, F. S.; Fredrickson, G. H. *Physics Today* **1999,** 52, 32-38.

109. Lennon, E. M.; Katsov, K.; Fredrickson, G. H. *Physics Review Letters* **2008,** 101, (13), 138302.

110. Matsen, M. W.; Bates, F. S. *Macromolecules* **1996,** 29, (4), 1091-1098.

111. Khandpur, A. K.; Foerster, S.; Bates, F. S.; Hamley, I. W.; Ryan, A. J.; Bras, W.; Almdal, K.; Mortensen, K. *Macromolecules* **1995,** 28, (26), 8796-8806.

112. Matsen, M. W.; Schick, M. *Physics Review Letters* **1994,** 72, (16), 2660-2663.

113. Bates, F. S. *Science* **1991,** 251, (4996), 898-905.

114. Bates, F. S.; Fredrickson, G. H. *Annual Review of Physical Chemistry* **1990,** 41, (1), 525-557.

115. Fredrickson, G. H.; Helfand, E. *The Journal of Chemical Physics* **1987,** 87, (1), 697-705.

116. Leibler, L. *Macromolecules* **1980,** 13, (6), 1602-1617.

117. Milner, S. T. *Macromolecules* **1994,** 27, (8), 2333-2335.

118. Pochan, D. J.; Gido, S. P.; Pispas, S.; Mays, J. W.; Ryan, A. J.; Fairclough, J. P. A.; Hamley, I. W.; Terrill, N. J. *Macromolecules* **1996,** 29, (15), 5091-5098.

119. Dyer, C.; Driva, P.; Sides, S. W.; Sumpter, B. G.; Mays, J. W.; Chen, J.; Kumar, R.; Goswami, M.; Dadmun, M. D. *Macromolecules* **2013,** 46, (5), 2023-2031.

120. Hadjichristidis, N.; Iatrou, H.; Behal, S. K.; Chludzinski, J. J.; Disko, M. M.; Garner, R. T.; Liang, K. S.; Lohse, D. J.; Milner, S. T. *Macromolecules* **1993,** 26, (21), 5812-5815.

121. Xenidou, M.; Beyer, F. L.; Hadjichristidis, N.; Gido, S. P.; Tan, N. B. *Macromolecules* **1998,** 31, (22), 7659-7667.

122. Lee, C.; Gido, S. P.; Poulos, Y.; Hadjichristidis, N.; Tan, N. B.; Trevino, S. F.; Mays, J. W. *Polymer* **1998,** 39, (19), 4631-4638.

123. Lee, C.; Gido, S. P.; Poulos, Y.; Hadjichristidis, N.; Tan, N. B.; Trevino, S. F.; Mays, J. W. *The Journal of Chemical Physics* **1997,** 107, (16), 6460-6469.

124. Olmsted, P. D.; Milner, S. T. *Macromolecules* **1998,** 31, (12), 4011-4022.

125. Whitmore, M. D.; Vavasour, J. D. *Acta Polymerica* **1995,** 46, (5), 341-360.

126. Vavasour, J. D.; Whitmore, M. D. *Macromolecules* **1993,** 26, (25), 7070-7075.

127. Zhu, Y.; Burgaz, E.; Gido, S. P.; Staudinger, U.; Weidisch, R.; Uhrig, D.; Mays, J. W. *Macromolecules* **2006,** 39, (13), 4428-4436.

128. Beyer, F. L.; Gido, S. P.; Büschl, C.; Iatrou, H.; Uhrig, D.; Mays, J. W.; Chang, M. Y.; Garetz, B. A.; Balsara, N. P.; Tan, N. B.; Hadjichristidis, N. *Macromolecules* **2000,** 33, (6), 2039-2048.

129. Laity, P. R.; Taylor, J. E.; Wong, S. S.; Khunkamchoo, P.; Norris, K.; Cable, M.; Andrews, G. T.; Johnson, A. F.; Cameron, R. E. *Polymer* **2004,** 45, (21), 7273-7291.

130. Puskas, J. E.; Kaszas, G. *Rubber Chem. Technol.* **1996,** 462, 69.

131. Aggarwal, S. L. *Polymer International* **1976,** 17, 938.

132. Puskas, J. E.; Antony, P.; ElFray, M.; Altstadt, V. *Eur. Polym.* **2003,** 39, 2041.

133. Staudinger, U.; Schlegel, R.; Weidisch, R.; Fritzsche, J.; Klüppel, M.; Heinrich, G.; Mays, J. W.; Uhrig, D.; Hadjichristidis, N. *European Polymer Journal* **2008,** 44, (11), 3790-3796.

134. Staudinger, U.; Weidisch, R.; Zhu, Y.; Gido, S. P.; Uhrig, D.; Mays, J. W.; Iatrou, H.; Hadjichristidis, N. *Macromolecular Symposia* **2006,** 233, (1), 42-50.

135. Schlegel, R.; Staudinger, U.; Thunga, M.; Weidisch, R.; Heinrich, G.; Uhrig, D.; Mays, J. W.; Iatrou, H.; Hadjichristidis, N. *European Polymer Journal* **2009,** 45, (10), 2902-2912.

136. Duan, Y.; Thunga, M.; Schlegel, R.; Schneider, K.; Rettler, E.; Weidisch, R.; Siesler, H. W.; Stamm, M.; Mays, J. W.; Hadjichristidis, N. *Macromolecules* **2009,** 42, (12), 4155-4164.

137. Baskaran, B., *Progress in Polymer Science* **2003**, 28, 521-581.

138. Baskaran, B.; Muller, A., Anioinc Vinyl Polymerization. In Matyjaszewski, K. Muller, A. (eds) *Contolled and Living Polymerizations: from Mechanisms to Applications.* Wiley-VCH: Weinheim, Germany. 2009; pp 1-56.

139. Naohiko, U.; Kenichi, H.; Masaji, K.; Tomohiro, O.; Sachie, Y.; Kazushige, I., Preparation Process of Acrylic Acid Ester Polymer. EP0945470 (A1), 29 Aug. 1999.

140. Kenichi, H.; Kazushige, I.; Masaji, K.; Sachie, Y., Anionic Polymerization Process, and Process for Producing a Polymer by the Anionic Polymerization Process. EP1078942 (A1), 28 Feb. 2001.

141. Tabuchi, K.; Kitayama, T.; Hatada, K., *Polymer* **2002**, 43, (25), 7185-7190.

142. Hamada, K.; Morishita, Y.; Kurihara, T.; Ishiura, K., Methacrylate-Based Polymers for Industrial Uses. In Hadjichristidis, N. and Hirao, A. (eds.) *Anionic Polymerization: Principles, Practice, Strength, Consequences and Applications*. Springer: Tokyo, Japan. 2015; pp1011-1031.

143. Tong, J.D.; Jerome, R., *Macromolecules* **2000**, 33, 470-479.

144. Boutillier, J.M., *Nanostrength®: Nanostructured Acrylic Copolymers Technology and Applications* [Powerpoint slides]. 22 Nov. 2012. Presented at Innovation days, Dijon, France. Retrived 9 Nov. 2015 from http://www.innovdays-plasturgie.com/innovdays/Illustrations/Documents/InnovDays/2012/20121122_Nanomateriaux/6_ARKEMA-Nanostrength_nov12.pdf

CHAPTER 2.

THE SYNTHESIS AND CHARACTERIZATION OF ALL-ACRYLIC MULTIGRAFT COPOLYMERS USING THE GRAFTING THROUGH APPROACH

Abstract

The synthesis of poly(*n*-butyl acrylate)-*g*-poly(methyl methacrylate) multigraft copolymers was accomplished *via* the grafting through approach. The two controlled polymerization techniques of anionic, using high vacuum conditions, followed by reversible addition-fragmentation chain transfer polymerization yielded the desired poly(methyl methacrylate) macromonomer and all-acrylic multigraft materials, respectively. Several multigraft samples with different side chain molecular weights, number of branch point junctions, and side chain volume percents were systematically produced. All the materials were carefully characterized using nuclear magnetic resonance spectroscopy and size exclusion chromatography for their structural and compositional determination, with the addition of matrix-assisted laser desorption/ionization time of flight spectrometry for monitoring the side chain polymerization and post polymerization reactions used to obtain the macromonomer.

2.1 Introduction

Graft and other branched architectures often exhibit superior physical and mechanical properties as compared to their linear counterparts, along with providing additional avenues for tailoring materials to achieve improved performance for numerous applications.[1-7] Thus, the control of the tunable macromolecular architecture parameters such as the side chain composition, side chain and backbone molecular weight, volume fraction between components, branch point incorporation and placement, and branch point symmetry have all been shown to influence bulk properties of dynamics, self-assembly, and mechanical strength.[8-11] For these reasons, the investigation into multigraft copolymers that incorporate both plastic and rubbery segments has been of interest for use in thermoplastic elastomer (TPE) and impact modifier applications. As discussed in the previous chapter, TPEs based on linear ABA block copolymers are composed of a low glass transition (T_g) middle segment with high T_g chain-end segments, however, recently TPEs based on multigraft copolymers have been demonstrated where the low T_g segment is the backbone and high T_g segment is the branched side chains.[8, 12] In this class of materials the most recognizable is styrene/diene (SIS or SBS) rubbers where the hard phase is polystyrene and the soft phase either isoprene of butadiene.

TPEs composed of all–acrylic monomers in ABA block copolymers, most commonly using poly(*n*-butyl acrylate) (P*n*BA) as the soft phase and poly(methyl methacrylate) (PMMA) as the hard phase, have been synthesized with their elastomeric

and adhesion properties thoroughly investigated.[13-15] Additionally, graft architectures exhibiting a P*n*BA backbone and PMMA side chains have been produced, but are not nearly as well studied as compared to their SIS and SBS branched counterparts.[16-23] Our interest in obtaining a better understanding of the structure-property relationship of the all-acrylic TPE system was the motivation to construct a novel synthetic method to produce defined branched architectures where various structural and compositional parameters could be altered for optimizing both the synthesis and mechanical properties observed by the desired material.

In this work, we report the synthesis and characterization of poly(*n*-butyl acrylate)-*g*-poly(methyl methacrylate) (P*n*BA-*g*-PMMA) multigraft copolymers *via* the grafting through approach. Initially, the construction, purification, and characterization of the PMMA macromonomer will be discussed, and subsequently followed by the copolymerization of the PMMA macromonomer with n-butyl acrylate to yield the final multigraft materials. Additionally, the structural differences of the all-acrylic multigraft samples produced will be addressed in preparation for the following chapters where the morphology and mechanical properties are discussed.

2.2 Experimental

2.2.1 Materials

Methyl methacrylate (MMA, Sigma-Aldrich, >99%), *n*-butyl acrylate (*n*BA, Sigma-Aldrich, >99%), tetrahydrofuran (THF, Sigma-Aldrich, ≥99%), 1,1-diphenylethylene (DPE, Sigma- Aldrich, >99%), benzene (Sigma-Aldrich, ≥99.9) and 1-(*tert*-butyldimethylsiloxy)-3-butyl lithium (*t*BDMS-Li, FMC Lithium) were all purified according to standards required for anionic polymerization as previously reported.[24, 25] 2,2-Azobisisobutyronitrile (AIBN, Aldrich 90%) was recrystallized before use and the S-1-dodecyl-S'-(α,α'-dimethyl-α''-acetic acid)trithiocarbonate chain transfer agent (CTA) was synthesized following the procedure previously published by Lai et al.[26] The *tert*-butylammonium fluoride (Sigma-Aldrich, 1.0 M in THF) was used as received. Triethylamine (TEA, Sigma-Aldrich, 98%) and acryloyl chloride (Sigma-Aldrich, ≥97%) were distilled over CaH_2, stored over activated molecular sieves, and purged with Argon prior to use.

2.2.2 Synthesis of the Poly(methyl methacrylate) Macromonomer

The anionic polymerization of the PMMA macromonomer was carried out in sealed, all-glass apparatus using well documented high-vacuum polymerization techniques.[24, 27] All the reagents in ampoules, including MMA, lithium chloride, DPE, and *t*BDMS-Li were attached to the reactor and introduced in the appropriate order after

purging the reactor with a lithium-based washing solution. The polymerization was performed in dry THF in a -78 ^{o}C acetone/dry ice bath. The polymerization of PMMA was initiated using a silyl-protected alkyl-lithium in order to yield a chain-end functional group functional site for subsequent post-polymerization reactions.[28-30] Prior to the introduction of MMA, the solution was a deep red color that is indicative of Li active DPE and becoming a pale yellow color with after the initiation of the MMA monomer. The living PMMA was quenched with methanol after 1h and precipitated in a methanol/water (10:3) solution, and vacuum dried overnight at 60 ^{o}C.

The synthetic procedure for producing hydroxyl-terminated PMMA was performed by the simple desilylation reaction of the protecting group with excess tetrabutylammonium fluoride in dry THF for 18h. The reaction took place under argon purge at room temperature. The resulting polymer was purified by removal of THF solvent and re-dissolving into chloroform for removal of salt and excess tetrabutylammonium fluoride by liquid-liquid extraction using chloroform and water. The hydroxyl-terminated PMMA was then re-precipitated using a methanol/water (10:1) mixture and dried in the vacuum-oven overnight.

The final step utilized the nucleophilic addition/elimination reaction between acryloyl chloride and the terminal alcohol present on the PMMA chain in the presence of TEA. The dried polymer from the previous step was re-dissolved using dry THF from the vacuum line and purged with argon atmosphere. Slight excess stoichiometric amounts of TEA and acryloyl chloride were syringed in according to the calculated amount of

hydroxyl-functionalized chain-ends (OH:TEA:acryloyl chloride, 1:1.5:1.5). The reaction was performed at room temperature and allowed to proceed for 18h. Again, the excess TEA and salt produced was removed using a chloroform-water extraction and followed by freeze-drying the polymer using benzene. This three step synthetic methodology produced quantitative yields of well-defined PMMA chains with a terminal polymerizable head group.

2.2.3 Synthesis of All-Acrylic Multigraft Copolymers

The PnBA-*g*-PMMA multigraft copolymers were successfully synthesized by RAFT radical polymerization using a trithiocarbonate chain transfer agent. The PMMA macromonomer, *n*BA, AIBN, and CTA reagents, amounts shown in Table 2.1, were added to a single-neck round-bottom flask, capped with a rubber septum, equipped with a single side-arm with a stopcock and male glass joint and dissolved in 15 -20 mL of benzene. The polymer/solution mixture was placed on the high-vacuum line and subjected to three freeze/thaw cycles. After the last freeze/thaw cycle the mixture was sealed using the stopcock, warmed to room temperature, placed under slight argon positive pressure, and then removed from the vacuum line. The apparatus was then place into a 75 ^{o}C oil bath and stirred vigorously. The reaction time was between 36-48 h and terminated by introducing a 1mL of methanol and rapidly cooling the reaction mixture with an ice bath for 5 minutes.

The purification of the newly synthesized multigraft copolymers was performed by adding THF to the solution to reduce the viscosity of the reaction solution and precipitating drop-wise into excess methanol. This procedure was performed twice; the first solution discarded will be milky in nature and contain partially soluble unreacted macromonomer PMMA chains while the second methanol precipitation yields a transparent discard solution. The pale yellowish, transparent material was then dried in the vacuum oven overnight at 60 ^{o}C before characterization or film casting (discussed in later chapters). The general nomenclature for the synthesized multigraft copolymers, first demonstrated in Table 2.1, is MG-*n*-*m*-*o*: where MG stands for multigraft, *n* represents the PMMA side chain molecular weight, *m* represents the average number of branch points per molecule, and *o* represents the PMMA volume percent.

2.3 Characterization

Number-average molecular weights, M_n, and polydispersity indices, M_w/M_n (PDI), of all samples were determined by size exclusion chromatography using a Polymer Labs GPC-120 unit equipped with a Precision Detector PD2040 (two-angle static light scattering detector), a Precision Detector PD2000DLS (dynamic light scattering detector), Viscotek 220 differential viscometer, and a Polymer Labs differential refractometer. The elution solvent is THF with a flow rate of 1ml/min at 40^{o}C. The column set is Polymer Labs PLgel; 7.5 x 300 mm; 10 µm; 500; 10E3, 10E5, and 10E6 Å. The calibration range was 600 to 7,500,000 Daltons using PMMA standards.

Table 2.1. Synthesis and characteristics of poly(*n*-butyl acrylate)-*g*-poly(methyl methacrylate) multigraft copolymers synthesized using RAFT polymerization

							Multigraft Copolymers	
Sample I.D.[a]	Graft PMMA M_n[b] (kg/mol)	Monomer[c] (mmol)	Macromonomer[d] x 10^2 (mmol)	CTA[c] x 10^2 (mmol)	Initiator[f] x 10^3 (mmol)	$M_{nTheor.}$[d] (kg/mol)	M_n[h] (kg/mol)	PDI[i]
MG 5.3-4.9-14.4	5.3	20.92	6.70	1.50	4.00	179	111	1.59
MG 5.3-2.0-16.7		10.46	4.70	3.50	4.00	38.3	29.5	1.64
MG 5.3-5.4-18.3		13.95	5.28	0.75	2.00	238	95.4	1.52
MG 5.3-9.2-25.7		10.46	7.15	0.75	2.00	179	93.3	1.55
MG 11.7-2.6-16.0	11.7	27.90	3.55	1.60	4.00	223	127	2.04
MG 11.7-5.3-22.2		20.93	4.05	0.75	2.00	358	179	2.38
MG 11.7-3.6-27.7		10.46	3.35	1.50	4.00	89.4	78.2	1.49
MG 11.7-6.1-34.0		13.95	3.97	0.75	2.00	238	93.9	1.78
MG 11.7-3.7-38.1		10.46	4.28	3.50	4.00	38.3	54.1	1.59

[a] Sample identification MG *n-m-o* where *n* is MM-PMMA side chain molecular weight observed by SEC, *m* is calculated average number of branch points using the M_p obtained from SEC and ratio of P*n*BA to PMMA by ^{1}H-NMR, and *o* is the calculated PMMA volume fraction using ^{1}H-NMR. [b] Number average molecular weight of PMMA side chains calculated by SEC. [c] RAFT chain transfer agent. [d] Theoretical calculated number average molecular weight for the P*n*BA backbone according to the ratio of [*n*BA]/[CTA]. [e] Maximum peak molecular weight of MG sample calculated by SEC. [f] Polydispersity indices for MG samples calculated by SEC.

Reported molecular weights were determined by light scattering using calculated dn/dc values PMMA and P*n*BA-*g*-PMMA samples. In addition to molecular weight, the determination of branching and the construction of a Mark-Houwink plot were completed using the available light scattering and viscosity detectors.

^{1}H- and ^{13}C-NMR spectroscopy was performed on a Varian Mercury 500 MHz spectrometer using $CDCl_3$ as a solvent. MALDI-TOF mass spectrometry was obtained on a Bruker Autoflex II model smart-beam instrument equipped with a nitrogen laser (λ=337 nm). The matrix used was trans-2-[3-(4-tert-butylphenyl)-2-methyl-2-propenylidene]malononitrile (DCTB, >99% Fluka) with sodium trifluoroacetate (NaTFA, >99% Fluka) in THF. A 1:20:0.5 ratio of PMMA:DCTB:NaTFA were the conditions used for plating.

2.4 Results and Discussion

2.4.1 Poly(methyl methacrylate) Macromonomer

Poly(methyl methacrylate) macromonomer samples were synthesized by anionic polymerization using high-vacuum and glass-blowing techniques in THF at -78 ^{o}C. The polymerization was initiated using a silyl-protected initiator and yielded the targeted molecular weights of 5.3 kg/mol and 11.7 kg/mol with PDIs of 1.07 and 1.04 respectively. Scheme 2.1 shows the polymerization methodology, as well as, the post-polymerization reactions of deprotection the initiating chain-end to produce hydroxyl-terminated PMMA and the final step of attaching the polymerizable head group by the

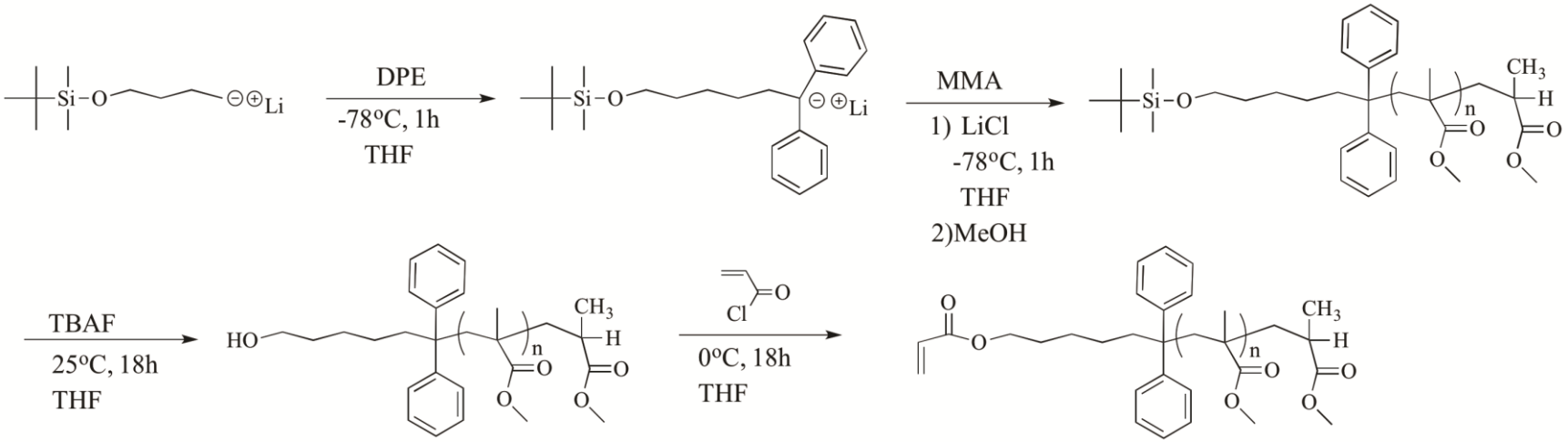

Scheme 2.1. The anionic polymerization of MMA and the post polymerization synthetic procedure to yield the desired PMMA macromonomer.

reaction with acryloyl chloride and the terminal alcohol. The PMMA samples were purified and treated between each step as described previously in this chapter.

The PMMA macromonomer and PMMA precursors were initially characterized by ^{1}H-NMR to confirm the manipulation of the polymer chain-end and quantify the conversion of each post polymerization step, depicted in Figure 2.1. The first step was confirming the successful synthesis of PMMA with the intact *t*-butyldimethylsiloxy protecting group at the chain-end. The black-line spectra in Figure 2.1 shows the characteristic signals at 3.53 ppm, 1.80 ppm, and 0.80 -1.00 ppm which corresponds to the methoxy protons, methyl protons, and vinyl backbone protons of the methyl methacrylate repeat unit. Most importantly the six proton signals of the Si-Me_2 silyl-protecting group is present at 0.0 ppm.

The first post-polymerization reaction was to produce a terminal hydroxyl-functionality at the chain-end by cleaving the silyl-protecting group using TBAF. The blue-line spectra in Figure 2.1 shows that the conversion to the desired HO-PMMA was quantitative and did not interrupt any part of the polymer chain because only the disappearance of the Si-Me_2 peak at 0.0 ppm and the *t*-butyl-Si peak at 0.75ppm was observed. The final synthetic step for completion of the PMMA macromonomer involved attaching a vinyl double bond at the chain-end that could be used to polymerize through in the next step. The red-line spectra in Figure 2.1 shows the presence of the three proton signals between 5.8 and 6.2 ppm and the integration of the peaks indicated >95% conversion for the reaction with acryloyl chloride. The CH_2=CH signals depicted

in the zoomed-in region and labeled according to the scheme shown in the figure.

Further confirmation of the α-terminal vinyl group of the macromonomer and the precursor materials was obtained using MALDI-TOF MS. Due to the inherent shortcomings associated with mass analysis of macromolecules a third PMMA macromonomer sample was prepared targeting lower molecular weight solely for obtaining a well-resolved mass spectrum. Figure 2.2 shows the MALDI spectrum of the PMMA macromonomer sample with the enlarged potion to show the monoisotopic peak value of 2,219.74 m/z. The corresponding 19-mer [307.17($C_{21}H_{23}O_2$) + 19 × 101.12($C_5H_9O_2$) + 22.98(Na^+) – 31.02(OCH_3)] peak has a calculated monoisotopic mass of 2,220.41 g/mol. The calculated mass includes the macromonomer-DPE head group, the methyl methacrylate monomer repeat units, the Na^+ proton source used to promote ionization, and the loss of 31.02 g/mol, which corresponds to the cyclization and extraction of the pendent methoxy-group located on the terminal monomer unit, previously reported in the MALDI-TOF analysis of PMMA.[31] Additionally, the MALDI-TOF spectra of the silyl-protected, hydroxyl-terminated, and final PMMA macromonomer can be viewed in Figure 2.3. The peaks are labeled to the calculated number of repeat units to show the 115.08 g/mol mass loss from cleaving of the *t*Bu-Si(Me_2) group (*t*BDMS-PMMA, bottom spectrum) to yield hydroxyl-terminated PMMA (HO-PMMA, middle spectrum). The PMMA macromonomer mass spectra (MM-PMMA, top spectrum) shows the addition of 55.59 g/mol corresponding to the addition of the acrylic terminal group.

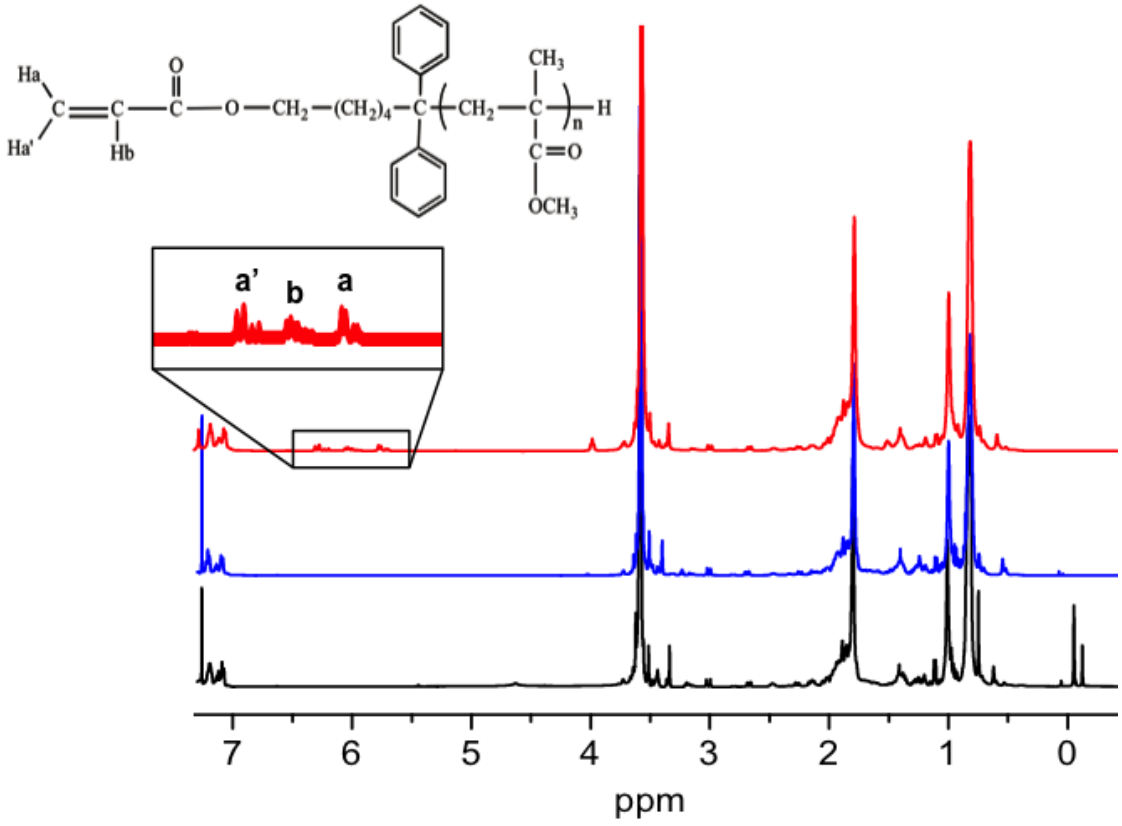

Figure 2.1. 1H-NMR spectra of the silyl protected PMMA (black), the hydroxyl-terminated PMMA (blue), and the desired PMMA macromonomer (red). The enlarged section indicates the appearance of the α-terminal vinyl group proton signals depicted in the scheme.

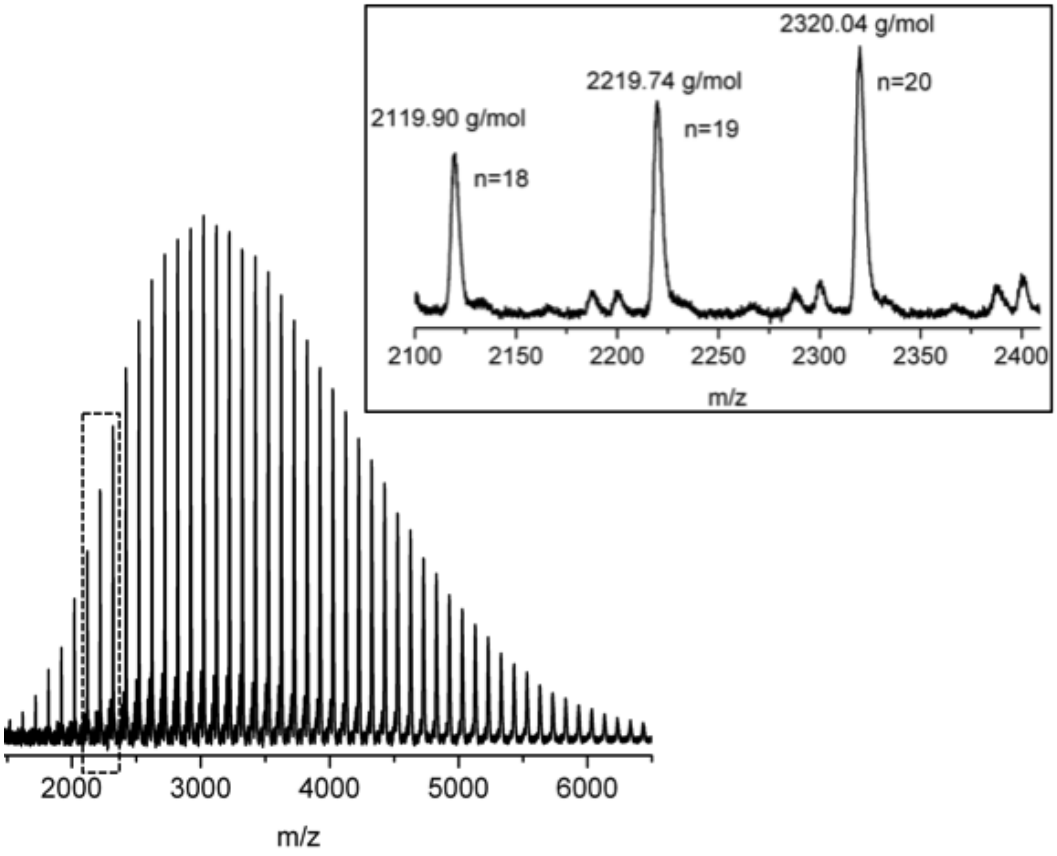

Figure 2.2. MALDI-TOF mass spectra of the PMMA macromonomer

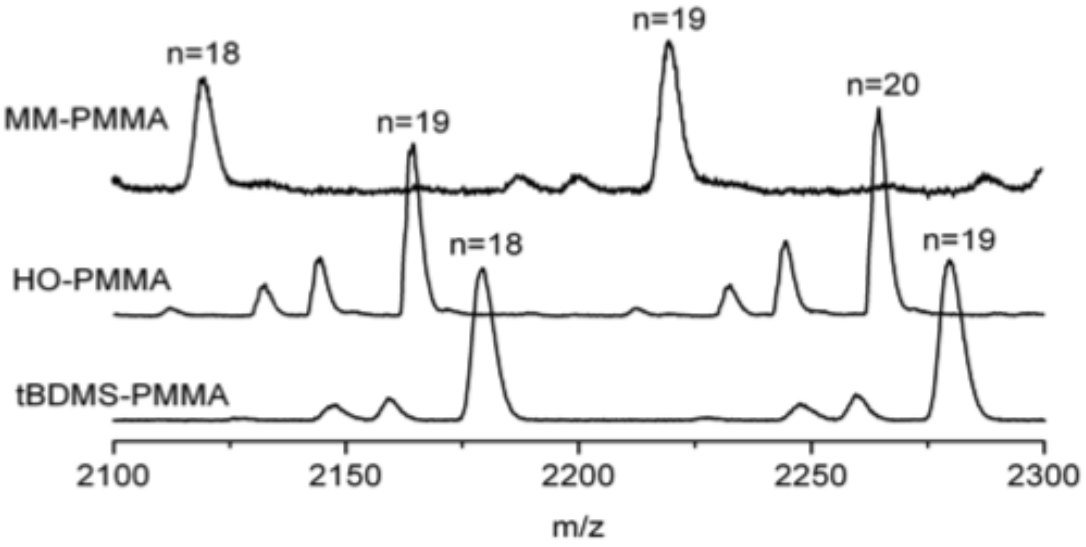

Figure 2.3. MALDI-TOF mass spectra overlay of the silyl protected PMMA (bottom), the hydroxyl-terminated PMMA (middle), and the desired PMMA macromonomer (top).

2.4.2 All-Acrylic Multigraft Copolymers

The synthesis of the all-acrylic multigraft copolymers were carried out by RAFT polymerization of nBA and a synthesized PMMA macromonomer *via* the grafting through approach (Scheme 2.2), the details of the synthetic method were previously described in an earlier section. The molecular weight and polydispersity indices of the graft copolymers were obtained by SEC equipped with light scattering, viscometry, and RI detectors and can be viewed in Table 2.2.

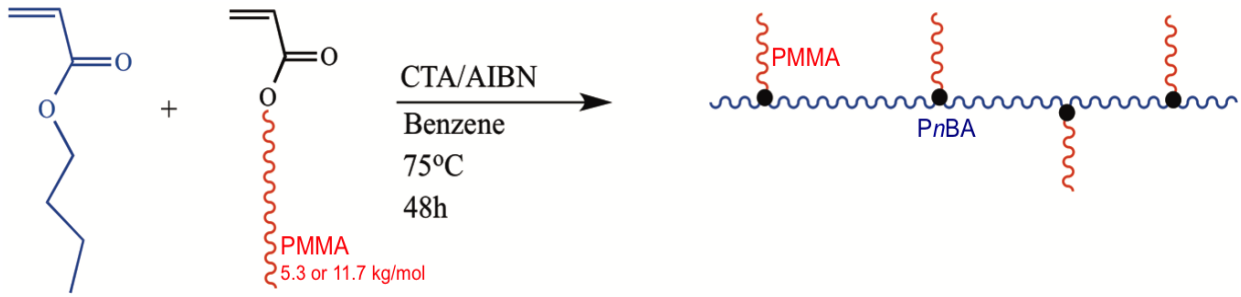

Scheme 2.2. The general synthetic procedure for poly(*n*-butyl acrylate)-*g*-poly(methyl methacrylate) multigraft copolymers by the grafting through approach using RAFT polymerization.

Additionally, the SEC curve in Figure 2.4 shows the purified multigraft copolymer and the PMMA macromonomer peak to demonstrate that there is no residual unreacted PMMA macromonomer present in the sample. The graft copolymer peaks show a unimodal distribution with PDIs between 1.5 and 2.4 for all of the samples. The broad

Table 2.2. Synthesis and characteristics of poly(*n*-butyl acrylate)-*g*-poly(methyl methacrylate) multigraft copolymers

		Multigraft Copolymer				
Sample I.D.[a]	Graft Chain M_n[b] (kg/mol)	M_n[c] (kg/mol)	M_p[d] (kg/mol)	PDI[e]	#[f]	Volume Percent[g] (%)
MG 5.3-4.9-14.4	5.3	111	168	1.59	4.9	14.4
MG 5.3-2.0-16.7		29.5	58.1	1.64	2.0	16.7
MG 5.3-5.4-18.3		95.4	139	1.52	5.4	18.3
MG 5.3-9.2-25.7		93.3	153	1.55	9.2	25.7
MG 11.7-2.6-16.0	11.7	127	175	2.04	2.6	16.0
MG 11.7-5.3-22.2		171	237	2.38	5.3	22.2
MG 11.7-3.6-27.7		78.2	119	1.49	3.6	27.7
MG 11.7-6.1-34.0		93.9	151	1.78	6.1	34.0
MG 11.7-3.7-38.1		54.1	76.4	1.59	3.7	38.1

[a] Sample identification MG *n-m-o* where *n* is MM-PMMA side chain molecular weight observed by SEC, *m* is calculated average number of branch points using the M_p obtained from SEC and ratio of P*n*BA to PMMA by ^{1}H-NMR, and *o* is the calculated PMMA volume fraction using ^{1}H-NMR. [b] Number average molecular weight of PMMA side chains calculated by SEC. [c] Number average molecular weight of MG sample calculated by SEC. [d] Maximum peak molecular weight of MG sample calculated by SEC. [e] Polydispersity indices for MG sample calculated by SEC. [f] Average number of branch points per MG chain calculated using ^{1}H-NMR and the M_p calculated by SEC. [g] Average PMMA volume percent per MG chain calculated using ^{1}H-NMR.

PDIs are a result of both the RAFT polymerization technique, which often yields polymers with PDIs between 1.2 and 1.5 for linear homopolymers, and an inherent consequence of the macromonomer approach to produce branched materials, where the addition of one branch junction produces a significant change in the overall molecular weight. This also explained why the PDIs for the MG samples composed of the longer, 11.7 kg/mol, PMMA side chains are generally broader than the samples with the lower molecular weight side chains.

The compositions of the graft copolymers were measured by ^{1}H-NMR, MG 11.7-6.1-34.0 represented by the blue spectra in Figure 2.5. The spectrum allows for the integration of the PMMA macromonomer methoxy proton signal (3.5 ppm) with the β-CH_2- proton signal of the P*n*BA butyl-pendent group (3.8 ppm) allowing for the calculation of the average number of branch points and the volume fraction of each acrylic monomer. Furthermore, the disappearance of any -CH_2- vinyl signals (5.8-6.2 ppm) confirms that the sample is free of both unreacted *n*BA monomer and PMMA macromonomer.

To confirm the presence of branching and the validity of the average number of branches calculated by NMR, viscometry was used with the triple detection system equipped on the GPC. Viscometry is often employed for determining the extent of branching in a polymer sample by exploiting the difference in size, or density, between linear and branched polymers. More specifically, because branching within a polymer chain allows for regions of higher density both the radius of gyration (R_g) and the

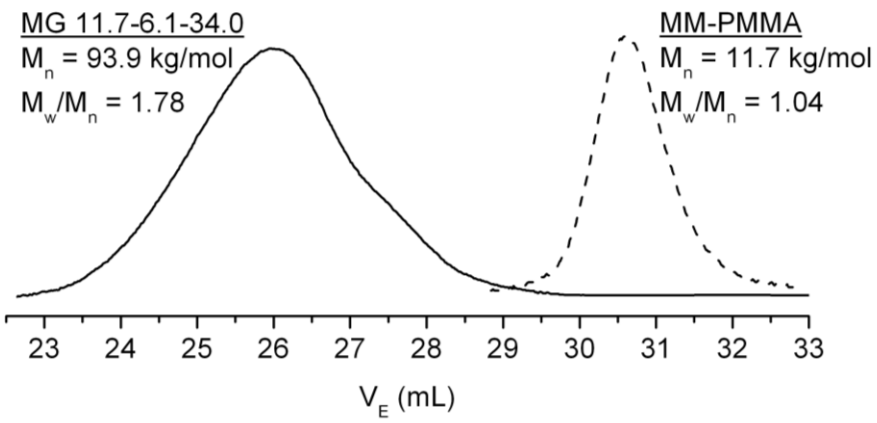

Figure 2.4. SEC elugram of a poly(*n*-butyl acrylate)-*g*-poly(methyl methacrylate) multigraft copolymers (solid line) and the PMMA macromonomer used in the polymerization (dashed line)

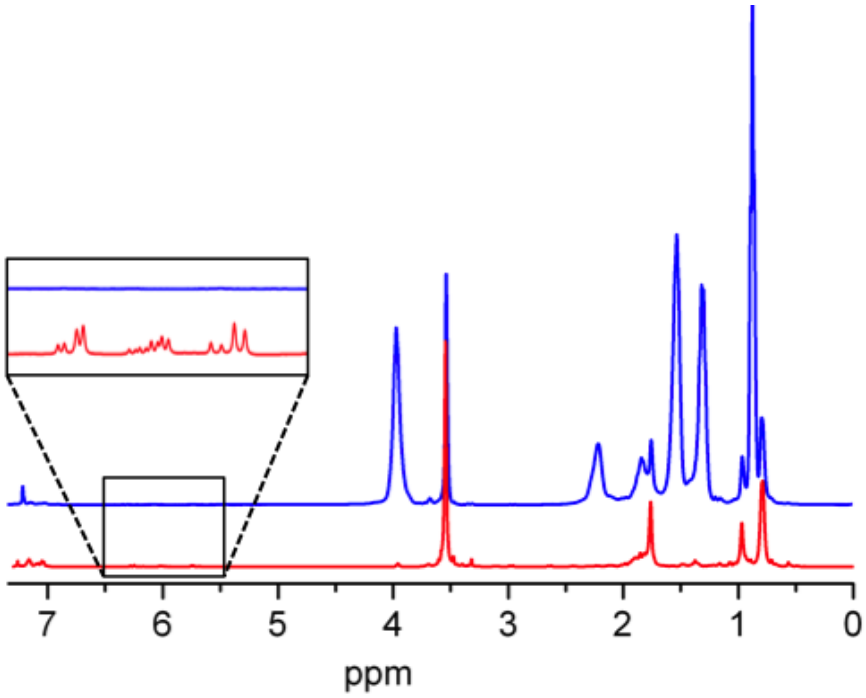

Figure 2.5. ^{1}H-NMR spectra of the 11.7 kg/mol PMMA macromonomer (red) and MG 11.7-6.1-34.0 (blue) after purification.

intrinsic viscosity ([η]) will be reduced at any given molecular weight. In Figure 2.6 the intrinsic viscosity and radius of gyration are plotted against the molecular weight where the reduction in both molecular size and viscosity can be easily observed over the entire molecular weight range. Additionally, the log-log plot of viscosity and weight-average molecular weight, also termed the Mark-Houwink plot, again demonstrates the lower observed intrinsic viscosity decrease with the increase in branch point junctions and shows very little dependence on the difference in molecular weight of the PMMA side chains (Figure 2.7). It is important to note that we were unable to directly calculate the degree of branching from the Mark-Houwink plot because the linear precursor does not contain a PMMA block with the same vol.% as each of the multigraft samples, but qualitatively it does support the branching number calculated by NMR.

2.5 Conclusion

All-acrylic multigraft copolymers composed of P*n*BA backbone as the rubbery phase and PMMA side chains as the plastic phase were synthesized using the grafting through approach. The PMMA macromonomer was produced using anionic polymerization and because of the nature of the living chain end of PMMA a protected initiator was employed to ensure complete chain-end functionalization, followed by two post polymerization reactions that showed nearly quantitative conversion. RAFT controlled radical polymerization was employed and optimized to produce the final branched structure with various copolymer compositions and side chain lengths. The

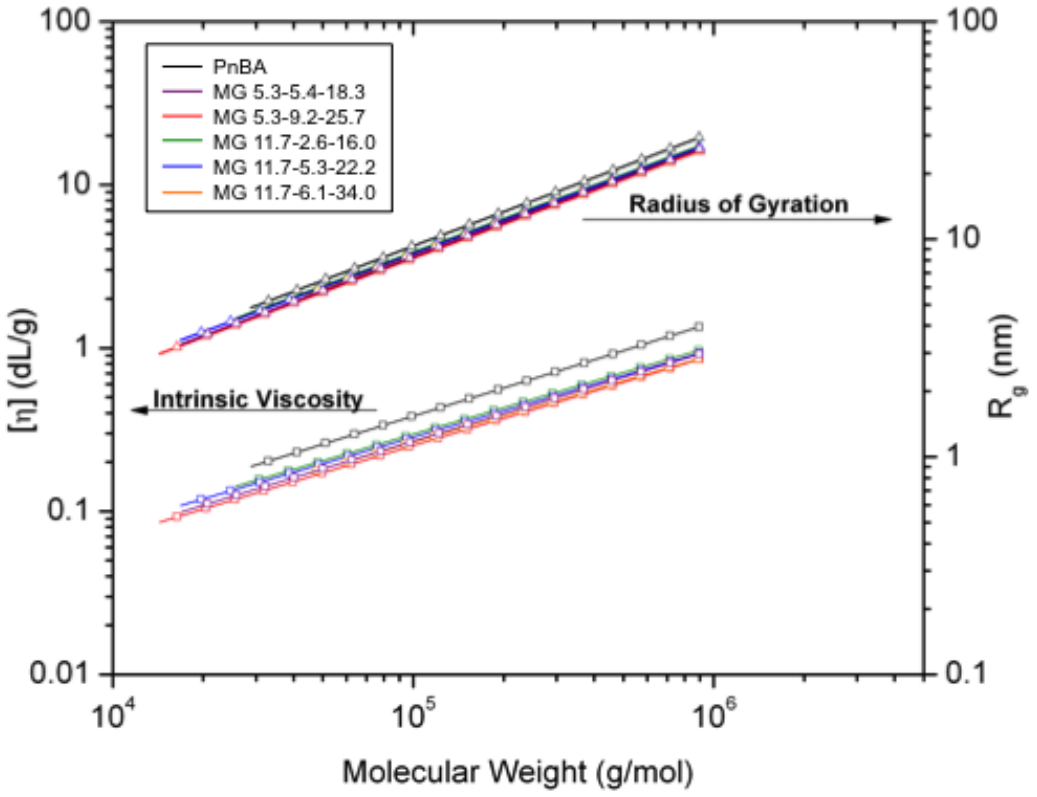

Figure 2.6. Intrinsic viscosity and R_g versus molecular weight for various multigraft samples to showing the lower viscosity and chain dimensions for the branched architectures compared to linear PnBA over the same molecular weight range.

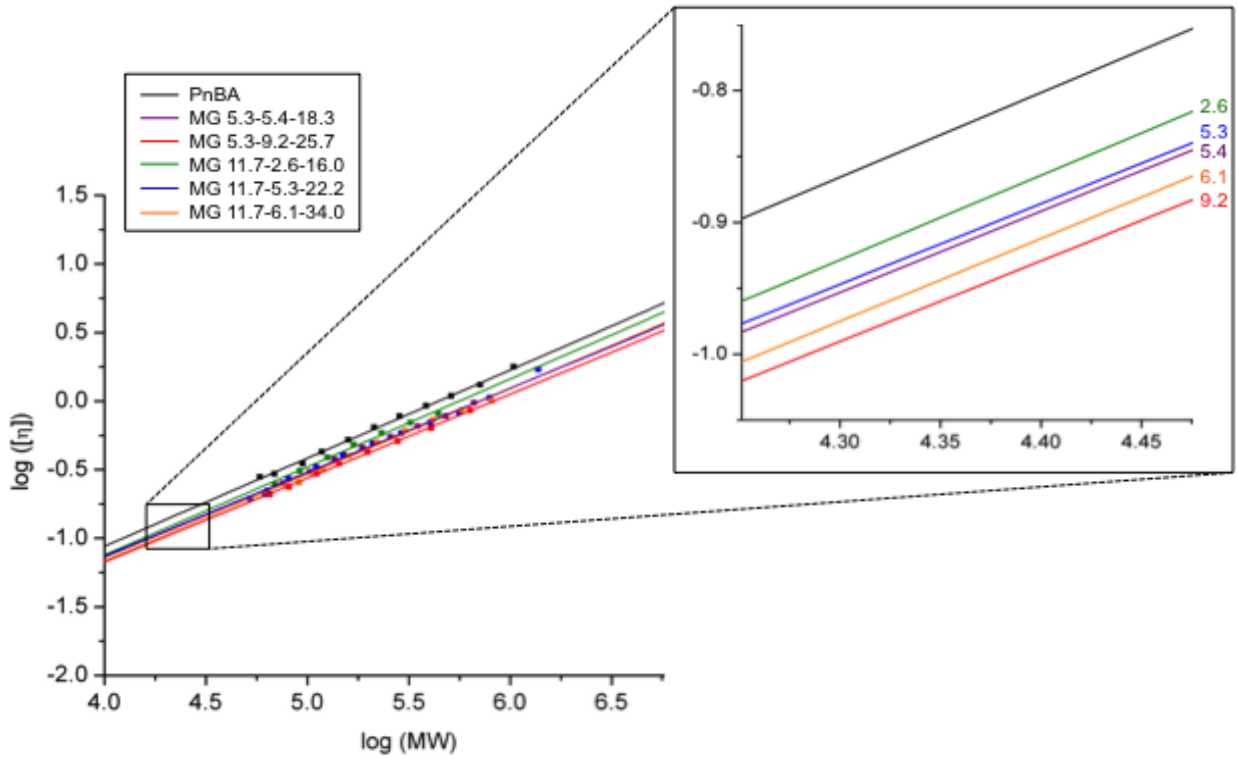

Figure 2.7. Mark-Houwink plot of log intrinsic viscosity versus log molecular weight of various multigraft samples. All branched materials exhibit a lower intrinsic viscosity than the linear PnBA standard, as well as, decrease according to the average number of branch points per polymer chain calculated by SEC and ^{1}H-NMR. Additionally, the enlarged selection displays the average number of branches per molecule in the in the same color of its respected line to show the decrease in the intrinsic viscosity with an increase in the number of branches.

use of anionic and controlled radical polymerization procedures allowed for molecular weights >100 kg/mol to be achieved with considerable control over branch point incorporation and the volume fraction of each segment. All materials were characterized using NMR and SEC to calculate molecular weight values, volume fraction of each component, and the average number of branch point junctions per chain; additionally MALDI-TOF was used for end group determination of the PMMA macromonomer.

References

1. Wang, W.; Wang, W.; Li, H.; Lu, X.; Chen, J.; Kang, N.-G.; Zhang, Q.; Mays, J. *Industrial & Engineering Chemistry Research* **2015,** 54, (4), 1292-1300.

2. Liu, B.; Quirk, R. P.; Wesdemiotis, C.; Yol, A. M.; Foster, M. D. *Macromolecules* **2012,** 45, (23), 9233-9242.

3. Hadjichristidis, N.; Iatrou, H.; Pitsikalis, M.; Mays, J. *Progress in Polymer Science* **2006,** 31, (12), 1068-1132.

4. Matsuo, A.; Watanabe, T.; Hirao, A. *Macromolecules* **2004,** 37, (17), 6283-6290.

5. Mays, J. W., Recent Developments in Anionic Synthesis of Model Graft Copolymers. In *Ionic Polymerizations and Related Processes*, Puskas, J.; Michel, A.; Barghi, S., Eds. Springer Netherlands: 1999; Vol. 359, pp 269-281.

6. Tsukahara, Y.; Mizuno, K.; Segawa, A.; Yamashita, Y. *Macromolecules* **1989,** 22, (4), 1546-1552.

7. Rahlwes, D.; Roovers, J. E. L.; Bywater, S. *Macromolecules* **1977,** 10, (3), 604-609.

8. Uhrig, D.; Mays, J. *Polymer Chemistry* **2011,** 2, (1), 69-76.

9. Mijović, J.; Sun, M.; Pejanović, S.; Mays, J. W. *Macromolecules* **2003,** 36, (20), 7640-7651.

10. Lee, C.; Gido, S. P.; Poulos, Y.; Hadjichristidis, N.; Tan, N. B.; Trevino, S. F.; Mays, J. W. *The Journal of Chemical Physics* **1997,** 107, (16), 6460-6469.

11. Hadjichristidis, N.; Iatrou, H.; Behal, S. K.; Chludzinski, J. J.; Disko, M. M.; Garner, R. T.; Liang, K. S.; Lohse, D. J.; Milner, S. T. *Macromolecules* **1993,** 26, (21), 5812-5815.

12. Hirao, A.; Goseki, R.; Ishizone, T. *Macromolecules* **2014,** 47, (6), 1883-1905.

13. Tong, J.-D.; Jerôme, R. *Macromolecules* **2000,** 33, (5), 1479-1481.

14. Matyjaszewski, K.; Shipp, D. A.; McMurtry, G. P.; Gaynor, S. G.; Pakula, T. *Journal of Polymer Science Part A: Polymer Chemistry* **2000,** 38, (11), 2023-2031.

15. Leclère, P.; Moineau, G.; Minet, M.; Dubois, P.; Jérôme, R.; Brédas, J. L.; Lazzaroni, R. *Langmuir* **1999,** 15, (11), 3915-3919.

16. Li, H.; Wang, W.; Li, C.; Tan, J.; Yin, D.; Zhang, H.; Zhang, B.; Yin, C.; Zhang, Q. *Journal of Colloid and Interface Science* **2015,** 453, 226-236.

17. Wyman, I. W.; Liu, G. *Polymer* **2013,** 54, (8), 1950-1978.

18. Jang, Y.; Hirai, T. *Soft Matter* **2011,** 7, (22), 10818-10823.

19. Kavitha, A. A.; Singha, N. K. *Macromolecules* **2010,** 43, (7), 3193-3205.

20. Tong, J. D.; Leclère, P.; Doneux, C.; Brédas, J. L.; Lazzaroni, R.; Jérôme, R. *Polymer* **2001,** 42, (8), 3503-3514.

21. Tong, J. D.; Leclère, P.; Rasmont, A.; Brédas, J. L.; Lazzaroni, R.; Jérôme, R. *Macromolecular Chemistry and Physics* **2000,** 201, (12), 1250-1258.

22. Tong, J. D.; Jerôme, R. *Polymer* **2000,** 41, (7), 2499-2510.

23. Radke, W.; Roos, S.; Stein, H. M.; Müller, A. H. E. *Macromolecular Symposia* **1996,** 101, (1), 19-27.

24. Uhrig, D.; Mays, J. W. *Journal of Polymer Science Part A: Polymer Chemistry* **2005,** 43, (24), 6179-6222.

25. Hadjichristidis, N.; Iatrou, H.; Pispas, S.; Pitsikalis, M. *Journal of Polymer Science Part A: Polymer Chemistry* **2000,** 38, (18), 3211-3234.

26. Lai, J. T.; Filla, D.; Shea, R. *Macromolecules* **2002,** 35, (18), 6754-6756.

27. Hadjichristidis, N.; Xenidou, M.; Iatrou, H.; Pitsikalis, M.; Poulos, Y.; Avgeropoulos, A.; Sioula, S.; Paraskeva, S.; Velis, G.; Lohse, D. J.; Schulz, D. N.; Fetters, L. J.; Wright, P. J.; Mendelson, R. A.; García-Franco, C. A.; Sun, T.; Ruff, C. J. *Macromolecules* **2000,** 33, (7), 2424-2436.

28. Dhara, M. G.; Sivaram, S. *Journal of Macromolecular Science, Part A* **2009,** 46, (10), 983-988.

29. Dhara, M.; Sivaram, S.; Baskaran, D. *Polymer Bulletin* **2009,** 63, (2), 185-196.

30. Dhara, M. G.; Baskaran, D.; Sivaram, S. *Journal of Polymer Science Part A: Polymer Chemistry* **2008,** 46, (6), 2132-2144.

31. Singha, N. K.; Rimmer, S.; Klumperman, B. *European Polymer Journal* **2004,** 40, (1), 159-163.

CHAPTER 3.

THERMAL AND MECHANICAL PROPERTIES OF ALL-ACRYLIC MULTIGRAFT COPOLYMERS WITH DIFFERENT GRAFT CHAIN MOLECULAR WEIGHT AND VOLUME FRACTION

Abstract

Multigraft copolymers composed of rubbery poly(*n*-butyl acrylate) backbones and randomly spaced glassy poly(methyl methacrylate) side chains were synthesized using a grafting through approach to produce materials that exhibit thermoplastic elastomeric properties. The multigraft materials were initially characterized by differential scanning calorimetry and thermal gravimetric analysis to gain insight into the thermal stability and molecular motion of the low and high T_g segments. The mechanical properties were investigated using a combination of dynamic mechanical analysis, rheology, and tensile testing to examine the viability for these materials to be used as next generation TPEs and to understand the role of side chain molecular weight, the number of branch points and volume fraction of the glassy segment on the physical properties displayed by the bulk material. This study sheds light on the mechanical behavior and reveals important new considerations for optimizing all-acrylic branched systems for use as TPEs.

3.1 Introduction

All-acrylic monomers in linear ABA triblock compositions, using P*n*BA as the rubbery matrix and PMMA as the glassy domains, have been extensively studied by numerous groups and are currently manufactured for commercial use as TPEs and adhesives by companies such as Arkema®. Typical MAM linear triblock TPEs display rupture elongations ranging from 200% to 600% strain with ultimate tensile stress values reported as low as 0.03 MPa to about 1.0 MPa.[1-3] The mechanical performance of these all-acrylic materials was found to be directly related to the extent of phase separation between the two polymer segments and the average molecular weight between chain entanglement of the rubbery phase, both of which are less suitable for dissipating deformation stress when compared to SIS and SBS triblock copolymers.[4-7] Analogous to the styrene-diene based systems, it was found that tailoring the volume fraction of the glassy phase to ~20 vol.% resulted in the best TPE characteristics, with the stiffness of the material being directly related to the PMMA content and increasing with an increase in the PMMA vol.%.[4, 6, 8, 9]

Branched materials, such as 3-arm P*n*BA-PMMA stars and regular-comb multigraft copolymers using PnBA and PMMA, have also been synthesized and studied in order to design materials with novel architectures and topologies to address elastomeric and stiffness issues associated with all-acrylic TPEs. [3, 10-13] The introduction of branching allowed further tailoring of the mechanical behavior of these materials while still allowing for phase separation between the hard and soft domains. These all-

acrylic branched architectures were reported to exhibited similar elongations at break as their linear counterparts, but ultimate tensile stresses were increased to >1.0 MPa and was again shown to be directly related to the amount PMMA content present in the sample.[3, 12]

In this chapter, we investigate the mechanical behavior of the P*n*BA-*g*-PMMA multigraft copolymers synthesized in Chapter 2 with particular interest in the PMMA side chain length and the number of branch point junctions on the observed physical properties. This work provided the basis for our understanding of how the all-acrylic multigraft system differs from the more well-studied styrene-diene system and allows for understanding of their structure-property relationships. Our branched materials highlighted in this chapter are comparable or superior to their linear TPE counterparts currently available on the commercial market. Additionally, the greater ability to tune structure and composition in branched materials allows us to produce materials that exhibit elastomeric behavior over a broad range of stiffness values.

3.2 Experimental

3.2.1 Synthesis of P*n*BA-*g*-PMMA multigraft copolymers

All experimental details for preparation of these materials are presented in Chapter 2. Additionally, Table 2.2 in the previous chapter contains structural and compositional details of the materials used in this chapter.

3.2.2 Mechanical properties: sample preparation

For characterization of the thermal properties, the multigraft copolymer samples were used directly as obtained after precipitating using methanol and drying under vacuum for 24h.

Film preparation for the characterization by dynamic mechanical analysis, tensile testing, and rheology were all performed using the same procedure. The precipitated and dried multigraft copolymer samples were dissolved in toluene overnight to form polymer solutions of ~2 w/v% in a sealed vial. The next day the solution was transferred into PTFE beakers and the toluene was slowly evaporated over five days. The PTFE beakers containing the polymer films were then placed into a clean, vacant, vacuum oven and dried for an additional week at room temperature and at 60^{o}C for five and two days, respectively. Using liquid nitrogen the films were retrieved from the beakers and cut to the desired dimensions prior to use.

3.3 Characterization

The T_g of each multigraft copolymer, precursor macromonomer, and linear P*n*BA analog was determined using a TA Instruments Q-1000 differential scanning calorimetry (DSC) over a temperature range of -80 ^{o}C to 150 ^{o}C, at a heating rate of 10 ^{o}C/min, with 2 minute isothermal holds at the minimum and maximum temperatures. The reported T_g was measured on the second of three scan cycles.

The thermal stability and decomposition thermogram were obtained for each multigraft copolymer, precursor macromonomer, and linear P*n*BA analog on a TA Instruments Q-50 TGA. A 10-20 mg sample was placed in a platinum pan and equilibrated at 30 ^{o}C. The temperature ramp rate was set to 10 ^{o}C/min over the range of 30-600 ^{o}C under nitrogen atmosphere.

The mechanical properties were examined using a TA Instruments Q-800 dynamic mechanical analyzer equipped with a single cantilever clamp. The controlled force experiments were run at 25 ^{o}C to observe the stress/strain curve and the temperature ramp/frequency sweep experiments were run at 0.5 Hz over temperature range of -80 ^{o}C to 150 ^{o}C. Additionally, tensile testing was performed on a Zwick Z010 mechanical tester at a deformation rate of 27 mm/min with an initial gauge length of 12 mm and sample type ISO 527-2/5B. The results for each sample is reported as the average of three runs.

The linear viscoelastic properties of the multigraft samples were evaluated using small amplitude oscillatory shear measurements on a Hybrid Rheometer 2 from TA Instruments. Polymer samples were analyzed using 3 mm and 20 mm parallel plates at low and high temperatures, respectively. The temperature was controlled by an Environmental Test Chamber with a nitrogen gas source.

3.4 Results and Discussion

3.4.1 Thermal Properties

Prior to investigating the mechanical properties of the synthesized multigraft copolymers, the materials were characterized using DSC and TGA in order to observe the T_g of the corresponding rubbery and plastic phases and determine their thermal stability. The results from TGA and DSC also provided preliminary results for the presence of phase separation within the materials and qualitatively confirmed the PMMA content, but more importantly these tests revealed what thermal conditions should be used for film casting and annealing. Initially, DSC of the PMMA macromonomer and a linear P*n*BA prepared by RAFT with a similar molecular weight and PDI to the backbones of the graft samples (M_n = 160 kg/mol and PDI = 1.48) were measured and each displayed a single, sharp T_g with a midpoint of -50 ^oC and 105 ^oC respectively. The DSC thermographs of the multigraft materials displayed a similar T_g for the rubbery P*n*BA component at -45 ^oC, however, the Tg corresponding to the glassy PMMA phase of the copolymers was masked in the majority of the samples. The high T_g curve is observed in samples MG 11.7-3.7-38.1 and MG 11.7-6.1-34.0 because of their higher, >30 vol.%, PMMA content. Figure 3.1 shows the DSC thermograph of sample MG 11.7-3.7-38.1 where the glass transition temperature of the PMMA side chains is observed, additionally, the zoomed potion of the figure shows the first derivative of heat flow versus temperature where the change in slope can be viewed more easily and matched nicely with that of the PMMA macromonomer precursor. This

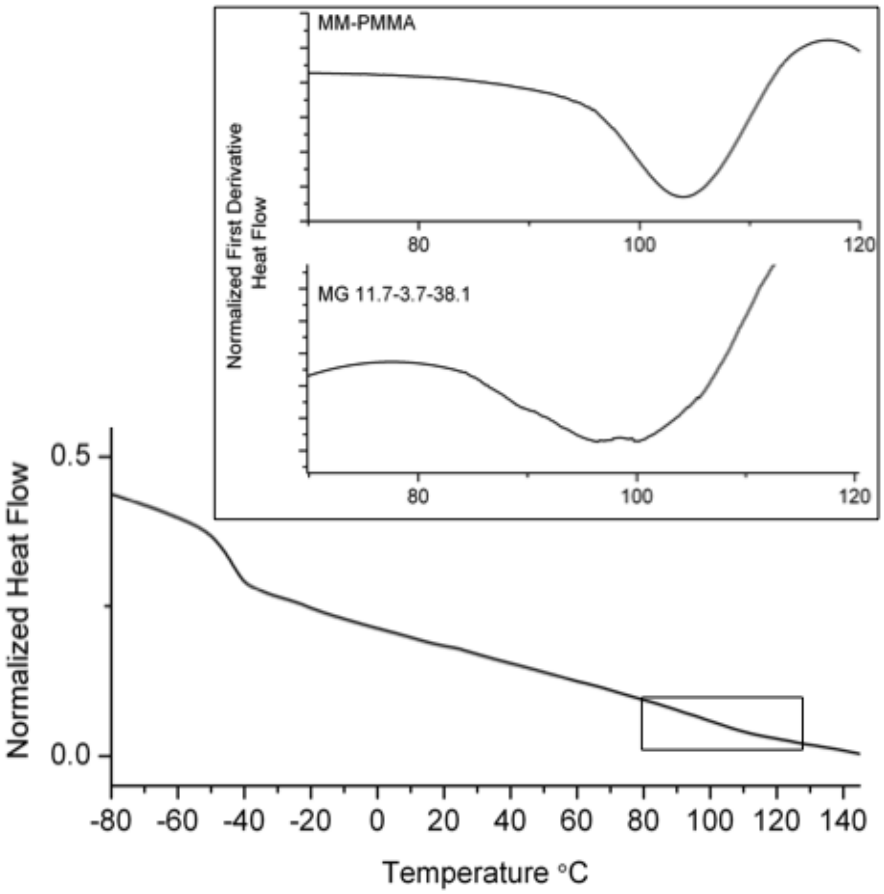

Figure 3.1. DSC thermograph of MG 11.7-3.7-38.1 which displays a glass transition temperature for each of the acrylic components. The zoomed portion displays the derivative heat flow versus temperature of the MG sample (bottom) over the highlighted region, which matches that of the PMMA macromonomer precursor (top).

result is in agreement with the findings published by Mijovic and co-workers, along with more recent work involving PI-*g*-PS copolymers with comb architectures.[14, 15] Their results concluded that the glassy PS domains consist of poorly ordered microphase segregated domains that effectively mask the high Tg material. Moreover, polydispersity of the graft copolymers can lead to the dissolution of the short randomly spaced PMMA segments into the soft P*n*BA phase, which again disguises the presence of the high T_g material.

After determining the presence of both the low and high T_g components, the thermal stabilities of the various multigraft samples, PMMA macromonomer, and a >100 kg/mol linear P*n*BA sample were established using TGA (Figure 3.2). The thermal decomposition of the PMMA macromonomer exhibits a two-step process with about 25% weight loss occurring around 295 ^oC and the remaining 75 % weight loss occurring over a temperature range of 320-405 ^oC. The linear P*n*BA displays a single-step decomposition over a much broader temperature range starting at around 270 ^oC with complete weight loss occurring by 405 ^oC. The graft copolymer TGA thermograms also demonstrates a two–step thermal decay resulting from the presence of the PMMA component and because the composition of PMMA is only ~10 to 35 vol.% of the multigraft copolymer the initial decay accounts for a lower weight loss percentage than the PMMA macromonomer alone, generally ranging from 10 to 15 weight %. In addition to the weight loss versus temperature, the derivative of weight change against temperature was plotted to show that the weight loss increases with increasing PMMA

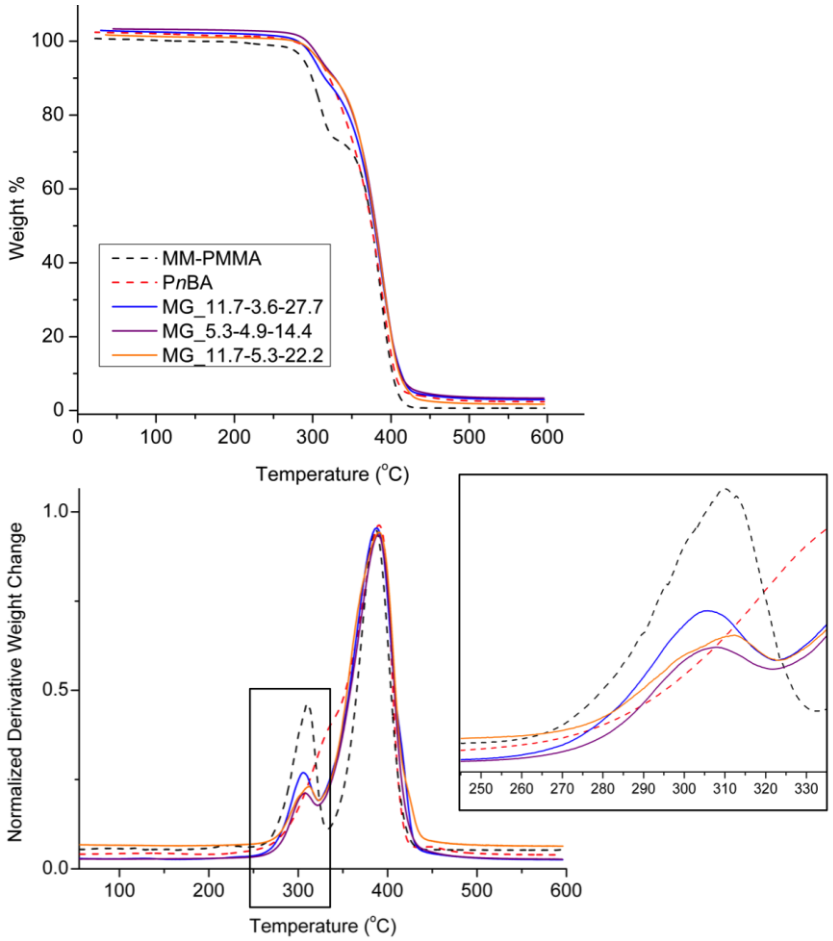

Figure 3.2. Thermal analysis of various MG samples using TGA. The weight % versus temperature (top) displays the presence of PMMA side chains because of the two-step decomposition. Additionally, the derivative weight change versus temperature (bottom) qualitatively supports the PMMA amount of each MG sample by increasing in weight loss with respect to PMMA content.

content, regardless of the molecular weight of the PMMA graft side chain, which confirms qualitatively that our characterization using NMR and triple detector SEC of the PMMA content is accurate.

3.4.2 Mechanical Properties

The effect of composition and side chain molecular weight on the mechanical properties of five branched copolymer samples were explored using DMA, tensile testing, and rheology. Previous works have shown, using styrene and isoprene multigraft copolymers, that architectural heterogeneity does effect the morphology of the graft copolymers and thus influences the mechanical properties of the material, however, the authors demonstrated that the number of branch point junctions and branch point functionality are much more impactful on enhancing the mechanical properties.[9] According to their results, we should suspect the bulk mechanical behavior for the all-acrylic system to be less influenced by branch point placement and heavily dominated by number of branch points and the volume ratio of the hard and soft components. To begin the characterization into the bulk mechanical properties of the all-acrylic multigraft materials, DMA was employed to obtain preliminary stress/strain values at room temperature and the storage and loss modulus as a function of temperature in order to see how these properties can be tuned by manipulation of the glassy PMMA side chain. The stress versus strain curves of five multigraft samples (Figure 3.3) depicts a large variation in the observed stress values of each sample

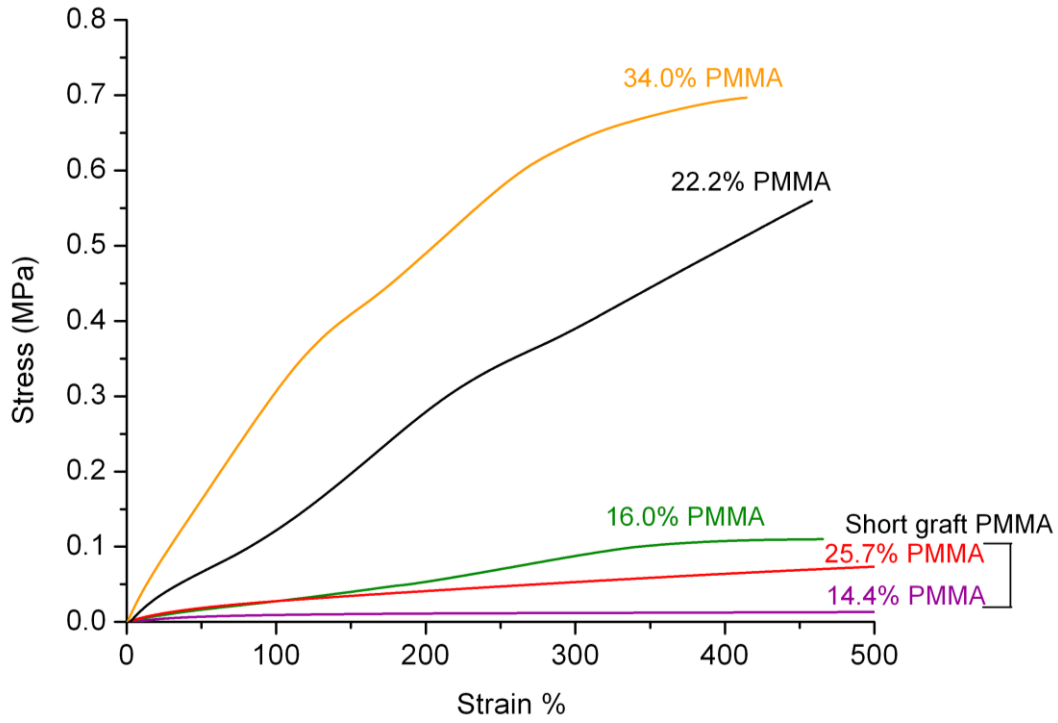

Figure 3.3. Stress versus strain values for several MG samples composed of both 5.3 and 11.7 kg/mol PMMA side chains. The final elongation values are not the elongation at rupture, but the displacement limitation of the DMA instrument, ~24 mm.

below 500 strain %, with one notable trend being the samples synthesized using the higher, 11.7 kg/mol, molecular weight side chains, exhibiting higher strength regardless of volume percent when compared to those with the lower, 5.3 kg/mol, molecular weight PMMA graft chains. These results indicate that by increasing the PMMA content of the multigraft copolymer the strength of the material can be enhanced, suggesting the presents of phase separation between the rigid PMMA domains and rubbery P*n*BA phases within the material, despite side chain molecular weight. Additionally, it is the multigraft materials composed of the higher molecular weight side chains that produce far superior elastic properties because of their increasing degree of tethering within the glassy domains, which effectively strengthens the physical crosslink of the hard phase and results in greater resistance during elongation.[8]

The same trend can be seen in Figure 3.4 where the elastic modulus and stress values at 400% strain versus PMMA volume percent further demonstrates the importance of side chain length, allowing for adequate chain entanglement by the PMMA side chains, followed by the percent of PMMA incorporated into the material. It is important to note that these strain values are not the strain at break of the material, but the limitations of the DMA instrument which has a maximum crosshead displacement of only ~24 mm.

DMA was also used to evaluate the storage modulus, loss modulus, and tan delta over a temperature range from -80 ^{o}C to 175 ^{o}C. Shown in Figure 3.5 are DMA data for sample MG 11.7-5.3-22.2, which contains 22.2 volume % PMMA. As expected

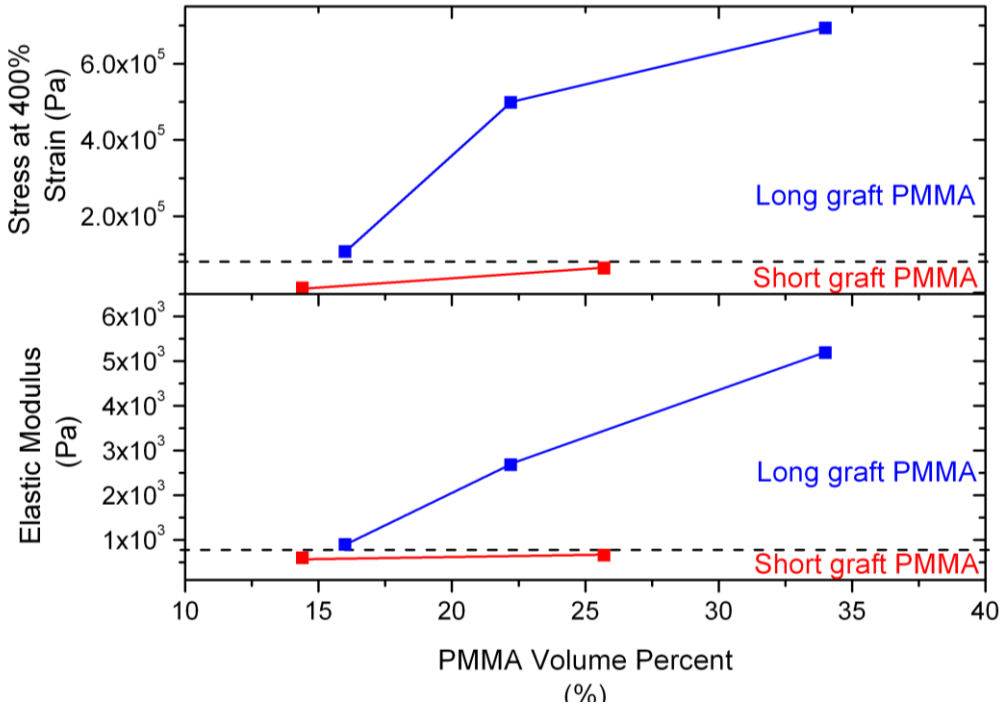

Figure 3.4. Elastic modulus (bottom) and stress value at 400 strain % (top) versus PMMA volume fraction of the five samples used in the previous stress/strain figure depicting the large reduction in strength with using short PMMA graft side chains.

we see two transition temperatures, one corresponding to the T_g of the rubbery P*n*BA matrix and the other from the T_g of the glassy PMMA domains, and because DMA is a much more sensitive technique for determining the thermal transition temperatures we are also able to observe the existence of phase blending by the T_g of the rubbery phase migrating from -45 ^oC in DSC to -20 ^oC. This result was observed in all multigraft samples and reflects the influence of the slow, controlled annealing process that leads to a greater number of PMMA domains, while also presenting soft segregated phase boundaries that will introduce an intermediate T_g similar to those previously reported.[10, 14, 16, 17] Additionally, the storage modulus plotted over the same temperature range for multiple multigraft samples is shown in Figure 3.6 and depicts that at low and intermediate temperatures the materials exhibit similar behavior, but undergo very different deformation and mechanical failure at high temperatures depending on the molecular weight of the PMMA side chains. As the temperature begins to reach that of the PMMA T_g the material composed of 25 PMMA vol. % of the 5.3 kg/mol molecular weight side chain undergoes a much greater deformation with exposed to milder forces and yields promptly when 100 ^oC is reached, while the longer graft PMMA materials do not exhibit complete mechanical failure until ~150 ^oC. Again, this provides insight into the morphology of the multigraft materials and shows that the degree of chain entanglement within the hard domains of the 5.3 kg/mol graft PMMA materials is substantially lower, allowing the PMMA chains to easily disentangle and slip by one another once the molecular motion of the PMMA side chains begins. The figure also

demonstrates the stiffness of the material throughout the rubbery plateau region is directly correlated to amount of PMMA present in the multigraft copolymer and increases with increasing PMMA volume percent.

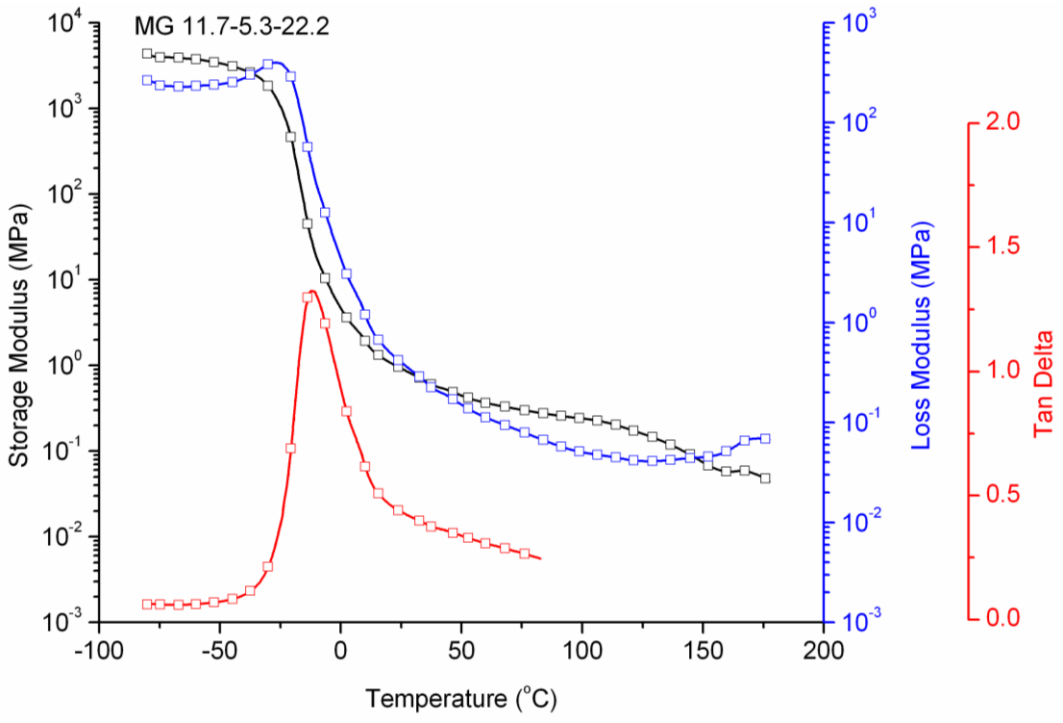

Figure 3.5. Storage modulus (black line), loss modulus (blue line), and tan delta (red line) of multigraft sample MG 11.7-5.3-22.2 depicting the characteristics of a thermoplastic elastomer, the T_gs of both the hard and soft segments, and the loss of phase separation experienced around 150°C.

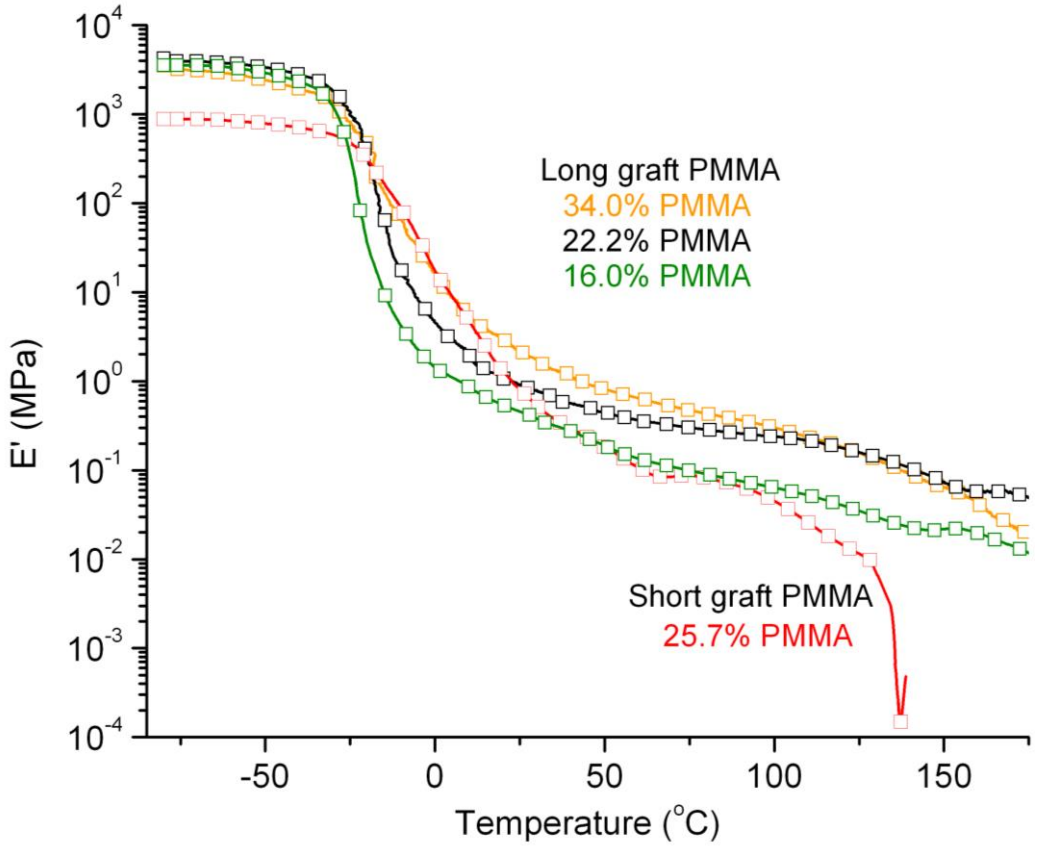

Figure 3.6. DMA of various MG samples to demonstrate the materials strength and mechanical failure temperature range dependence to side chain length.

In-depth tensile testing was performed by collaborators at the Fraunhofer Institute (Halle, Germany) to measure the properties of strain at break and the stress/strain behavior of the material corresponding to the gauge length, allowing for the determination of Young's modulus. Figure 3.7 and Table 3.1 display the stress/strain results for the multigraft materials, both of which were composed of the 11.7 kg/mol PMMA side chains, with 34.0 and 22.2 vol.% of PMMA. The two major differences we see when comparing to the stress versus strain curves previously discussed in this chapter is that the maximum stress (σ_M) observed by each of the material is nearly doubled, while the elongation is significantly reduced from that represented in Figure 3.4. This reduction in elongation percent was to be expected as a result of measuring the gauge length apposed to the cast-film over the entire crosshead length, which includes sample deformation at the clamp prior to and throughout tensile testing, seen previously in the SIS system previously reported.[18, 19] Regardless, both samples still exhibited the desired elastomeric properties with much improved strength. Additionally, the log-log plot of stress and draw ratio (Figure 3.8) allowed for the calculation of Young's modulus, which was obtained between 0.5-1.0% strain and calculated to be 0.38 MPa for MG 11.7-6.1-34.0 and 0.14 MPa for MG 11.7-5.3-22.2. Figure 3.8 also illustrates that at 22 PMMA vol.% the material behavior very much as both a plastic and a rubber, however, at 34 vol.% of PMMA the multigraft material exhibits a more plastic-like response during the early region of elongation, 25-150 strain % or 1-2 log draw ratio in Figures 3.7 and 3.8 respectively.

Table 3.1. The mechanical characterization of multigraft copolymers composed of the larger PMMA side chains

Sample[a]	σ_M (MPa)		ε_B[d] (%)	E[e] (MPa)
	Crosshead length[b]	Gauge length[c]		
MG 11.7-5.3-22.2	**0.56**	**0.98**	**279**	**0.14**
MG 11.7-6.1-34.0	**0.70**	**1.34**	**239**	**0.38**

[a] Sample identification MG *n-m-o* where *n* is MM-PMMA side chain molecular weight observed by SEC, *m* is calculated average number of branch points using the M_p obtained from SEC and ratio of P*n*BA to PMMA by ^{1}H-NMR, and *o* is the calculated PMMA volume fraction using ^{1}H-NMR. [b] Ultimate tensile stress measured on the TA Instruments Q-800 DMA of the film from the top to bottom clamp. [c] Ultimate tensile stress measured on the Zwick Z010 of the gauge length. [d] The elongation at break of the gauge length measured by the Zwick Z010. [e] Young's Modulus calculated using the region of 0.5-1.0 strain%.

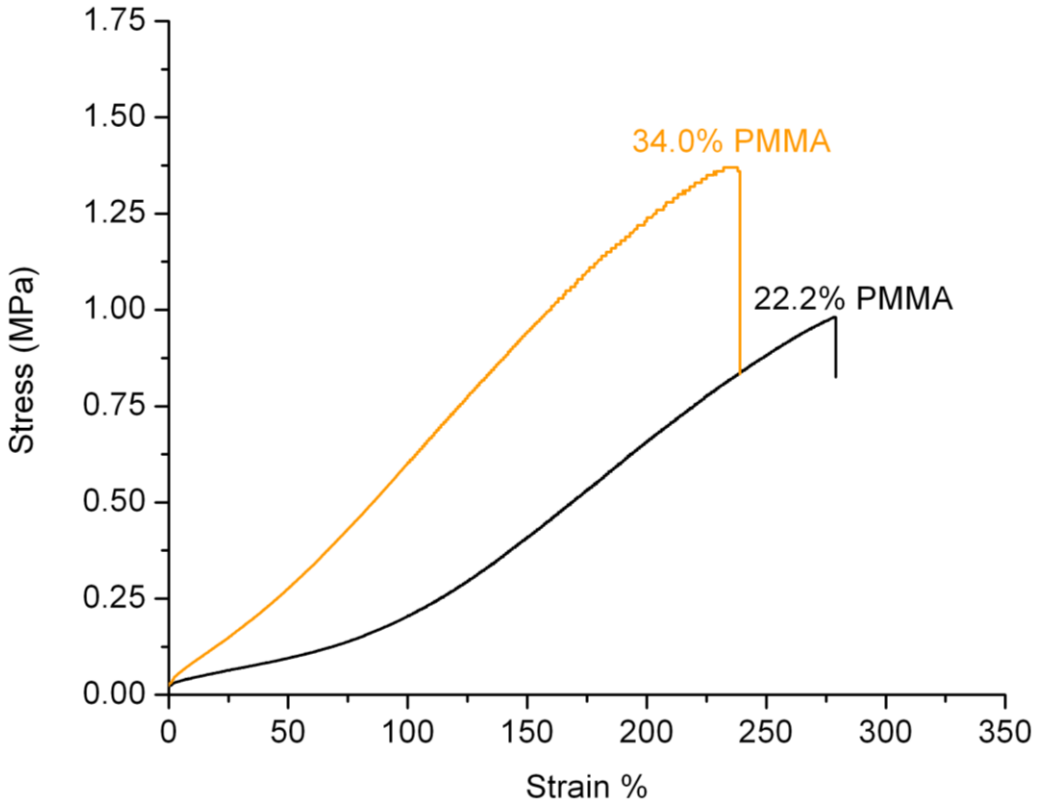

Figure 3.7. Stress versus strain of MG samples with 11.7 kg/mol PMMA side chains with 34.0 (orange) and 22.2 (black) vol. %. This figure represents the average of 3 runs for each sample.

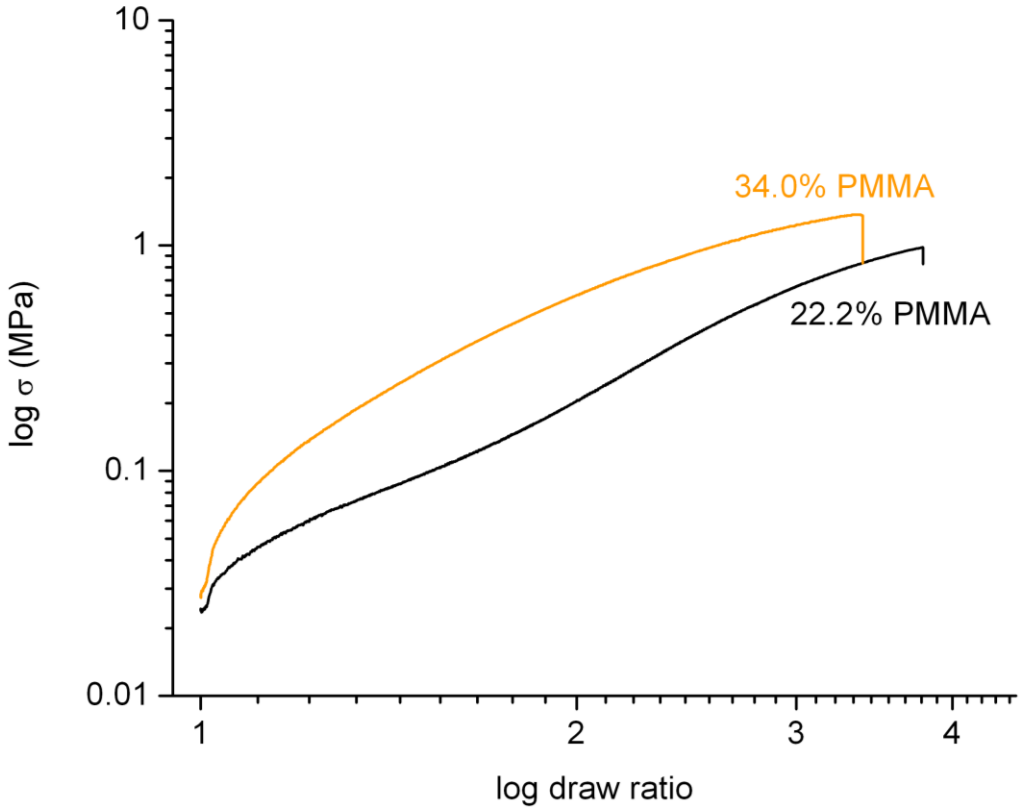

Figure 3.8. The log-log plot of stress versus draw ratio of MG samples composed of 11.7 kg/mol PMMA side chains and vol. % of 34.0 (orange) and 22.2% (black) to illustrate the more plastic-like behavior exhibited by the 34.o vol.% containing sample.

Lastly, small amplitude oscillatory shear measurements were also carried out on a rotational rheometer to further evaluate the mechanical behavior of the branched materials. Figure 3.9 is the Cole-Cole plot of mostly the same multigraft samples used for DMA and shows that all the samples exhibit thermo-rheological complexity. Additionally, it is again shown that the stiffness of the material is directly related to the PMMA percent incorporated into the multigraft copolymer, and by using the larger molecular weight PMMA side chains the rubbery plateau of the material is more pronounced.

The dynamic viscoelastic spectra at three representative temperatures: -35, 30 and 150 ^{o}C (Figure 3.10) further illustrate the physical properties of the multigraft copolymers, as well as, insight into the phase separation behavior and how these properties are effected by the side chain molecular weight and PMMA volume fraction. At low temperatures, the mechanical behavior of the material is dominated by the branched polymer's T_g and by the number of branch points incorporated into the backbone. The storage modulus for the polymers composed of the larger molecular weight PMMA side chains increase with increasing PMMA composition, however, at -35 ^{o}C the multigraft copolymer with the shorter, 5.3 kg/mol, side chains demonstrates the largest storage modulus value. This can be explained by the fact that the multigraft sample has to contain roughly twice the amount of branch point junctions per copolymer because of the lower molecular weight side chains, resulting in shorter P*n*BA backbone segments before being interrupted by an PMMA branch point that effectively enhances

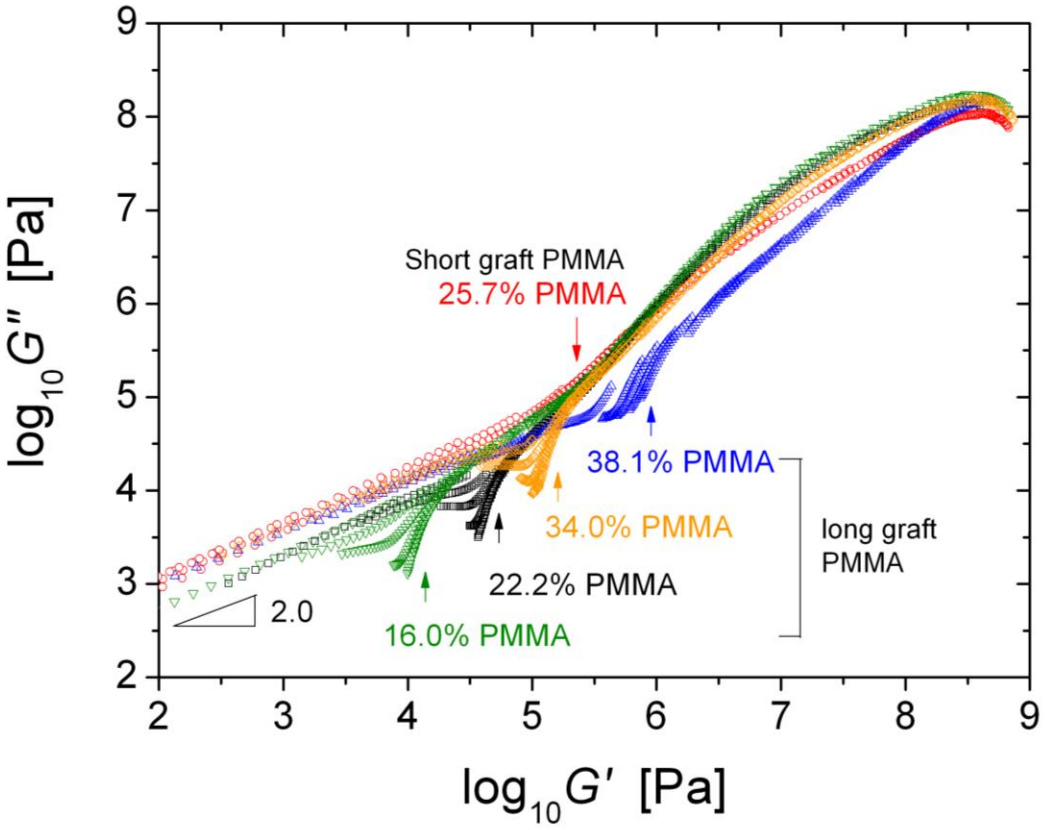

Figure 3.9. Cole-Cole plot of various MG copolymer samples composed of both 5.3 and 11.7 kg/mol PMMA side chains, with various PMMA vol. %, depicting how side chain length effects both the strength and rubbery phase of the material.

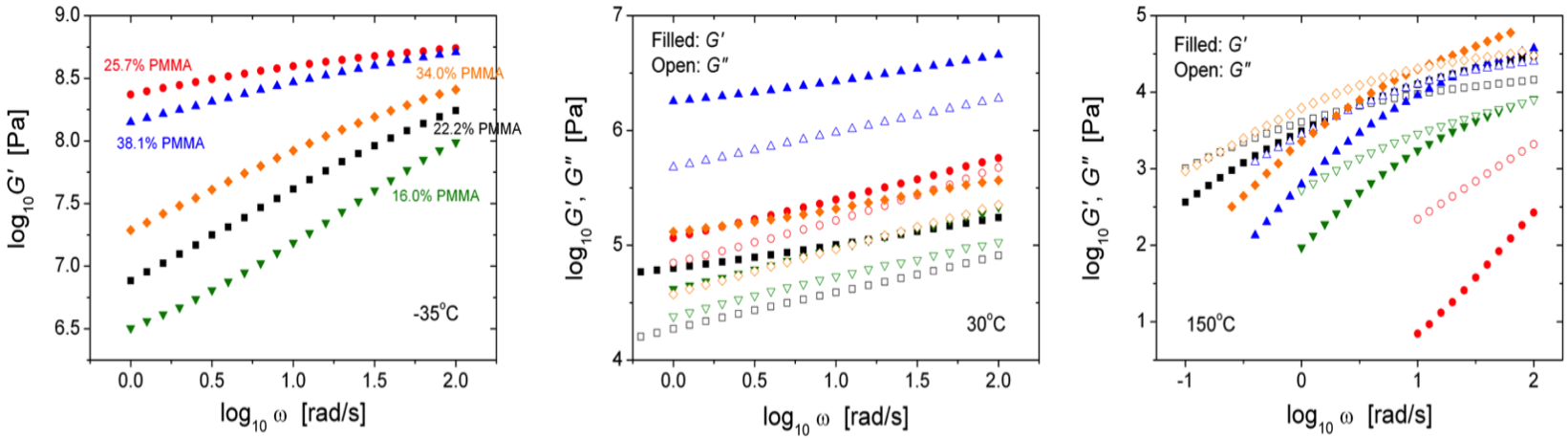

Figure 3.10. Dynamic viscoelastic spectra of various MG samples at -35 (left), 30 (middle), and 150 °C (right) to display the effect of temperature on the strength, working mechanical temperature range, and phase separation of the film.

the overall T_g of the branched copolymer. At intermediate temperatures we again experience the same reduction in the resistance to deformation of the shorter side chain length containing material and the samples increase in the storage modulus with increasing PMMA content. It is at high temperatures, 150 ^oC, that we again obtain evidence that the physical crosslink is much weaker and less entangled within the shorter graft PMMA side chains sample because of the immediate liquid-like behavior with the onset of the T_g of the glassy component. The multigraft copolymer samples with the larger molecular weight side chains also go through a transition from solid-like to liquid-like at this temperature, but because there still exists phase-separated regions the transition is prolonged.

3.4.3 Application of the non-affine tube model to elastomer systems

To further understand the physical properties exhibited by the bulk multigraft material based on the micro-mechanical properties, the non-affine tube model was fit to the observed stress-strain of the all-acrylic samples MG 11.7-5.3-22.2 and MG 11.7-6.1-34.0 that underwent tensile testing at the Fraunhofer Institute. The two common models applied to describe the stress response versus the elongation ratio, in terms of the chemical (G_c) and physical (G_e) cross-link modulus, for elastomeric materials are the slip-tube model and the non-affine tube model.[20, 21] The advantage of the latter model is that it covers all experimental model by taking into account finite chain extensibility and

offers a minimum set of parameters which are easily correlated to the materials behavior, however, it does require the experimental elongation/recovery to undergo several iteration cycles to conclusively correlate the model fitting to the observed stress-strain characteristics.[22] Additionally, the non-affine tube model also yields a parameter representing the portion of elastically active entanglements (n), which is defined by n_e/T_e, where T_e is the Langley trapping factor and describes the probability of that a certain entanglement becomes permanently trapped.[22, 23]

Application of the non-affine tube model to the all-acrylic multigraft copolymers composed of 22.2 and 34.0 vol. % PMMA of the longer 11.7 kg/mol side chains is shown in Figure 3.11(a) and (b), respectively. Again, the application of the rubber elasticity model is not recommended in the first deformation cycle because of the significant amount of viscoelastic and plastic deformation and is the result of the large theoretical deviation at elongation ratios (λ) >2.0. More specifically, during the first deformation cycle the physical cross-links are not fully stable and the grafted hard phase may be pulled out of their domains or interactions between other grafted, hard phase, domains will be fragmented. For this reason the fit range was limited to λ=1-1.5 for sample MG 11.7-6.1-34.0 and λ=1-2 for sample MG 11.7-5.3-22.2. The observed G_c, G_e, and n values for each sample are outlined in Table 3.2. As expected both G_c and G_e increase with the increased PMMA vol.% resulting in an increase of the chemical cross-link modulus and greater amount of chain pullout or fracturing of the initial plastic domains (resolving of 'physical' cross-links). A similar observation can be made for n,

where a larger amount of PMMA content also correlates to an increase in the number of branch point junctions resulting in shorter molecular weight P*n*BA-spacer segments between branches and consequently a lesser number of rubbery segmental entanglements between physically cross-linked domains. Additionally, the absence of a yield point in both the experimental (black line) and modeled (blue line) stress-strain curves indicates that the hard phase is not continuous, which is preferred for this class of elastomers.

Table 3.2. The deformation characteristics parameters using the non-affine

Sample	G_c [kPa]	G_e [kPa]	n	fit range
MG 11.7-5.3-22.2	**53.7±2.9**	**43.7±0.3**	**7.7±0.3**	**λ=1-2**
MG 11.7-6.1-34.0	**207±35**	**129±16**	**3.7±0.5**	**λ=1-1.5**

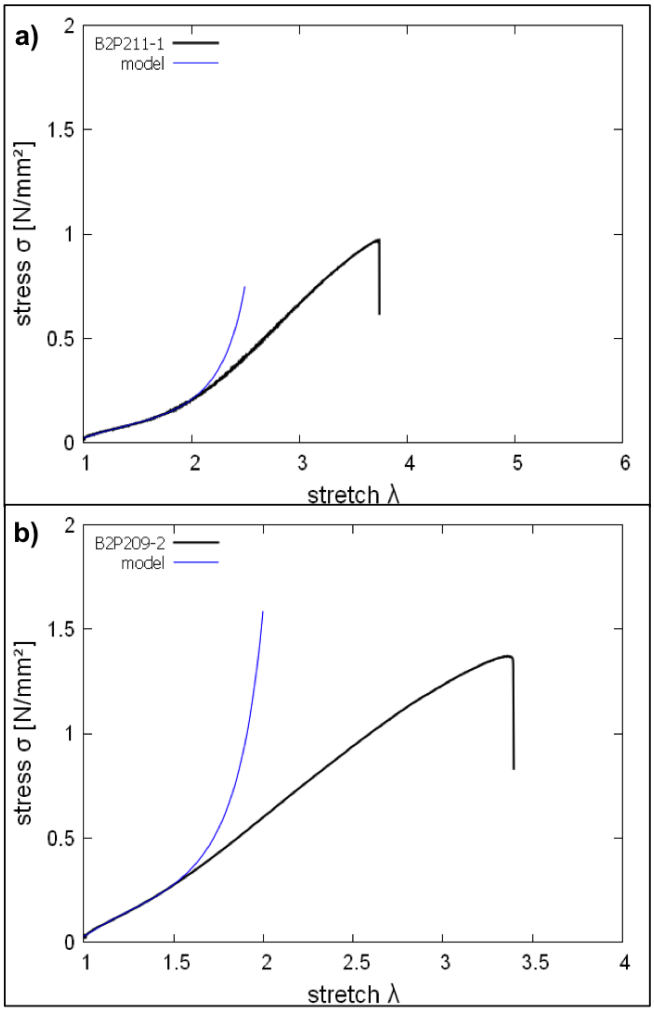

Figure 3.11. The experimental results for stress-strain by tensile testing (black line) and deformation characteristics modeled by the non-affine tube model (blue line) of MG 11.7-5.4-22.2 (a) and MG 11.7-6.1-34.0 (b).

3.5 Conclusion

This investigation into the thermal and mechanical properties of the newly synthesized all-acrylic multigraft copolymers demonstrated that by introducing the rigid segments as branches off the rubbery material, as opposed to the terminal ends of a linear block copolymer, we were able to produce TPEs with superior properties to their current commercial linear analogs. In addition, we also demonstrated the capability to improve the resistance to elongation by three orders of magnitude through manipulating the molecular weight of the side chain and volume percent of PMMA. It was shown that generally >20 vol. % of PMMA of the higher molecular weight side chains was need to obtain superior elastomeric properties, while materials composed of <20 PMMA vol. % or short PMMA graft side chains still produced materials with similar elongations without rupture but with much lower resistance to- and recovery from elongation. As predicted the strongest materials were those composed of the largest percent of PMMA and with the longer PMMA side chains, however, this work provides novel experimental insight into the presence and significance of the physically cross-linked domains of these all-acrylic materials. The results obtained in this chapter thoroughly demonstrate the potential to systematically tailor all-acrylic multigraft copolymers for use as next generation TPEs and for other impact resistant applications.

References

1. Jang, Y.; Hirai, T. *Materials Sciences and Applications* **2011,** Vol.02No.03, 4.

2. Jang, Y.; Hirai, T. *Soft Matter* **2011,** 7, (22), 10818-10823.

3. Radke, W.; Roos, S.; Stein, H. M.; Müller, A. H. E. *Macromolecular Symposia* **1996,** 101, (1), 19-27.

4. Tong, J. D.; Leclère, P.; Doneux, C.; Brédas, J. L.; Lazzaroni, R.; Jérôme, R. *Polymer* **2001,** 42, (8), 3503-3514.

5. Tong, J. D.; Leclère, P.; Rasmont, A.; Brédas, J. L.; Lazzaroni, R.; Jérôme, R. *Macromolecular Chemistry and Physics* **2000,** 201, (12), 1250-1258.

6. Tong, J. D.; Jerôme, R. *Polymer* **2000,** 41, (7), 2499-2510.

7. Tong, J.-D.; Jerôme, R. *Macromolecules* **2000,** 33, (5), 1479-1481.

8. Zhu, Y.; Burgaz, E.; Gido, S. P.; Staudinger, U.; Weidisch, R.; Uhrig, D.; Mays, J. W. *Macromolecules* **2006,** 39, (13), 4428-4436.

9. Staudinger, U.; Weidisch, R.; Zhu, Y.; Gido, S. P.; Uhrig, D.; Mays, J. W.; Iatrou, H.; Hadjichristidis, N. *Macromolecular Symposia* **2006,** 233, (1), 42-50.

10. Li, H.; Wang, W.; Li, C.; Tan, J.; Yin, D.; Zhang, H.; Zhang, B.; Yin, C.; Zhang, Q. *Journal of Colloid and Interface Science* **2015,** 453, 226-236.

11. Matyjaszewski, K. *Macromolecules* **2012,** 45, (10), 4015-4039.

12. Dufour, B.; Koynov, K.; Pakula, T.; Matyjaszewski, K. *Macromolecular Chemistry and Physics* **2008,** 209, (16), 1686-1693.

13. Shim, J. S.; Asthana, S.; Omura, N.; Kennedy, J. P. *Journal of Polymer Science Part A: Polymer Chemistry* **1998,** 36, (17), 2997-3012.

14. Wang, W.; Wang, W.; Li, H.; Lu, X.; Chen, J.; Kang, N.-G.; Zhang, Q.; Mays, J. *Industrial & Engineering Chemistry Research* **2015,** 54, (4), 1292-1300.

15. Mijović, J.; Sun, M.; Pejanović, S.; Mays, J. W. *Macromolecules* **2003,** 36, (20), 7640-7651.

16. Pu, G.; Dubay, M. R.; Zhang, J.; Severtson, S. J.; Houtman, C. J. *Industrial & Engineering Chemistry Research* **2012,** 51, (37), 12145-12149.

17. Nelliappan, V.; El-Aasser, M. S.; Klein, A.; Daniels, E. S.; Roberts, J. E.; Pearson, R. A. *Journal of Applied Polymer Science* **1997,** 65, (3), 581-593.

18. Mays, J. W.; Uhrig, D.; Gido, S.; Zhu, Y.; Weidisch, R.; Iatrou, H.; Hadjichristidis, N.; Hong, K.; Beyer, F.; Lach, R.; Buschnakowski, M. *Macromolecular Symposia* **2004,** 215, (1), 111-126.

19. Weidisch, R.; Gido, S. P.; Uhrig, D.; Iatrou, H.; Mays, J.; Hadjichristidis, N. *Macromolecules* **2001,** 34, (18), 6333-6337.

20. Rubinstein, M.; Panyukov, S. *Macromolecules* **2002,** 35, (17), 6670-6686.

21. Klüppel, M.; Schramm, J. *Macromolecular Theory and Simulations* **2000,** 9, (9), 742-754.

22. Schlegel, R.; Duan, Y. X.; Weidisch, R.; Hölzer, S.; Schneider, K.; Stamm, M.; Uhrig, D.; Mays, J. W.; Heinrich, G.; Hadjichristidis, N. *Macromolecules* **2011,** 44, (23), 9374-9383.

23. Klüppel, M., The Role of Disorder in Filler Reinforcement of Elastomers on Various Length Scales. In *Filler-Reinforced Elastomers/Sanning Force Microscopy*, Capella, B.; Geuss, M.; Klüppel, M.; Munz, M.; Schulz, E.; Sturm, H., Eds. Springer Berlin Heidelberg: 2003; Vol. 164, pp 1-86.

CHAPTER 4.

MORPHOLOGY OF ALL-ACRYLIC MULTIGRAFT COPOLYMERS BY ATOMIC FORCE MICROSCOPY

Abstract

In this chapter atomic force microscopy was employed to observe the presence of phase separation within the poly(*n*-butyl acrylate)-*g*-poly(methyl methacrylate) samples synthesized *via* the grafting through approach. It was found that both the volume ratio between the acrylic segments and the chain length of the grafted side chains affect the formation and size of PMMA rich domains. Force modulation imaging with atomic force microscopy was able to confirm the phase separation observed in the phase contrast images through directly probing the elastic modulus of the imaged region. The results observed in this section are correlated to the mechanical properties measured in the previous chapter for these samples.

4.1 Introduction

There is an increasing importance for linear and branched mulit-block polymers because of their unique, and tunable, properties in the solid state.[1, 2] In the solid state these molecules have the tendency to phase segregate and self-assemble into ordered microdomains. The details of self-assembly and a discussion on the effects of the Flory-Huggins interaction parameter, volume fraction of each component, and molecular architecture on the observed morphology can be found in Chapter 1 of this dissertation. In the context of TPEs, self-assembly and solid-state morphology play a critical role in the exhibited bulk physical properties and ultimately the available applications that can be targeted. The class of materials termed TPEs are especially sensitive to compositional and morphological changes because of their reliance on T_gs and the formation of thermoplastic domains that effectively act as cross-links within the elastomeric domain.[1] In general, ABA linear triblock copolymers for use as TPEs require a continuous rubbery matrix with spherical or cylindrical glassy domains, which is determined by the volume ratio of the hard, glassy end blocks to the rubbery middle segment, of the high T_g segment throughout the rubbery phase.

Expanding these findings and concepts to branched architectures, it was shown that complex graft copolymers could be understood morphologically as a series of fundamental building blocks characterized by the local structure of the branch point intersections.[3-5] In the case of PI-*g*-PS multigraft copolymers with regular tri-, tetra-, and hexafunctional branch point junctions, the authors demonstrated how the branch point

functionality and branch point number would affect the observed morphology and domain spacing, which exhibited consequences on the measured tensile properties.[3, 6-9] The authors concluded that the functionality of the branch point causes the described morphology change according to the Milner phase diagram, and that the increase in the number of branch points per molecule resulted in a decrease in the grain size of the microphase-separated domains and a reduction in long range ordering.[3, 10] Additional work with the analogous system that exhibited random branch point placement also displays the characteristic microphase separated domains but disordered morphology resulting from the architectural disparity along the backbone causing different parts of the molecule to locally prefer a different morphology.[5, 11] Furthermore, the lack of long-range order did not seem to have much effect on the mechanical properties.[5, 9, 11]

Structural studies of block copolymers are most often carried out using transmission electron microscopy (TEM), coupled with x-ray scattering (SAXS) for morphology conformation and domain spacing by the ratio and spacing of q*, but the use of this technique for soft matter requires selective staining of one component to create contrast within the image. The selective staining is well-documented and easily performed in systems containing conjugated and non-conjugated double bonds using compounds such as RuO_4 and OsO_4, respectively.[12, 13] However, imaging phase segregation by TEM in all-acrylic systems requires more complicated staining technique of the PMMA phase using phosphotungstic acid (PTA) described in literature.[14-17] As a result of the more complicated staining and imagining process associated with all-acrylic

copolymers, atomic force microscopy (AFM) has been regularly employed to image the phase separation by scanning over an area of the sample in contact mode where the cantilever tip interacts with the samples surface differently according to the softness or rigidity of the material.[18-21] In the specific cases of linear MAM triblock copolymers, the cantilever oscillation change can be related to the elastic modulus and therefore the phase signal of the AFM image clearly indicates microphase separation.[1, 22-27] It is important to note that the AFM profile is not directly relatable to the bulk morphology of the material, but because the image is generated by the local contrast in the mechanical properties it can be used as a clear indication of phase separation between different segments.[28]

Another important consideration of phase segregation and self-assembly of P*n*BA-*b*-PMMA materials is the relatively low Flory-Huggins interaction parameter, reported in literature to be χ=0.04.[17, 29, 30] For comparison to other commercially available TPE materials based on PS-PI-PS triblock copolymers, PS/PI χ=0.09, leading to more defined phase boundaries and less phase blending.[31, 32] Phase separation and ordered morphologies have been reported for linear diblock and triblock P*n*BA/PMMA copolymers, but the authors also acknowledge phase blending between the two acrylic phases, which is known to increase with factors such as increasing PDIs, using low molecular weight block segments, and by introducing structural irregularity.[25, 27, 30]

In this chapter the use of AFM and force modulated AFM to confirm the presence of phase separation between the P*n*BA elastic phase and the plastic PMMA phase will

be discussed. Additionally, the changes in PMMA domain size and overall morphological behavior will be correlated to the structural and compositional changes of the branched materials. The work presented in this section to illustrate the structure-property relationship of these materials was obtained exclusively by AFM, which does not always reflect the bulk morphology of a material. For this reason, in-depth TEM and SAXS experiments are ongoing in order to observe the multigrafts bulk morphology and relate results presented in this chapter by AFM to other imaging and morphological experiments.

4.2 Experimental

4.2.1 Synthesis of PnBA-g-PMMA multigraft Copolymers

All experimental details for preparation of these materials refer to Chapter 2. Additionally, Table 2.2 in the previous chapter contains detailed structural and compositional details of the materials used in this chapter.

4.2.2 Sample preparation for AFM imaging

Sample preparation began by spin casting a polymer/toluene solution (2.0 w/v%) onto a Si-wafer, at 1500 rpm for 30 s and slowing to 300 rpm for an additional 30 s, to yield a film ~ 300-600 nm thick. The samples were then placed under vacuum for 24 h at room temperature. The annealing process consisted of slowly heating the samples

under vacuum to 150 °C, increasing the temperature by 50 °C increments and equilibrating over a 24 h period, and allowing 48 h at 150 °C for the thermodynamic self-assembly process to be completed. The temperature was then slowly decreased under the same conditions and placed in the freezer for a few days prior to imaging.

4.3 Characterization

Scanning probe microscopy measurements were performed with an OmegaScope AIST-NT (Novato, U.S.). A HiRes-C19/Cr-Au (MikroMasch) with a less than 2 nm curvature radius probe was used at 65 kHz resonance.

4.4 Results and Discussion

All-acrylic multigraft copolymers consisting of a rubbery P*n*BA backbone with glassy PMMA side chains were synthesized by a combination of anionic and grafting through via RAFT polymerization. The methodology developed for the synthesis of these materials allowed for the parameters of volume ratio between the hard and soft phases, control of side chain molecular weights, and number of branches per polymer chain to be altered in order to relate the compositional and architectural changes to the corresponding mechanical and morphological characteristics. In order to evaluate the structure-property relationship of these materials, four multigraft samples (Table 4.1) were chosen systematically to observe the presence and variations of phase separation on the basis of PMMA side chain molecular weight and PMMA vol.%.

Table 4.1. Multigraft copolymers characteristics

Sample[a]	Graft Chain	Multigraft				
	M_n[b] (kg/mol)	M_n[c] (kg/mol)	M_p[d] (kg/mol)	PDI[e]	#[f]	Volume Percent[g] (%)
MG 5.3-4.9-14.4	5.3	111.3	168.2	1.59	4.9	14.4
MG 5.3-9.2-25.7		93.3	153.2	1.55	9.2	25.7
MG 11.7-2.6-16.0	11.7	126.8	175.0	2.04	2.6	16.0
MG 11.7-6.1-34.0		93.9	150.7	1.78	6.1	34.0

[a] Sample identification MG *n-m-o* where *n* is MM-PMMA side chain molecular weight observed by SEC, *m* is calculated average number of branch points using the M_p obtained from SEC and ratio of P*n*BA to PMMA by ^{1}H-NMR, and *o* is the calculated PMMA volume fraction using ^{1}H-NMR. [b] Number average molecular weight of PMMA side chains calculated by SEC. [c] Number average molecular weight of MG sample calculated by SEC. [d] Maximum peak molecular weight of MG sample calculated by SEC. [e] Polydispersity indices for MG sample calculated by SEC. [f] Average number of branch points per MG chain calculated using ^{1}H-NMR and the M_p calculated by SEC. [g] Average PMMA volume percent per MG chain calculated using ^{1}H-NMR.

To begin, samples MG 5.3-4.9-14.4 and MG 5.3-9.2-25.7 were imaged using Tapping-Mode AFM (TMAFM) to observe the annealed films topology and phase separation between the rubbery and plastic segments. The first interesting observation is seen in Figure 4.1 of the MG 5.3-4.9-14.4 sample, which depicts no phase separation. This is attributed to both the partial dissolution of the short PMMA chains into the PnBA matrix, and the low PMMA content which does not seem to be adequate to produce PMMA rich clusters or domains. In contrast, the AFM images seen in Figure 4.2 of MG 5.3-9.2-25.7 do exhibit phase separation between the PMMA (bright regions) and PnBA (dark regions) segments, and confirm that the side chain molecular weight is entirely responsible for the existence, or absence, of phase separation within the material. Furthermore, it indicates the significance of the number of branch point junctions, and as a result shorter molecular spacing between branch point junctions, in encouraging the formation of hard domains. Since the sample containing 25.7 vol.% PMMA has roughly twice as many branching junctions, the PMMA side chains are in closer proximity to one another, which seemingly reduces the dissolution of the side chains into the soft matrix and leads to a low degree of self-organization between the phases at the nanoscale. Additionally from the phase image in figure 4.2, it can be seen that the PMMA domains are large in size and loosely packed domains produced by a low degree of chain entangled of the low molecular weight PMMA side chain segments.

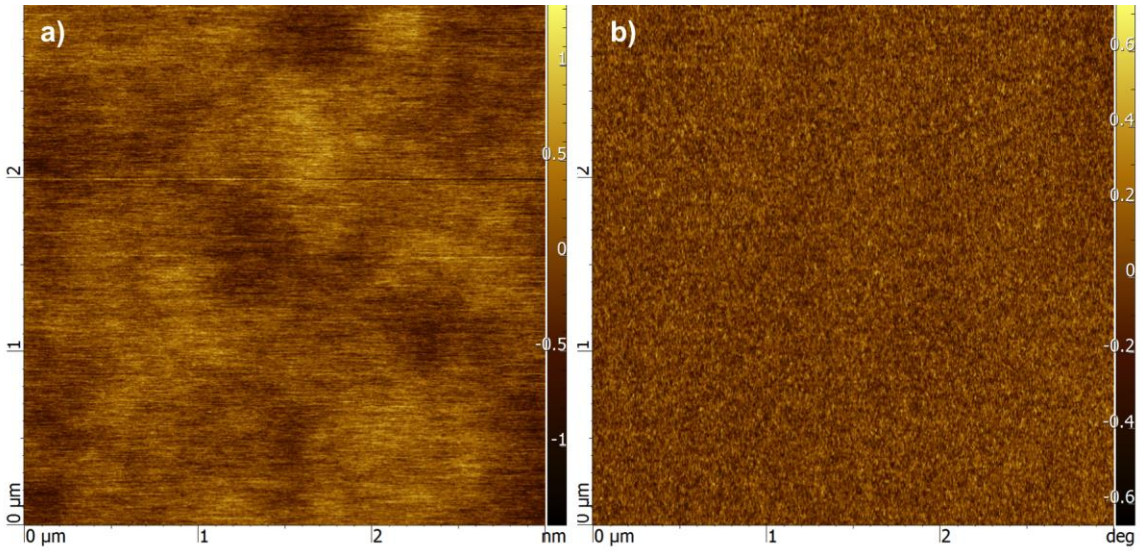

Figure 4.1. TMAFM height image (a) and phase contrast image (b) of sample MG 5.3-4.9-14.4

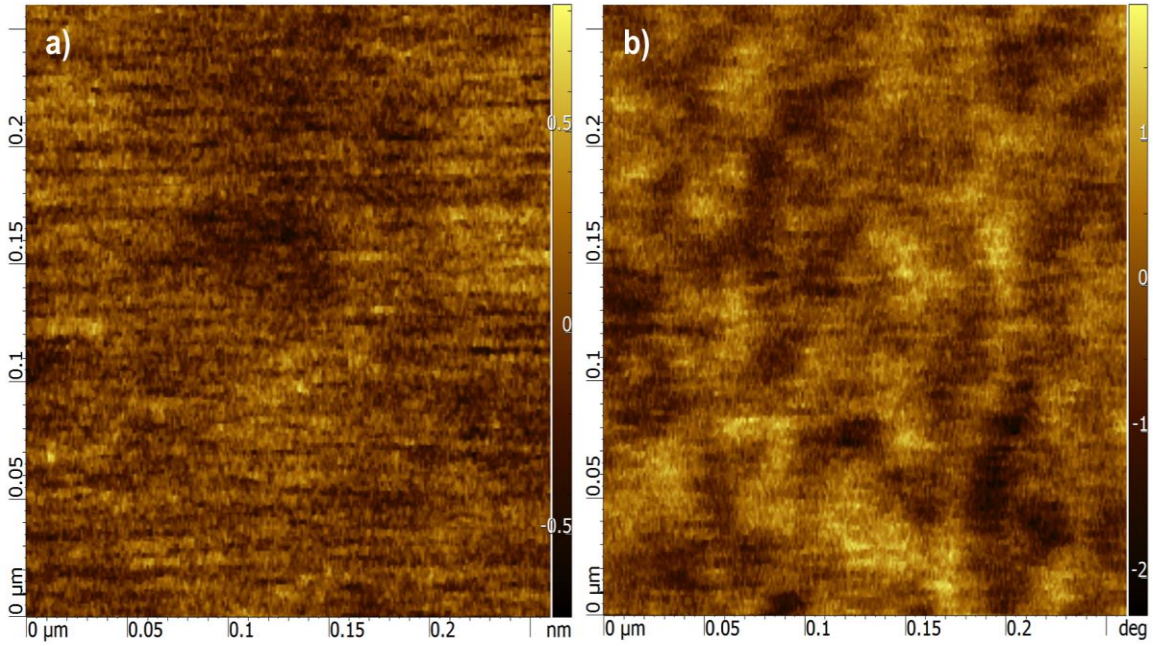

Figure 4.2. TMAFM height image (a) and phase contrast image (b) of sample MG 5.3-9.2-25.7

In order to investigate the morphological behavior of the randomly branched all-acrylic materials in regard to the side chain length, the MG 11.7-2.6-16.0 and MG 11.7-6.1-34.0 were also imaged by TMAFM. The two multigraft samples composed of the longer PMMA side chains both exhibit phase separation and display generally comparable spherical, more defined, hard domains. Looking in detail at Figure 4.3, sample MG 11.7-2.6-16.0, the small spherical and worm-like aggregates are clearly visible throughout the imaged region and correspond to a mean size of 15 nm. Similarly, Figure 4.4 of sample MG 11.7-6.1-34.0, depicts a similar, random arrangement, of spherical and worm-like PMMA rich aggregates.

Further comparison of the phase images of the MG 11.7-2.6-16.0 and MG 11.7-6.1-34.0 samples (Figure 4.3 and 4.4, respectively) the domain size in each image is similar. This is confirmed in Figure 4.5 which provides a mean domain size of 15 and 19 nm, for the 16.0 and 34.0 vol.% samples, respectively. The primary notable difference between the two samples is the number of PMMA domains is much greater for the MG 11.7-2.6-16.0 sample. We attribute the increased number of PMMA domains for the 16.0 vol.% sample to the longer P*n*BA segments between branch point junctions which leads to less available PMMA side chain segments to incorporate into the each hard domain, because of PMMA chain proximity, and leading to the formation of additional PMMA domains.

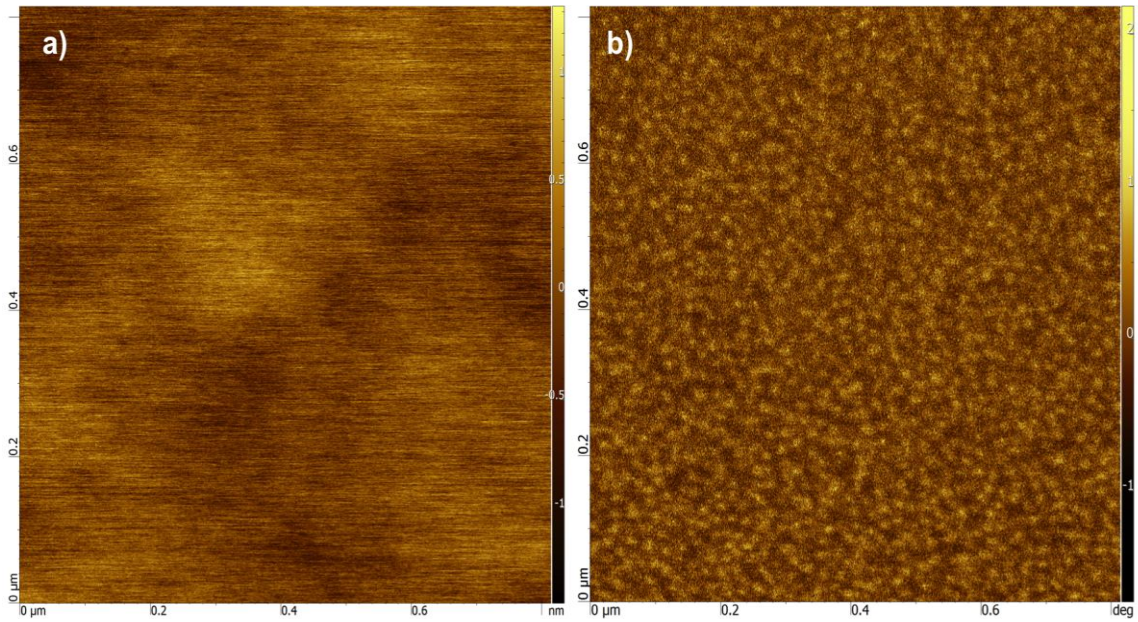

Figure 4.3 TMAFM height image (a) and phase contrast image (b) of sample MG 11.7-2.6-16.0

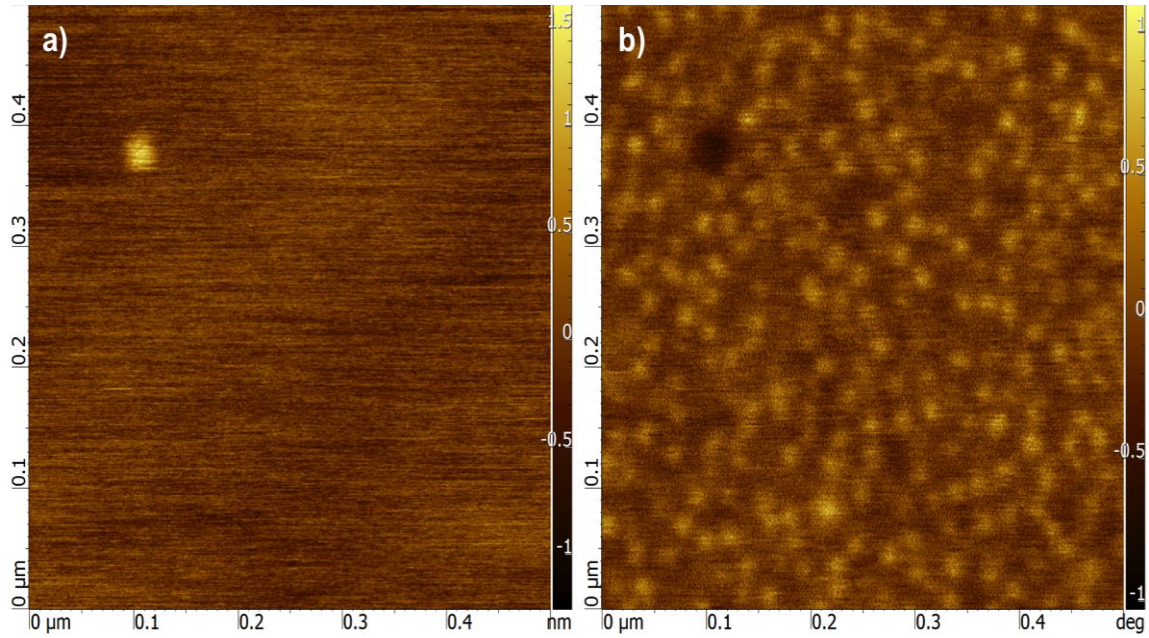

Figure 4.4 TMAFM height image (a) and phase contrast image (b) of sample MG 11.7-6.1-34.0

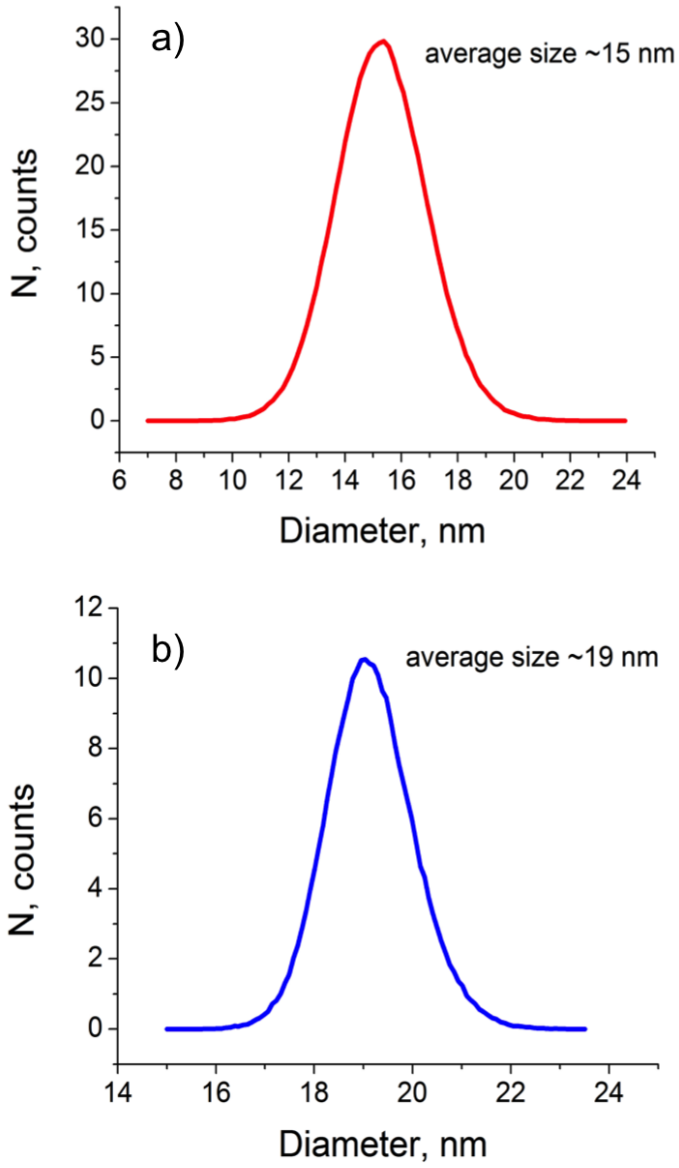

Figure 4.5. Size distribution profiles for MG 11.7-2.6-16.0 (a) and MG 11.7-6.1-34.0 (b).

In addition to conventional TMAFM, the secondary imaging technique of Force Modulation (FMAFM), which is a dynamic imaging mode that maps the elastic moduli of the material was used to confirm our previously reported results from the phase images.[33-36] In FMAFM the cantilever is in contact with the sample and is given a small vertical oscillation, where the tip oscillation is much greater than the raster scan rate, allowing the variation in the cantilever amplitude to be directly related to the relative stiffness of the material. This technique is often employed for elastic materials because of the ability to discriminate a samples local change in stiffness at nanometer scale. Figure 4.6 is the FMAFM image of the two multigraft samples that are composed of the 11.7 kg/mol PMMA side chains where the change in the materials elasticity, which is directly being measured in this AFM imaging mode, is visible and confirms the presence of phase separation between P*n*BA and PMMA.

4.5 Conclusion

The presence of phase separation in the all-acrylic multigraft copolymers was shown using TMAFM and further demonstrated through dynamic interaction with the films surface by FMAFM. The side chain molecular weight and PMMA vol.% played a critical role in both the size and formation of PMMA rich domains. The phase images show that the MG 5.3-9.2-25.7 sample does display PMMA domains, but are large and loosely packed aggregates when compared to the samples composed of the larger 11.7 kg/mol PMMA side chains. Additionally, no long-range ordering or definite morphology

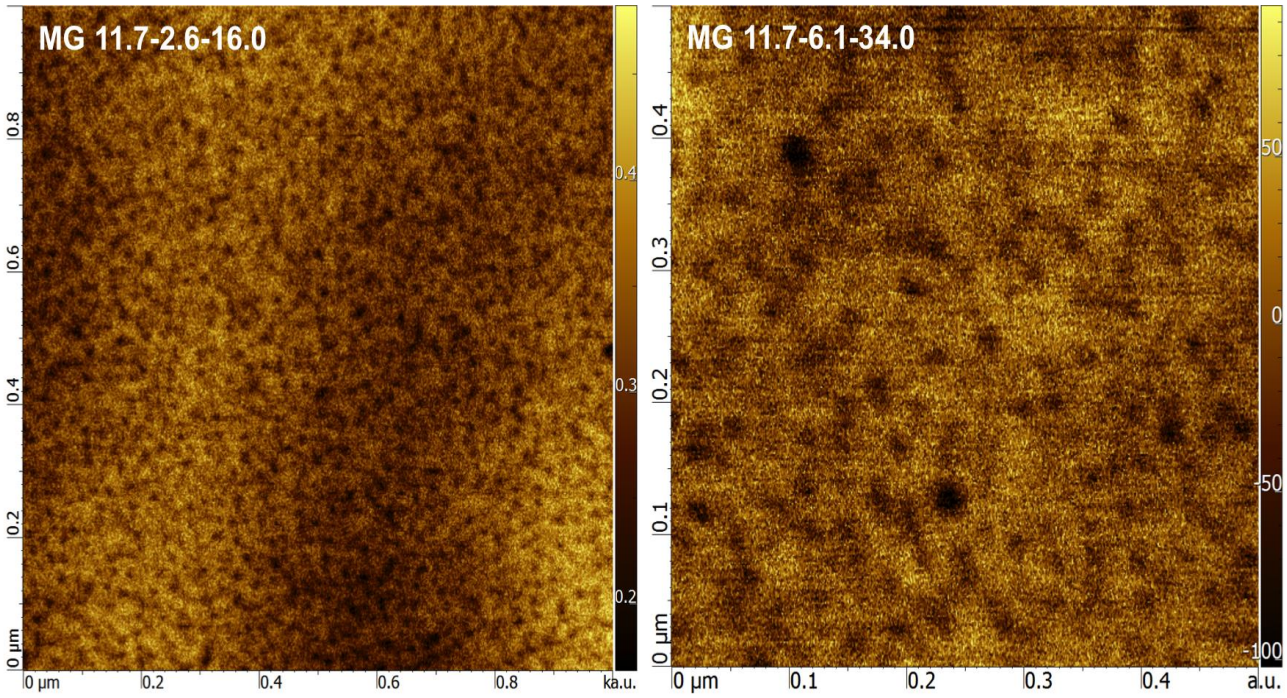

Figure 4.6 FMAMF images of MG 11.7-2.6-16.0 (left) and MG11.7-6.1-34.0 (right) depicting both regions of PnBA rich continuous matrix and PMMA rich domains

was observed as a result of the heterogeneity throughout the bulk material occurring from random branching and broad PDIs.

The images discussed throughout this chapter can also be correlated to results on the mechanical properties where the longer PMMA side chains demonstrate more defined regions of phase separation, producing superior strength and recovery as seen in DMA, rheology, and tensile testing. It was also shown that doubling the PMMA vol.% of the longer PMMA graft side chains resulted in only a slight increase in the mean domain size, ~4 nm, but the number of domains was greatly reduced. The reduction in the number of PMMA domains could lead to more densely packed and entangled PMMA aggregates which would result in the superior strength of the MG 11.7-6.1-34.0 reported in the previous chapter.

References

1. Leclère, P.; Lazzaroni, R.; Brédas, J. L.; Yu, J. M.; Dubois, P.; Jérôme, R. *Langmuir* **1996,** 12, (18), 4317-4320.

2. Riess, G.; Bahadur, P., *Encyclopedia of polymer science and engineering*. Wiley: New York, 1989; p 324.

3. Zhu, Y.; Burgaz, E.; Gido, S. P.; Staudinger, U.; Weidisch, R.; Uhrig, D.; Mays, J. W. *Macromolecules* **2006,** 39, (13), 4428-4436.

4. Beyer, F. L.; Gido, S. P.; Büschl, C.; Iatrou, H.; Uhrig, D.; Mays, J. W.; Chang, M. Y.; Garetz, B. A.; Balsara, N. P.; Tan, N. B.; Hadjichristidis, N. *Macromolecules* **2000,** 33, (6), 2039-2048.

5. Xenidou, M.; Beyer, F. L.; Hadjichristidis, N.; Gido, S. P.; Tan, N. B. *Macromolecules* **1998,** 31, (22), 7659-7667.

6. Schlegel, R.; Wilkin, D.; Duan, Y.; Weidisch, R.; Heinrich, G.; Uhrig, D.; Mays, J. W.; Iatrou, H.; Hadjichristidis, N. *Polymer* **2009,** 50, (26), 6297-6304.

7. Schlegel, R.; Staudinger, U.; Thunga, M.; Weidisch, R.; Heinrich, G.; Uhrig, D.; Mays, J. W.; Iatrou, H.; Hadjichristidis, N. *European Polymer Journal* **2009,** 45, (10), 2902-2912.

8. Staudinger, U.; Schlegel, R.; Weidisch, R.; Fritzsche, J.; Klüppel, M.; Heinrich, G.; Mays, J. W.; Uhrig, D.; Hadjichristidis, N. *European Polymer Journal* **2008,** 44, (11), 3790-3796.

9. Staudinger, U.; Weidisch, R.; Zhu, Y.; Gido, S. P.; Uhrig, D.; Mays, J. W.; Iatrou, H.; Hadjichristidis, N. *Macromolecular Symposia* **2006,** 233, (1), 42-50.

10. Milner, S. T. *Macromolecules* **1994,** 27, (8), 2333-2335.

11. Xenidou, M.; Hadjichristidis, N. *Macromolecules* **1998,** 31, (17), 5690-5694.

12. Hasegawa, H., Block Copolymers and Miktoarm Star-Branched Polymers. In *Anionic Polymerization: Principles, Practice, Strength, Consequences and Applications*, Hadjichristidis, N.; Hirao, A., Eds. Springer: Japan, 2015; pp 843-859.

13. Hadjichristidis, N.; Pispas, S.; Floudas, G., *Block Copolymers: Synthetic Strategies, Physical Properties, and Applications* . John Wiley & Sons, Hoboken : New Jersey, 2003.

14. Ma, J.; Lu, M.; Zhang, H. *Journal of Macromolecular Science, Part A* **2014,** 51, (4), 279-285.

15. Jang, Y.; Hirai, T. *Soft Matter* **2011,** 7, (22), 10818-10823.

16. Jang, Y.; Hirai, T. *Materials Sciences and Applications* **2011,** Vol.02No.03, 4.

17. Ruzette, A.-V.; Tencé-Girault, S.; Leibler, L.; Chauvin, F.; Bertin, D.; Guerret, O.; Gérard, P. *Macromolecules* **2006,** 39, (17), 5804-5814.

18. Bar, G.; Brandsch, R.; Whangbo, M.-H. *Langmuir* **1998,** 14, (26), 7343-7347.

19. Brandsch, R.; Bar, G.; Whangbo, M. H. *Langmuir* **1997,** 13, (24), 6349-6353.

20. Cleveland, J. P.; Anczykowski, B.; Schmid, A. E.; Elings, V. B. *Applied Physics Letters* **1998,** 72, (20), 2613-2615.

21. Magonov, S. N.; Elings, V.; Whangbo, M.-H. *Surface Science* **1997,** 375, L385-L391.

22. Jeusette, M.; Leclère, P.; Lazzaroni, R.; Simal, F.; Vaneecke, J.; Lardot, T.; Roose, P. *Macromolecules* **2007,** 40, (4), 1055-1065.

23. Chatterjee, D. P.; Mandal, B. M. *Macromolecules* **2006,** 39, (26), 9192-9200.

24. Tong, J. D.; Leclère, P.; Rasmont, A.; Brédas, J. L.; Lazzaroni, R.; Jérôme, R. *Macromolecular Chemistry and Physics* **2000,** 201, (12), 1250-1258.

25. Tong, J. D.; Jerôme, R. *Polymer* **2000,** 41, (7), 2499-2510.

26. Tong, J.-D.; Jerôme, R. *Macromolecules* **2000,** 33, (5), 1479-1481.

27. Leclère, P.; Moineau, G.; Minet, M.; Dubois, P.; Jérôme, R.; Brédas, J. L.; Lazzaroni, R. *Langmuir* **1999,** 15, (11), 3915-3919.

28. Tong, J. D.; Leclère, P.; Doneux, C.; Brédas, J. L.; Lazzaroni, R.; Jérôme, R. *Polymer* **2001,** 42, (8), 3503-3514.

29. Sriprom, W.; James, M.; Perrier, S.; Neto, C. *Macromolecules* **2009,** 42, (8), 3138-3146.

30. Tong, J. D.; Moineau, G.; Leclère, P.; Brédas; Lazzaroni, R.; Jérôme, R. *Macromolecules* **2000,** 33, (2), 470-479.

31. Lodge, T. P.; Hanley, K. J.; Pudil, B.; Alahapperuma, V. *Macromolecules* **2003,** 36, (3), 816-822.

32. Huang, C.-i.; Chapman, B. R.; Lodge, T. P.; Balsara, N. P. *Macromolecules* **1998,** 31, (26), 9384-9386.

33. Schön, P.; Bagdi, K.; Molnár, K.; Markus, P.; Pukánszky, B.; Julius Vancso, G. *European Polymer Journal* **2011,** 47, (4), 692-698.

34. Menshikov, E. A.; Bol'shakova, A. V.; Yaminskii, I. V. *Moscow University Physics Bulletin* **2009,** 64, (2), 166-171.

35. Raghavan, D.; VanLandingham, M.; Gu, X.; Nguyen, T. *Langmuir* **2000,** 16, (24), 9448-9459.

36. Kopp-Marsaudon, S.; Leclère, P.; Dubourg, F.; Lazzaroni, R.; Aimé, J. P. *Langmuir* **2000,** 16, (22), 8432-8437.

CHAPTER 5.

THE SYNTHESIS OF ALL-ACRYLIC MULTIGRAFT COPOLYMERS CONSISTING OF AMPHIPHILIC BLOCK SIDE CHAINS

Abstract

This chapter highlights the advantages of the grafting through approach of an acrylic macromonomer, synthesized using anionic polymerization, because of the ability to synthesize multigraft copolymers with three-phases where the side chains consist of an acrylic block copolymer. We demonstrate, using similar methodology as in chapter 2, the synthesis and characterization of poly(*n*-butyl acrylate)-*g*-poly(methyl methacrylate-b-*t*-butyl acrylate) and subsequently poly(*n*-butyl acrylate)-*g*-poly(methyl methacrylate-b-acrylic acid). The final material consists of the same rubbery backbone and branched architecture but with amphiphilic block side chains, where both blocks of the graft side chains exhibit a T_g >100 ^oC and phase separate from poly(*n*-butyl acrylate). All the materials were carefully characterized using nuclear magnetic resonance spectroscopy and size exclusion chromatography for their structural and compositional determination. Additionally, the thermal properties were investigated using thermogravimetric analysis and differential scanning calorimetry, and used to confirm the material's structure.

5.1 Introduction

All-acrylic copolymers consisting of rubbery and glassy segments are currently used as TPEs in the commercial market. One aspect that makes these materials attractive is the extensive library of usable acrylic monomers so that the desired properties such as oil or UV resistance and optical transparency can be retained while introducing the ability to further tailor physical properties like glass transition temperatures or to incorporate segments bearing functional groups to enhance the material's solubility and physical properties. This can be extremely attractive for industries that manufacture cross-linked acrylic materials because it can imbed UV or thermal cross-linking sites during the initial polymerization and will not require post-polymerization reactions or materials that increase cost and labor.

Currently in the commercial market companies like Arkema® have begun to produce functional triblock copolymers under their BlocBuilder® technology which has the capability to introduce and control the polymerization of a broad range of acrylate and methacrylate monomers. This enables the introduction of functional monomers into either the rubbery middle-block or the glassy end-blocks in a random arrangement. This produces the desired acrylic elastomer with tunable nanostructures and physical properties such as adhesion and absorbance. However, no branched architectures of all-acrylic compositions analogous to the above linear triblocks that incorporate functional monomers have been reported or demonstrated for use in TPE applications.

Our approach to producing all-acrylic multigraft copolymers using the grafting-through method of an anionically polymerized macromonomer enables us to synthesize a novel system that consists of amphiphilic diblock copolymers as the high T_g side chains. In this chapter, the synthesis of a poly(methyl methacrylate-*b*-*t*-butyl acrylate) (PMMA-*b*-P*t*BA) macromonomer in order to produce a poly(*n*-butyl acrylate)-*g*-poly(methyl methacrylate-*b*-acrylic acid) (P*n*BA-*g*-(PMMA-*b*-PAA)) multigraft copolymers will be discussed. The final all-acrylic branched architecture containing PMMA-*b*-PAA side chains was targeted to investigate both the changes in mechanical behavior and self-assembly. Physically, incorporating the hydrophilic PAA block provides the ability to retain the low Tg backbone and high Tg side chain composition, both PMMA and PAA have T_gs >100 ^oC, with an advantage of introducing a block that can increase the physical crosslinking in the glassy domains by secondary, non-covalent interactions. Also, from a morphological perspective, this approach attempts to create more defined phase boundaries between the glassy PMMA/PAA domains and the rubbery PnBA matrix, resulting from the larger Flory-Huggins interaction parameter for PAA/P*n*BA (χ=0.25), as compared to PMMA/P*n*BA (χ=0.044).[1, 2]

5.2 Experimental

5.2.1 Materials

Methyl methacrylate (MMA, Sigma-Aldrich, >99%), *t*-butyl acrylate (*t*BA, Sigma-Aldrich, >99%) *n*-butyl acrylate (*n*BA, Sigma-Aldrich, >99%), tetrahydrofuran (THF,

Sigma-Aldrich, ≥99%), 1,1-diphenylethylene (DPE, Sigma- Aldrich, >99%), benzene (Sigma-Aldrich, ≥99.9) and 1-(*tert*-butyldimethylsiloxy)-3-butyl lithium (*t*BDMS-Li, FMC Lithium) were all purified according to standards required for anionic polymerization as previously reported.[3-5] 2,2-Azobisisobutyronitrile (AIBN, Aldrich 90%) was recrystallized before use and the S-1-dodecyl-S'-(α,α'-dimethyl-α''-acetic acid)trithiocarbonate chain transfer agent (CTA) was synthesized following the procedure previously published by Lai et al.[6] The *tert*-butylammonium fluoride (Sigma-Aldrich, 1.0 M in THF) and *p*-toluenesulfonic acid monohydrate (Sigma-Aldrich, 98%) was used as received. Triethylamine (TEA, Sigma-Aldrich, 98%) and acryloyl chloride (Sigma-Aldrich, ≥97%) were distilled over CaH_2, stored over activated molecular sieves, and purged with Argon prior to use.

5.2.2 Synthesis of the PMMA-*b*-P*t*BA Macromonomer

The anionic polymerization to produce the PMMA-*b*-P*t*BA macromonomer was carried out in sealed, all-glass apparatus using well documented high-vacuum polymerization techniques.[7, 8] All the reagents in ampoules, including MMA, *t*BA, lithium chloride, DPE, and tBDMS-Li were attached to the reactor and introduced in the appropriate order after purging the reactor with a lithium-based washing solution. When constructing a diblock copolymer using sequential addition anionic polymerization the nucleophilicity of the living carbanion at the chain end of the first block must be greater in order to attack and begin the polymerization of the second block. The nucleophilicity

of most acrylates are similar so in this case both MMA and *t*BA can be initiated by the other, however, according to literature the yield is higher when using PMMA as the first block, and why we chose to follow that methodology.[9-13] The polymerization was performed in dry THF in a -78 ^{o}C acetone/dry ice bath. The polymerization of PMMA was initiated using a silyl-protected alkyl-lithium in order to yield a chain end functional group functional site for subsequent post-polymerization reactions.[3-5] Prior to the introduction of MMA, the solution was a deep red color that is indicative of the living diphenylethyllithium species and becoming a pale yellow color with after the initiation of the MMA monomer. After 1h the *t*BA ampoule was cooled to -78 ^{o}C and the monomer was quickly introduced into the reactor. The living PMMA-*b*-P*t*BA was quenched with methanol after a total reaction time of 2 h and precipitated in a methanol/water (10:3) solution, and vacuum dried overnight at 60 ^{o}C.

The synthetic procedure for producing hydroxyl-terminated PMMA-*b*-P*t*BA was performed by the simple desilylation reaction of the protecting group with excess tetrabutylammonium fluoride in dry THF for 18 h. The reaction took place under argon purge at room temperature. The resulting polymer was purified by removal of THF solvent and re-dissolving it into chloroform for removal of salt and excess tetrabutylammonium fluoride by liquid-liquid extraction using chloroform and water. The hydroxyl-terminated block copolymer was then re-precipitated and dried in the vacuum-oven overnight.

The final step utilized the nucleophilic addition/elimination reaction between

acryloyl chloride and the terminal alcohol present on the chain, in the presence of TEA. The dried polymer from the previous step was re-dissolved using dry THF from the vacuum line and purged with argon atmosphere. Slight excess stoichiometric amounts of TEA and acryloyl chloride were syringed in according to the calculated amount of hydroxyl-functionalized chain ends (-OH:TEA:acryloyl chloride, 1:1.5:1.5). The reaction was performed at room temperature and allowed to react for 18 h. Again, the excess TEA and salt produced was removed using a chloroform-water extraction and followed by freeze drying the polymer using benzene. This three step synthetic methodology produced quantitative yields of well-defined PMMA-*b*-P*t*BA chains with a terminal polymerizable head group.

5.2.3 Synthesis of P*n*BA-*g*-(PMMA-*b*-PAA)

Initially the PnBA-*g*-(PMMA-*b*-P*t*BA) multigraft copolymer was successfully synthesized by RAFT radical polymerization using a trithiocarbonate chain transfer agent. The PMMA-b-P*t*BA macromonomer, *n*BA, AIBN, and CTA reagents, were added to a single-neck round-bottom flask, capped with a rubber septum, equipped with a single side-arm with a stopcock and male glass joint and dissolved in 15 -20 mL of benzene. The polymer/solution mixture was placed on the high-vacuum line and subjected to 3 freeze/thaw cycles. After the last freeze/thaw cycle the mixture was sealed using the stopcock, warmed to room temperature, placed under slight argon positive pressure, and then removed from the vacuum line. The apparatus was then

place into a 75 ^{o}C oil bath and stirred vigorously. The reaction time was between 36-48 h and terminated by introducing a 1 mL of methanol and rapidly cooling the reaction mixture with an ice bath for 5 minutes.

The purification of the newly synthesized multigraft copolymers was performed by adding THF to the solution, in order to reduce the viscosity of the reaction solution, and precipitating drop-wise into excess methanol. This procedure was performed twice; the first solution discarded will be milky in nature and contain partially soluble unreacted macromonomer while the second methanol precipitation yields a transparent discard solution. The pale yellowish, transparent material was then dried in the vacuum oven overnight at 60^{o}C. A small amount ~100 mg of PnBA-*g*-(PMMA-*b*-P*t*BA) multigraft copolymers was for characterization and the rest was used for the final step of the synthesis to obtain the all-acrylic multigraft copolymer with amphiphilic side chains.

The last step of the synthesis was to cleave the pendant *t*-butyl group of the P*t*BA block portion of the graft side chains in order to obtain the desired alcohol functionality. This step was performed according to previous literature where excess *p*-toluenesulfonic acid was introduced to the multigraft copolymer/toluene solution in a distillation apparatus. The solution was then heated to slight reflux, ~110 ^{o}C, where the solution went from cloudy to transparent and left for 24 h. After allowing the solution to cool to room temperature, where the newly formed toluenesulfonic salt precipitated out, the solution was filtered and the excess toluene solvent was removed on the rotary vacuum. The polymer mixture was then dissolved in chloroform to purify by chloroform-

water extraction and dried under vacuum at 60 ^{o}C for several days. The final product was a yellowish transparent material.

5.3 Characterization

Number-average molecular weights M_n and polydispersity indices M_w/M_n (PDI) of all samples were determined by size exclusion chromatography using a Polymer Labs GPC-120 unit equipped with a Precision Detector PD2040 (two-angle static light scattering detector), a Viscotek 220 differential viscometer, and a Polymer Labs differential refractometer. The elution solvent was THF with a flow rate of 1 ml/min at 40 ^{o}C. The column set is Polymer Labs PLgel; 7.5 x 300 mm; 10 µm; 500; 10E3, 10E5, and 10E6 Å. The calibration range was 600 to 7,500,000 g/mol using PMMA standards. Reported molecular weights were determined by light scattering using reported dn/dc values PMMA-b-P*t*BA and P*n*BA-*g*-(PMMA-*b*-P*t*BA) samples, the refractive indices used were 0.087 mL/g for PMMA, 0.0512 mL/g for P*t*BA, and 0.085 mL/g for P*n*BA.[14-17] The dn/dc value for the diblock and terpolymers were calculated using the expression:

$$(dn/dc)_{terpolymer} = x\,(dn/dc)_A + y\,(dn/dc)_B + z\,(dn/dc)_C$$

where x, y, and z are the weight fractions of the A, B, and C components calculated by ^{1}H-NMR.[18]

^{1}H-NMR spectroscopy was performed on a Varian Mercury 500 MHz spectrometer using $CDCl_3$ as a solvent.

The T_g of each multigraft copolymer, precursor macromonomer, and linear P*n*BA analog was determined by a TA Instruments Q-1000 differential scanning calorimetry (DSC) from a temperature range of -80 ^oC to 150 ^oC, at a heating rate of 10 ^oC/min, and 2 minute isothermal holds at the minimum and maximum temperatures. The reported T_g was measured on the second of three scan cycles.

The thermal stability and decomposition thermogram were obtained for each multigraft copolymer, precursor macromonomer, and linear P*n*BA analog on a TA Instruments Q-50 TGA. A 10-20 mg sample was placed in a platinum pan and equilibrated at 30 ^oC. The temperature ramp rate was set to 10 ^oC/min over the range of 30-600 ^oC under nitrogen atmosphere.

5.4 Results and Discussion

5.4.1 PMMA-*b*-P*t*BA Macromonomer

The PMMA-*b*-P*t*BA macromonomer was synthesized by anionic polymerization under high vacuum by glass-blowing techniques. The desired block copolymer was obtained by using sequential polymerization of MMA followed by the introduction of the second *t*BA monomer in THF at -78 ^oC. Scheme 5.1 shows the polymerization methodology, as well as, the post-polymerization reactions to produce the PMMA-*b*-P*t*BA with a M_n of 9.6 kg/mol and a P.D.I. of 1.04 calculated by SEC, and exhibiting the desired vinyl head-group capable of copolymerizing using the grafting-through approach.

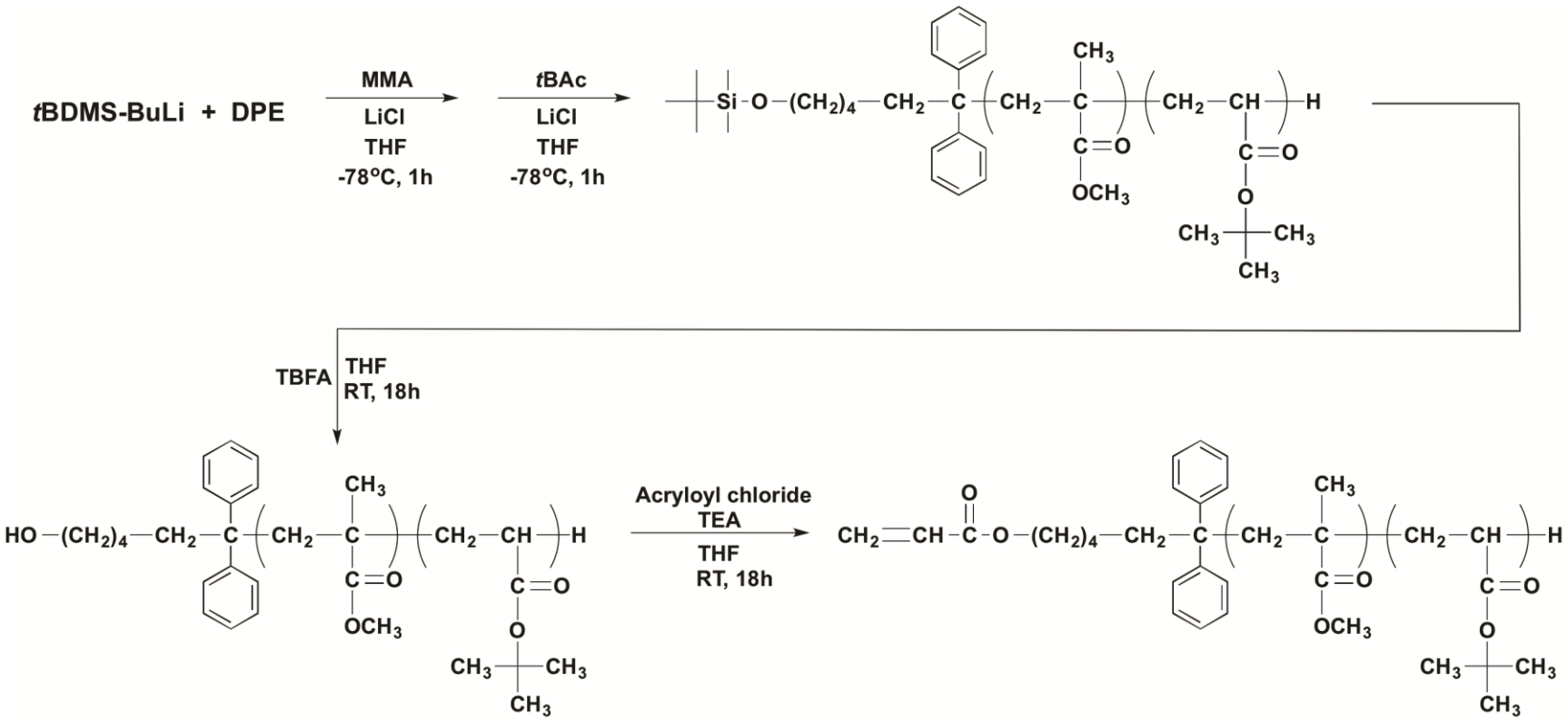

Scheme 5.1. Synthetic procedure for PMMA-*b*-P*t*BA and macromonomer PMMA-*b*-P*t*BA

The newly synthesized macromonomer was initially characterized using ^{1}H-NMR to confirm the successful polymerization of the diblock copolymer, calculate the mole percentage (mol.%) of each acrylic block, and view manipulation of the polymer chain end to produce the block macromonomer. Figure 5.1 shows the NMR spectra of the terminal silyl-protected PMMA-*b*-P*t*BA (black), the hydroxyl terminated PMMA-*b*-P*t*BA (blue), and the PMMA-*b*-P*t*BA macromonomer (red). Additionally, the PMMA-*b*-P*t*BA with the silyl-protected initiator was used to calculate the mol. % of each block by integrating the area under the pendent *t*-butyl group signal (9 H's) of the P*t*BA block at 1.43 ppm and the methoxy signal (3 H's) of the PMMA block at 3.59 ppm. The mol.% calculated the block ratio to be 66.1 % for PMMA and 33.9 % of P*t*BA, corresponding to a M_n of 6.1 kg/mol and 3.5 kg/mol for PMMA and P*t*BA respectively. The figure also shows the desired disappearance of the Si-$(CH_3)_2$ protons at 0.00 ppm and the appearance of the vinyl signals between 5.80 and 6.20 ppm corresponding to the double bond present at the initiating chain end.

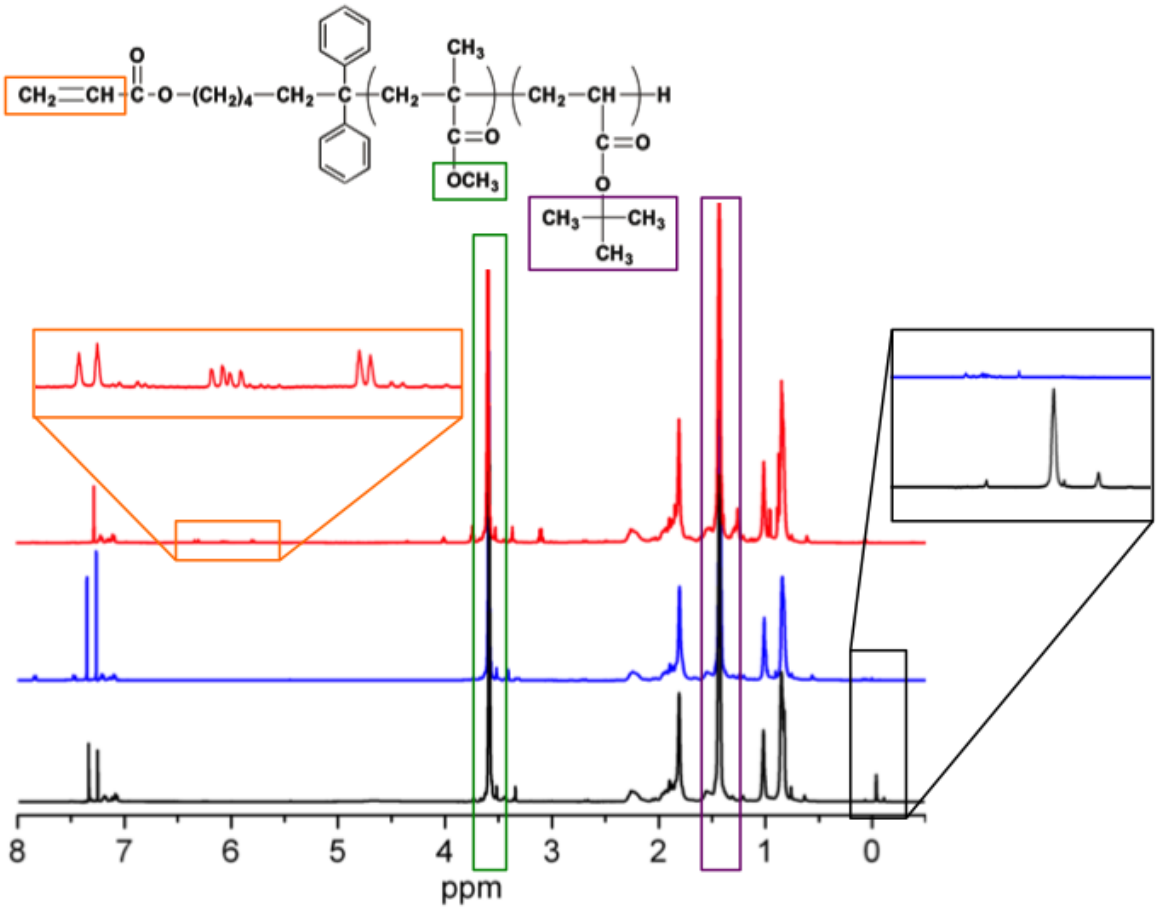

Figure 5.1. ^{1}H-NMR spectra of the synthesized silyl-protected PMMA-*b*-P*t*BA (black), HO-PMMA-*b*-P*t*BA (blue), and MM-PMMA-*b*-P*t*BA (red). The enlarged portions are to display the disappearance of the silyl-protecting group (black box) and the appearance of the vinyl double bond of the macromonomer head group (orange box)

5.4.2 All-Acrylic Multigraft Copolymers with Amphiphilic Graft Chains

The all-acrylic multigraft copolymers with PMMA-*b*-PAA side chains were synthesized by RAFT polymerization of *n*BA and the PMMA-*b*-P*t*BA macromonomer using the grafting-through approach, followed by the post-polymerization reaction to cleave the *t*-butyl group to convert this block to the desired PAA composition (Scheme 5.2). The molecular weight and polydispersity were obtained by SEC equipped with light scattering detectors and can be viewed in Figure 5.2 where both the PnBA-*g*-(PMMA-*b*-P*t*BA) and PMMA-*b*-P*t*BA macromonomer are presented. The precursor multigraft copolymer was used for molecular weight determination for two reasons, the first is to more accurately calculate and monitor the chain growth when compared to the macromonomer since it also exhibits the same composition and secondly to reduce the interaction with the silica gel columns that is generally experienced with polar functional groups, such as pyridines and alcohols, when using THF as the mobile phase.[19, 20] The calculated M_n and PDI are 83.4 kg/mol and 1.67, respectively.

The compositions of the multigraft copolymers were determined by ^{1}H-NMR and represented in Figure 5.3. The spectra initially allowed for the qualitative incorporation of the PMMA-*b*-P*t*BA graft side chains seen by the characteristic signals of the *t*-butyl pendent group signal at 1.43 ppm of the P*t*BA block and the methoxy signal at 3.59 ppm of the PMMA block present in the PMMA-*b*-P*t*BA macromonomer (black spectrum)

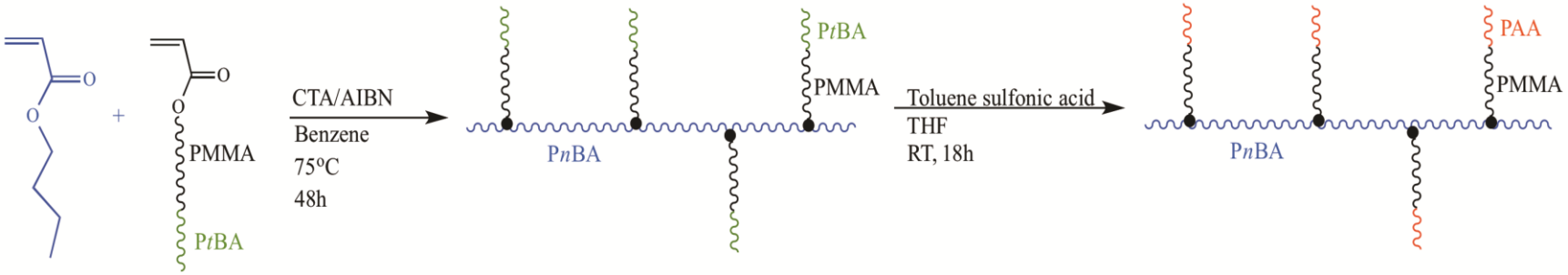

Scheme 5.2. The synthetic procedure of grafting through using the anionically polymerized PMMA-*b*-P*t*BA macromonomer to produce PnBA-*g*-(PMMA-*b*-P*t*BA) and the hydrolysis reaction to produce PnBA-*g*-(PMMA-*b*-PAA).

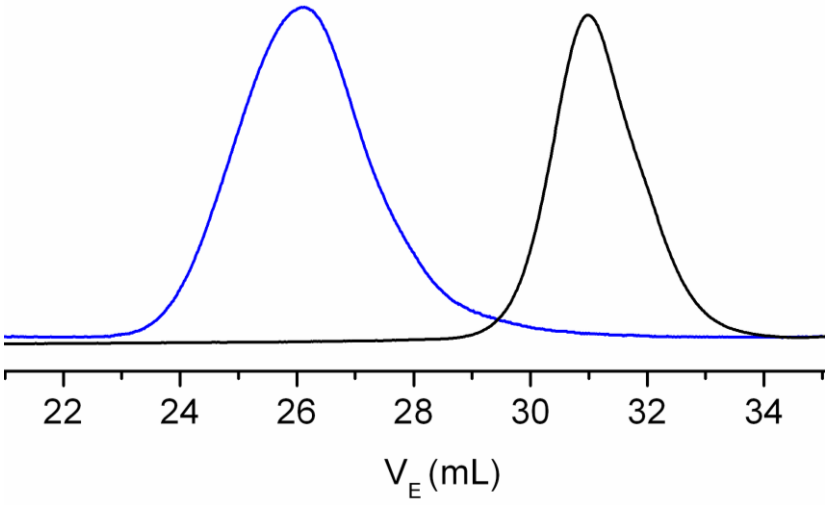

Figure 5.2. SEC of PnBA-*g*-(PMMA-*b*-P*t*BA) (blue) and the MM-PMMA-*b*-P*t*BA precursor (black).

matches that of the P*n*BA-*g*-(PMMA-*b*-P*t*BA) (blue spectrum). Additionally, in the P*n*BA-*g*-(PMMA-*b*-PAA) spectrum (red) the disappearance of the $C(CH_3)_3$ signal indicates the quantitative cleaving of the *t*-butyl pendant group to yield the COOH functional group, thus converting the second block of the graft side chains to PAA. More specifically, the P*n*BA-*g*-(PMMA-*b*-P*t*BA) spectrum (blue) allowed for the calculation of other necessary parameters such as average number of branch point junctions and volume percent (vol.%) of each component by integrating the methoxy proton signal of PMMA at 3.59 ppm) to that of the β-CH2- proton signal at 3.84 ppm of the PnBA backbone. The results are seen in Table 5.1.

The thermal properties were investigated for the PMMA-*b*-P*t*BA and PMMA-*b*-PAA multigraft materials, as well as the corresponding block macromonomers and linear PnBA analog, to not only gain insight into their thermal stability but to obtain additional confirmation that the desired MGCP had been synthesized. Initially, DSC was performed to accurately characterize the glass transition temperature for the overall material and to see if the T_gs corresponding to the side chains are visible. Figure 5.4 shows the DSC thermograms of the P*n*BA-*g*-(PMMA-*b*-P*t*BA) and P*n*BA-*g*-(PMMA-*b*-PAA) multigraft copolymers where the T_g of the rubbery backbone is clearly visible around -50 ^oC is each sample. In order to investigate the presence of the PtBA, PAA, and PMMA blocks the region from 35 to 145 ^oC was enlarged in Figure 5.5, where both the PMMA-*b*-P*t*BA and PMMA-*b*-PAA macromonomers (top), as well as, the P*n*BA-*g*-(PMMA-*b*-P*t*BA) and P*n*BA-*g*-(PMMA-*b*-PAA) multigraft copolymers (bottom).

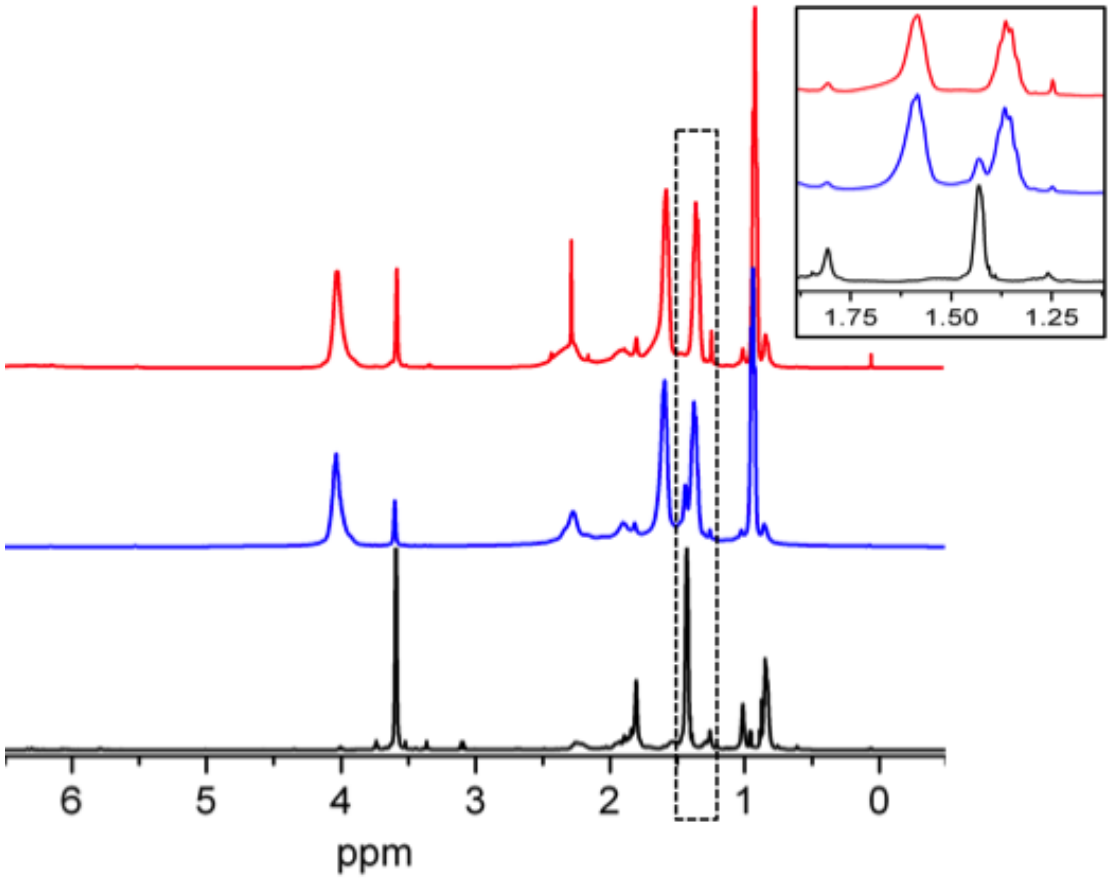

Figure 5.3. 1H-NMR of the PMMA-*b*-P*t*BA macromonomer (black), the P*n*BA-*g*-(PMMA-*b*-P*t*BA) multigraft copolymer (blue), and the P*n*BA-*g*-(PMMA-*b*-PAA) multigraft copolymer (red). The enlarged portion illustrates the disappearance of the *t*-butyl pendent group after the post polymerization hydrolysis reaction.

Table 5.1. Molecular composition of the PMMA-b-PtBA macromonomer and the resulting Multigraft Copolymers

				Multigraft Copolymer		
Sample I.D.[a]	Graft Chain M_n[b] (kg/mol)	Volume Percent[c] (%)		M_p[d] (kg/mol)	PDI[e]	#[f]
MM PMMA-*b*-P*t*BA	**9.7**	**56.54**	**43.46**	**-**	**-**	**-**
MG PMMA-*b*-P*t*BA	**9.7**	**13.22**	**10.16**	**153.4**	**1.67**	**3.6**
MG PMMA-*b*-PAA		**13.97**	**5.03**			

[a]The sample identification corresponds to either the macromonomer (MM) or the multigraft copolymer (MG) and the corresponding block copolymer side chain. [b]The number average molecular weight calculated by SEC. [c]The calculated volume percent of PMMA (first column) and P*t*BA or PAA (second column) using NMR. [d]Peak maximum molecular weight calculated by SEC. [e]Polydispersity index calculated by SEC. [f]The average number of branch point junctions calculated by a combination of NMR and SEC.

The plot of the PMMA-*b*-P*t*BA macromonomer (top, blue line) exhibits a T_g for each block at 46.3 ^oC and 101.8 ^oC for P*t*BA and PMMA respectively. After cleaving the *t*-butyl pendent group using *p*-toluenesulfonic acid, to yield PMMA-*b*-PAA, the Tg at 46.3 ^oC is no longer present and the high T_g region was broadened and the median temperature increased to 112.3 ^oC, resulting from the overlap of the PMMA and the PAA block transition temperature. The enlarged region corresponding to P*n*BA-*g*-(PMMA-*b*-P*t*BA) and P*n*BA-*g*-(PMMA-*b*-PAA) materials do not clearly definitively depict the T_gs for the blocks of the graft side chains, which is often reported for graft architectures as a result of phase blending, side chain length, and mole ratio of the side chain monomer to the backbone monomer.[21-24] However, there seems to be a slight change in the slope around 55 ^oC in the P*n*BA-*g*-(PMMA-*b*-P*t*BA) sample (bottom, blue line) that is not present in the P*n*BA-*g*-(PMMA-*b*-PAA) sample (bottom, black line) that would match that of the transition displayed by the linear side chain thermograms.

TGA was used to investigate the thermal stability of the multigraft materials and compared to that of the block macromonomers. Figure 5.6 depicts the percent weight loss versus temperature for the P*n*BA-*g*-(PMMA-*b*-P*t*BA) and the P*n*BA-*g*-(PMMA-*b*-PAA) plotted over their corresponding block copolymer side chains. It is immediately visible that the *t*-butyl group degrades very quickly around 220 ^oC and leaves a very sharp loss in weight with the remainder of the PMMA-*b*-P*t*BA polymer and P*n*BA-*g*-(PMMA-*b*-P*t*BA) occurring over 300 to 430 ^oC, while the PMMA-*b*-PAA and P*n*BA-*g*-(PMMA-*b*-PAA) polymers degrade over a gradual three step process at temperatures of

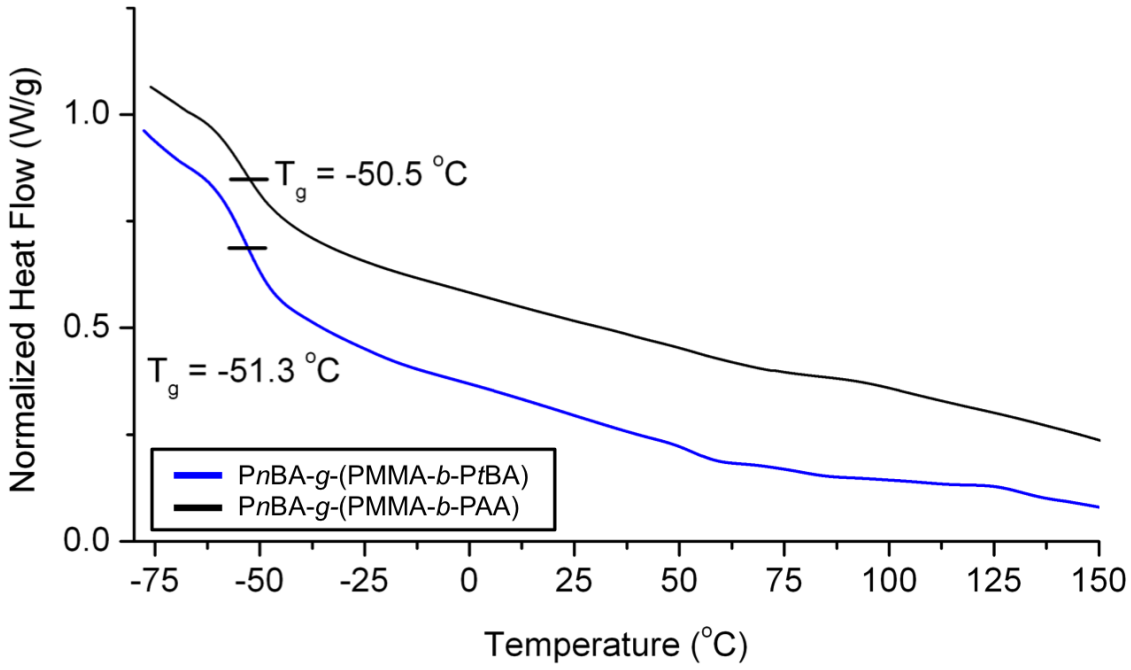

Figure 5.4. DSC thermogram of the synthesized P*n*BA-*g*-(PMMA-*b*-P*t*BA) (blue) and P*n*BA-*g*-(PMMA-*b*-PAA) (black). The major T_g of the rubbery PnBA is visibly present and indicated around -50 °C.

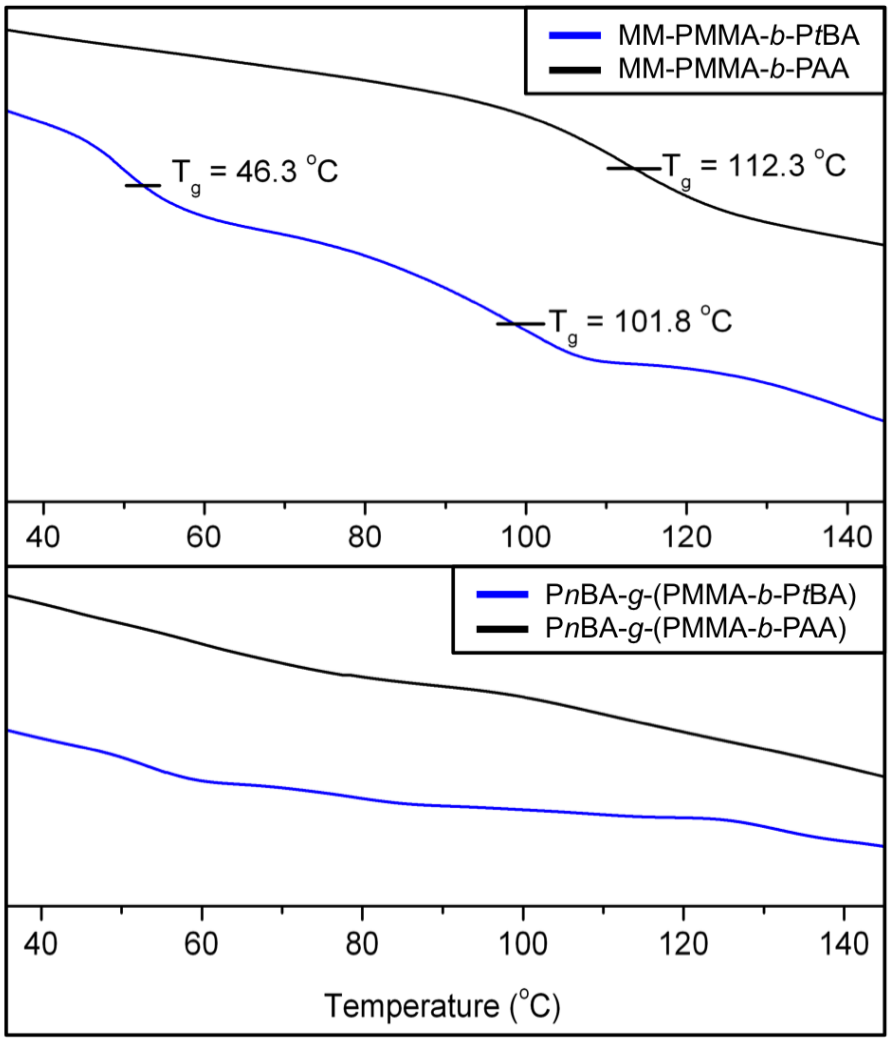

Figure 5.5. Enlarged and zoomed region of the DSC thermogram of the poly(PMMA-*b*-P*t*BA) (top, blue line) and poly(PMMA-*b*-PAA) (top, black line) macromonomers and the P*n*BA-*g*-(PMMA-*b*-P*t*BA) (bottom, blue line) and P*n*BA-*g*-(PMMA-*b*-PAA) (bottom, black line) multigraft materials.

200-275 °C and the remainder from 300 to 430 °C. Additionally, the same trend can be seen in the derivative weight loss versus temperature in Figure 5.7, further confirming the incorporation the PMMA-*b*-P*t*BA macromonomer and the cleaving of the *t*-butyl group to yield the MGCP with amphiphilic grafted side chains.

5.5 Conclusion

All-acrylic multigraft copolymers composed of block copolymer side chains were synthesized using the same reaction strategy as that employed for the first generation PnBA-*g*-PMMA materials, but by using a PMMA-*b*-P*t*BA macromonomer synthesized by sequential addition using anionic polymerization. We have demonstrated the wide variety of all-acrylic compositions that can be incorporated into these multigraft terpolymer TPEs. By using RAFT polymerization we were able to produce a branched polymer which incorporated multiple branch point junctions per chain and reached ~100 kg/mol, with a fairly narrow PDI. The MGCP and the precursor materials were characterized using NMR, SEC, DSC, and TGA to not only qualitatively show the incorporation of the block macromonomer into the polymer backbone, but to also calculate molecular weight, volume fraction of each component, and number of branch points per MGCP.

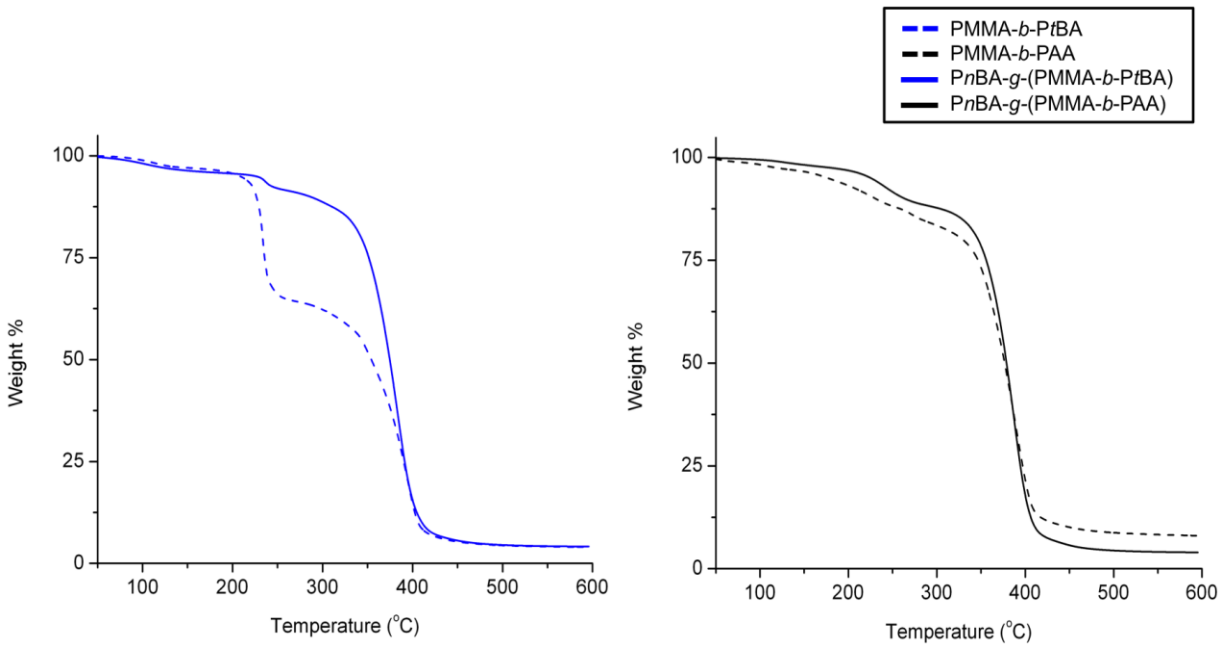

Figure 5.6. TGA thermogram of the poly(PMMA-*b*-P*t*BA) macromonomer and P*n*BA-*g*-(PMMA-*b*-P*t*BA) multigraft copolymer overlay (left) and the poly(PMMA-*b*-PAA) macromonomer and P*n*BA-*g*-(PMMA-*b*-PAA) multigraft copolymer overly (right).

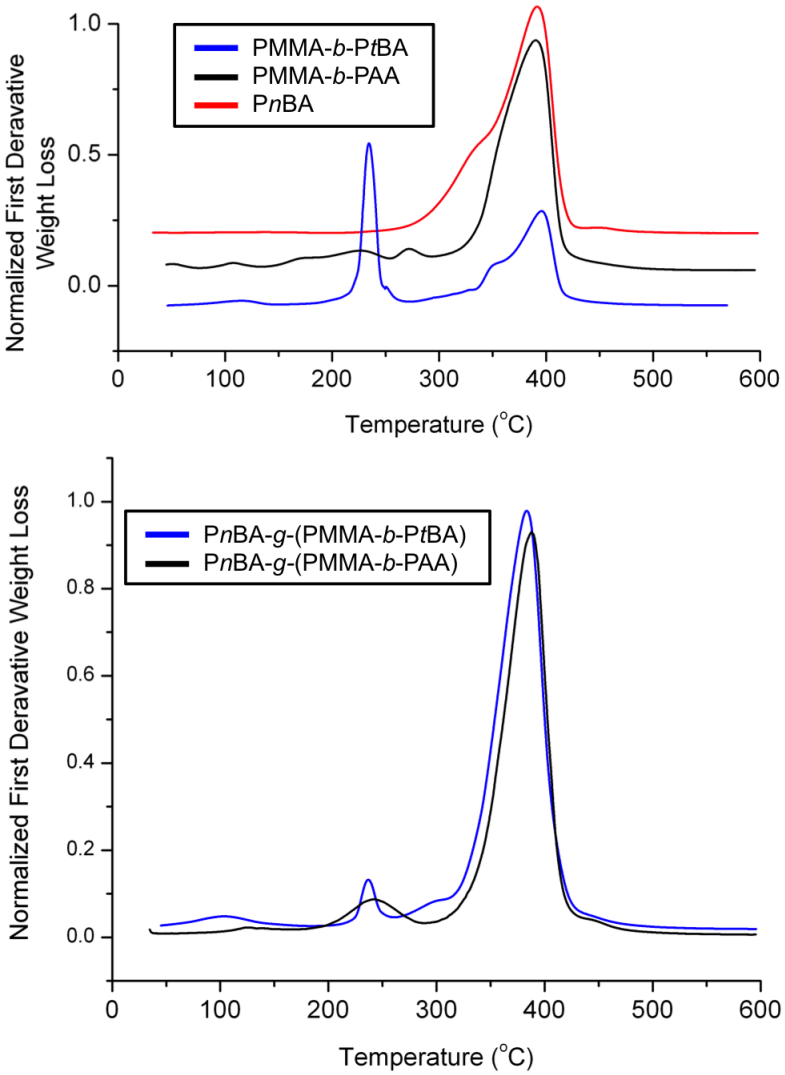

Figure 5.7. TGA thermogram of the derivative weight loss versus temperature of the precursor macromonomers and the PnBA backbone analog (top) and both the P*n*BA-*g*-(PMMA-*b*-P*t*BA) and P*n*BA-*g*-(PMMA-*b*-PAA) (bottom) to show the disappearance of the sharp t-butyl degradation peak after the hydrolysis reaction.

References

1. Sriprom, W.; James, M.; Perrier, S.; Neto, C. *Macromolecules* **2009,** 42, (8), 3138-3146.

2. Jacquin, M.; Muller, P.; Talingting-Pabalan, R.; Cottet, H.; Berret, J. F.; Futterer, T.; Théodoly, O. *Journal of Colloid and Interface Science* **2007,** 316, (2), 897-911.

3. Dhara, M. G.; Sivaram, S. *Journal of Macromolecular Science, Part A* **2009,** 46, (10), 983-988.

4. Dhara, M.; Sivaram, S.; Baskaran, D. *Polymer Bulletin* **2009,** 63, (2), 185-196.

5. Dhara, M. G.; Baskaran, D.; Sivaram, S. *Journal of Polymer Science Part A: Polymer Chemistry* **2008,** 46, (6), 2132-2144.

6. Lai, J. T.; Filla, D.; Shea, R. *Macromolecules* **2002,** 35, (18), 6754-6756.

7. Uhrig, D.; Mays, J. W. *Journal of Polymer Science Part A: Polymer Chemistry* **2005,** 43, (24), 6179-6222.

8. Hadjichristidis, N.; Xenidou, M.; Iatrou, H.; Pitsikalis, M.; Poulos, Y.; Avgeropoulos, A.; Sioula, S.; Paraskeva, S.; Velis, G.; Lohse, D. J.; Schulz, D. N.; Fetters, L. J.; Wright, P. J.; Mendelson, R. A.; García-Franco, C. A.; Sun, T.; Ruff, C. J. *Macromolecules* **2000,** 33, (7), 2424-2436.

9. Kaditi, E.; Mountrichas, G.; Pispas, S. *European Polymer Journal* **2011,** 47, (4), 415-434.

10. Hadjichristidis, N.; Pispas, S.; Floudas, G., Block Copolymer Applications. In *Block Copolymers*, John Wiley & Sons, Inc.: 2003; pp 383-408.

11. Hadjichristidis, N.; Pispas, S.; Floudas, G., *Block Copolymers: Synthetic Strategies, Physical Properties, and Applications* . John Wiley & Sons, Hoboken : New Jersey, 2003.

12. Varshney, S. K.; Jacobs, C.; Hautekeer, J. P.; Bayard, P.; Jerome, R.; Fayt, R.; Teyssie, P. *Macromolecules* **1991,** 24, (18), 4997-5000.

13. Baer, M. *Journal of Polymer Science Part A: General Papers* **1964,** 2, (1), 417-436.

14. Podzimek, S., *Light Scattering, Size Exclusion Chromatography and Asymmetric Flow Field Flow Fractionation: Powerful Tools for the Characterization of Polymers, Proteins and Nanoparticles*. Wiley: 2011.

15. Mrkvičková, L.; Pokorná, V.; Pecka, J. *Macromolecular Symposia* **2000,** 162, (1), 227-234.

16. Hiorns, R. *Polymer International* **2000,** 49, (7), 807-807.

17. Helmstedt, M.; Gast, K., *Data Evaluation in Light Scattering of Polymers*. Wiley: 2000.

18. Iatrou, H.; Hadjichristidis, N. *Macromolecules* **1992,** 25, (18), 4649-4651.

19. Wu, C. S., *Handbook Of Size Exclusion Chromatography And Related Techniques: Revised And Expanded*. CRC Press: 2003.

20. Cazes, J. *Journal of Chemical Education* **1970,** 47, (7), A461.

21. Wang, W.; Wang, W.; Li, H.; Lu, X.; Chen, J.; Kang, N.-G.; Zhang, Q.; Mays, J. *Industrial & Engineering Chemistry Research* **2015,** 54, (4), 1292-1300.

22. Li, H.; Wang, W.; Li, C.; Tan, J.; Yin, D.; Zhang, H.; Zhang, B.; Yin, C.; Zhang, Q. *Journal of Colloid and Interface Science* **2015,** 453, 226-236.

23. Nicolas, J.; Ruzette, A.-V.; Farcet, C.; Gérard, P.; Magnet, S.; Charleux, B. *Polymer* **2007,** 48, (24), 7029-7040.

24. Mijović, J.; Sun, M.; Pejanović, S.; Mays, J. W. *Macromolecules* **2003,** 36, (20), 7640-7651.

CHAPTER 6.

CONCLUDING REMARKS AND FUTURE WORK

Abstract

Throughout the last four chapters we have tried to systematically understand all-acrylic TPEs and furthermore what advantages are displayed by altering the architecture of the traditional linear MAM triblock copolymers. The initial step is to synthesize multigraft materials and illustrate how the synthetic procedure allows a level of control over composition and degree of branching for the bulk material. From here we were able to begin investigating what effect the glassy side chains would have on the mechanical properties of the material and in turn how this was correlated to the morphology displayed using AFM. After obtaining insight into the structure-property relationship of the simplest all-acrylic multigraft structure, we targeted a three-phase system where the glassy side chains were composed of block copolymers which both had a Tg >100 ^{o}C but with different side chain polarity, which was achieved and demonstrates the versatility of the all-acrylic system and of the synthetic approach. Our work here serves to be the basis of future targeted compositions and architectures of multigraft copolymers in order to obtain, and tailor, recyclable materials for uses as elastic and impact resistant applications. Concluding remarks and future direction will be discussed in this chapter.

6.1 Concluding Remarks

As stated in the introduction, there are currently thermoplastic elastomers in the commercial market based on the linear triblock copolymers, with the examples of SIS, SBS, and MAM being the most prevalent. Although the stiffness and elongation of the all-acrylic materials are not comparable to the values seen in SIS TPEs, it has been demonstrated previously in the literature and throughout this dissertation that manipulating the architecture of the general ABA linear analog results in improvements of both the elongation and strength of the material. Future attention to optimizing and producing new materials of this type must be diligently investigated as a result of commercial demands and the available niche market for novel, and superior, technologies based on non-chemically cross-linked TPEs.

The initial goal for this project was to demonstrate a synthetic procedure that can produce all-acrylic branched materials with the ability to alter the composition, structure, extend to include additional blocks and/or functional units, and to yield enough material to undergo thorough mechanical characterization; which usually requires multiple grams of material. In chapters 2 and 5 we have shown that the use of anionic and controlled radical polymerization to produce the acrylic macromonomer and the randomly branched all-acrylic structure *via* the grafting through approach to be successful in achieving all of the desired synthetic goals. In addition to the synthesis, this methodology also allowed for in depth structural and compositional characterization by NMR, GPC, viscometry, and MALDI-TOF, allowing for the quantification of volume

fractions, branch point incorporation, molecular weights, and molecular weight distributions. Additionally, DSC and TGA were employed to confirm the presence of each domain and to establish the materials' thermal characteristics, more specifically T_gs and degradation temperatures, which are prerequisites to mechanical testing and annealing conditions for morphology studies.

The characterization of the bulk mechanical properties exhibited by the all-acrylic multigraft samples was performed by DMA, rheology, and tensile testing to investigate the strength and elasticity, and their dependence on the side chain molecular weight, number of branch point junctions, and volume ratio between the plastic and elastic phases. The results obtained by DMA and rheology both illustrate the importance of higher molecular weight PMMA side chains to both increase the films stiffness and extend the working temperature range by roughly 25 ^{o}C. Furthermore, tensile testing confirmed the thermoplastic elastomer behavior and again showed increased stiffness with increasing PMMA content.

AFM was used to observe the presence of phase separation and to understand the role of morphology in regards to the observed mechanical properties. AFM was able to detect the presence of phase separation between the PMMA side chains and the PnBA backbone by mapping the elastic moduli of the plastic nanoscale domains and the continuous rubbery matrix. The results showed that the longer PMMA side chain produces more defined phase boundaries with more densely packed hard domains when compared to the shorter, 5.3 kg/mol, PMMA graft side chains as a result of

increasing the χN value. Additionally, by increasing the PMMA vol.% of the larger molecular weight PMMA side chain the mean domain size remained relatively constant, but did result in fewer hard domains present over the probed area. Work included in the morphology section, chapter 4, is on-going and we intend to support the AFM results with TEM and SAXS through collaboration to definitively report the bulk morphology and phase domain characteristics of the all-acrylic multigraft copolymer system reported in this dissertation.

In conclusion this project has been successful in synthesizing all-acrylic multigraft copolymers with trifunctional branch point junctions, along with conducting a fundamental investigation into the influence of compositional and branching parameters on their physical properties and morphology. We have also shown how TPEs made of acrylic monomers have the additional obstacles of higher entanglement molecular weights of the rubbery phase and the less favorable Flory-Huggins interaction parameter, when compared to isoprene-styrene systems, which results in materials with very distinct mechanical properties. However, manipulating the molecular architecture has resulted in an increase in the materials performance and allows for novel structures and compositions to be aspired to.

6.2 Future Work

The versatile approach to produce all-acrylic branched materials using the grafting through approach demonstrated in this dissertation and the large library of

available acrylates will lead to more complex architectures to enhance the desired physical properties exhibited by acrylic containing TPEs. The immediate focus will be on synthesizing a catalog of multigraft materials containing amphiphilic side chains and characterizing their physical properties and bulk morphologies. Additionally, in chapter 5 we highlighted the ability to synthesize the block macromonomer using sequential addition and that the acrylic monomer order is not restricted. This allows the ability to investigate the effect of the difference of the hydrophilic block of the side chain in relation to the backbone by synthesizing a PAA-b-PMMA macromonomer, with similar volume fraction to the PMMA-b-PAA macromonomer, and subsequently comparing their physical properties and morphology.

The second focus will be on attempts to produce an all-acrylic multigraft copolymer with the ‘centipede’ architecture by synthesizing a difunctional (double tailed) macromonomer. The increase in number of PMMA side chains at a branch point junction should increase the strength of the material by enhancing the physical cross linked domains and allowing to increase the PMMA vol. % without having to interrupt the molecular weight of the backbone between branch point junctions. The successful production of a multifunctional macromonomer would again allow for seemingly endless opportunities to expand the available catalog of all-acrylic TPEs in order to produce well-tailored materials based on the fundamental, and systematic, changes in composition and architecture. All in all, we expect all-acrylic TPEs to continue in the

direction of tailoring architecture and the incorporation of functional monomer segments guided by what is currently being produced and used in the commercial market.

VITA

Andrew Brown Goodwin was born the only child to Debbie and Ronnie Goodwin in Nashville, Tennessee. At a young age he moved with his family to Plant City, Florida but returned to the middle Tennessee area in 2001 where he attended Oakland and Siegel High School in Murfreesboro, Tennessee. He was active in athletics at this time and lettered in both baseball and track. After graduating in 2005, he attended the University of Tennessee, Knoxville. He obtained his Bachelors of Science degree in Chemistry from UT in May of 2010. The following fall he began graduate school at UT with aspirations of achieving his doctorate degree. His research expertise is in the synthesis of well-defined branched materials by anionic polymerization that was guided by his major professor Dr. Jimmy Mays. In December of 2015, he completed the requirements for a PhD in chemistry.